



University of Naples Federico II

Dosimetry in the Space
The radiation protection of astronauts during space missions

Filomena Loffredo

PhD student in Novel Technologies for Materials, Sensors and Imaging
XXVII cycle

Supervisors
Dott.ssa Mariagabriella Pugliese
Ing. Renato Aurigemma

Coordinator
Prof. Antonio Cassinese

Academic year 2014-2015

Contents

Introduction	3
1 Space Radiation	7
1.1 Van Allen radiation belts	7
1.2 Galactic Cosmic Rays	8
1.3 Solar Particle Events	11
1.4 Radiation protection quantities	13
1.5 Exposure limits	15
2 Shielding	17
2.1 Interaction between radiation and matter	19
2.2 Fragmentation of heavy ions	22
2.3 Interaction protons - matter	24
2.3.1 Intra-nuclear cascade (INC)	25
2.3.2 De-excitation	26
2.4 Products spallation	28
3 Geant4 -GEometry ANd Tracking	31
3.1 Simulation	31
3.2 Monte Carlo Method	31
3.3 State of Art	32
3.4 Development of the Geant project	33
3.5 Object-Oriented Programming	33
3.6 General structure of the software Geant4	34
3.7 The main Geant4 components	36
4 SPace ENVironment Information System SPENVIS	42
4.1 Generator of orbits	42
4.2 Radiation Sources	43
4.3 Radiation Protection	44
4.4 Multi-layer protective: MULASSIS	45
4.5 Analysis of microdosimetry: GEMAT	48
4.6 Sector Shielding Analysis Tool (SSAT)	50
4.7 Geant Radiation analysis space (GRAS)	51

5	Geant4 Results	55
5.1	PhysicsList	55
5.1.1	Electromagnetic Interactions	56
5.1.2	Hadronic Interactions	56
5.1.3	Determination of the interaction point	57
5.2	STP	59
5.2.1	Experimental Setup	59
5.2.2	G4hIonisation	59
5.2.3	Continuos energy loss	60
5.2.4	δ -rays	61
5.2.5	STP Results	62
5.3	<i>Dose</i>	64
5.3.1	Experimental Setup	64
5.3.2	<i>G4ProtonInelasticProcess</i>	65
5.4	<i>Dose</i> Results - Al Target	66
5.5	<i>Dose</i> Results- Nomex Target	80
5.6	<i>Dose</i> Results- PMMA Target	86
6	Spennis Results	93
6.1	Experimental setup	93
6.2	Results Mulassis	95
	Conclusions	99
	References	100

Introduction

The aim of my PhD work is the study of the effectiveness, in terms of reduction of dose to the astronauts, of materials with particular characteristics for applications in space.

The risks of a space mission can be:

1. Physiological problems caused by reduced gravity:

The physiological changes in weightlessness have been extensively studied, especially during long-term missions on space stations (ISS and, previously, Mir) in low-Earth orbit (LEO). Bone loss, kidney stone formation, skeletal muscle mass reduction, cardiovascular alterations, impaired sensorymotor capabilities, and immune system dysfunctions are among the consequences of prolonged permanence in microgravity. The risks are well characterized and several countermeasures are available.

2. Psychological and medical problems caused by isolation:

Isolation may lead to serious neurobehavioral problems caused by poor psychosocial adaptation (NASA, 2009). Isolation also brings the problem of autonomous medical care (AMC), i.e., the capability to handle sickness or accidents in complete isolation. Countermeasures for AMC risks are mostly technological, i.e., rely on the development of portable medical equipment and telemedicine (M.Durante and F.A.Cucinotta, 2011).

3. Acute and Late problems caused by exposure to radiation;

The Cosmic Radiation (CR) represents a serious health risk for astronauts during space travels. The radiation in space is very different from that on the Earth. In the space, high-energy (E) and charge (Z) particles (HZE) provide the main contribute to the equivalent dose, whereas on Earth, γ rays and low-energy α particles are major contributors.

The risks related to exposure to space radiation can be acute and late effects, because of the complex nature of the space radiation environment. Acute effects can be associated only to intense solar particle events (SPE) not adequately shielded. Late effects including cancer and other old age diseases are associated with the chronic exposure to galactic cosmic radiation (GCR), which is substantially different both qualitatively and quantitatively from the Earth's radiation natural background. On the Earth, three parameters can be considered to limit the exposure to radiation: exposure time, distance between source and target and shielding. Instead, the radiation protection in the space is a very complex problem because the only possibility to provide it is the shielding. The different radiation causes a high uncertainty on the estimated radiation health risk (including cancer and non cancer effects), and makes difficult the choice of a possible shielding. It should have important features: first

of all, it has to be light, because very heavy shields are impractical on spaceships and especially must take into account the interaction of radiation with the materials, which produce secondary radiation that can be very harmful to the health of astronauts.

The space radiation consists of a mixed field of radiations where, it is possible to distinguish three categories: i) Van Allen radiation belts, ii) Galactic Cosmic Radiation (GCR) and iii) Solar Particle Events (SPE) (Cucinotta and Durante, 2011). In particular the SPE, composed for 98% of protons with energies up to several GeV and high fluences ($\sim 10^{11}$ particles/cm²), represent one of the main health risk for long duration manned interplanetary missions (McGuire et al., 1986). The study of the behavior of protons at energies of about 1 GeV seems to be very interesting because the main contribution to the equivalent dose is provided by them and the remaining is attributed to heavy ions (10%). The Solar Particles Events show a maximum intensity during maximum solar intensity and represent the greatest danger to the unshielded crew.

For the health risk assessment transport codes are used, but these have a high degree of uncertainty, due to the fact that the experimental data available for the validation of different calculation models are still few. Since the limits of career recommended for activities in Low Earth Orbit (LEO) by the National Council on Radiation Protection and Measurements (NCRP) are estimated by combining data from personal dosimeters of astronauts with the results obtained using the model calculations, it is clear the importance of implementing the model calculations using all the information resulting from research conducted both in flight, aboard the International Space Station (ISS), on land, at accelerators dedicated (at the NASA Space Radiation Laboratory at Brookhaven and the National Institute of Radiological Sciences in Chiba).

My work was carried out in the LaRa (Radioactivity Laboratory) at the Physics Department of the University of Naples, Federico II, in collaboration with "Società Aerospaziale Mediterranea (SAM)" company.

In this work, by using Geant4, the validation of the electromagnetic physical processes was performed in a range of energy characteristic of SPE and the validation of the hadronic physical processes was performed for protons with 1GeV of energy. During the PhD's period, I performed an intership with the company SAM, "Validation of the electromagnetic physical processes with software Spenvis" and I used a different software Spenvis- MULASSIS.

By using MULASSIS, the validation of the electromagnetic physical processes was performed in a range of energy characteristic of SPE. The simulation was performed assuming a slab of aluminum of $20g/cm^2$ as shielding, whose thickness characterizes the shelter used by the crew in case of emergency caused by intense SPE. To validate the electromagnetic physical processes with both software, the primary beam consists of protons of energy varying between 800 to 1200 MeV. The results of the electromagnetic Stopping Power obtained with MULASSIS and Geant4-9.6p2, for different values of energy, and the comparison with the NIST data are reported. To validate the hadronic physical processes the simulated experimental setup is constituted by a source of 1 GeV protons, placed at 30 cm from the center of the aluminum target, in air. Validation and comparison among trends has

been performed. After a study of the behavior in terms of the equivalent dose, of different materials, aluminum ($\rho=2.70 \text{ g/cm}^3$), PMMA ($\rho=1.19 \text{ g/cm}^3$), or Nomex ($\rho=1.15 \text{ g/cm}^3$) of parallelepiped shape, of a thickness 20g/cm^2 in the incidence direction of the primary beam and base surfaces $30\times 30 \text{ cm}^2$, has been carried out.

The dose values are obtained by simulating the presence of a tissue equivalent ionisation chamber produced by Far West Technology, Inc., IC-17 model.

Validation of an application developed in Geant4, for the study and optimization of shielding in the exposure conditions to SPE, was performed by comparison with data of the NIST database PSTAR, available online, and experimental data (Mancusi et al. 2007).

The results that will be presented show a comparison of the performance of dose, in the same conditions of the experimental setup for different target materials, hydrogenated material (PMMA) and Nomex compared with aluminum. The comparison, as well as already present in the literature, confirms that the hydrogenated materials have a better shielding effectiveness.

This work can be subdivided into these parts:

1. Chapter 1: Introduction to the different Cosmic Radiation, Radiation protection quantities of interest and exposure limits;
2. Chapter 2: Interaction between radiation and matter;
3. Chapter 3: Geant4 -GEometry ANd Tracking that is a versatile and powerful toolkit to simulate the passage of particles through matter;
4. Chapter 4: Spenvis-MULASSIS that is an interactive tool developed by the European Space Agency;
5. Chapters 5 and 6: Geant4 and Spenvis Results.

1 Space Radiation

The radiation field present in the space is mixed and it is possible to distinguish three categories:

1. Van Allen radiation belts are formed by charged particles, in particular electrons and protons, retained by the Earth's magnetic field due to the Lorentz force.
2. Galactic Cosmic Radiation (GCR) is composed of protons, α – particles and heavy ions.
3. Solar Particle Event (SPE) is the issuance of a particularly violent flow of charged particles (protons, helium and heavy ions).

1.1 Van Allen radiation belts

Space missions passing through the Van Allen belts, leaving the protection of the Earth's magnetic field.

The name Van Allen belts comes from its discoverer, the American astronomer and physicist J.A. Van Allen (1914-2006), that between 1958 and 1960 deduced the existence through the study of the data transmitted from the first US satellite, Explorer1.

The Van Allen Belts are an important component of the Earth's magnetosphere, the region of space in which the motion of the charged particles of the solar wind and cosmic radiation, not too much energy, is conditioned by the Earth's magnetic field. Its origin is due to the interaction of the Galactic Cosmic Radiation and Solar particle with the Earth's magnetic field and atmosphere. Van Allen radiation belts are formed by charged particles, in particular electrons and protons, retained by the Earth's magnetic field due to the Lorentz force.

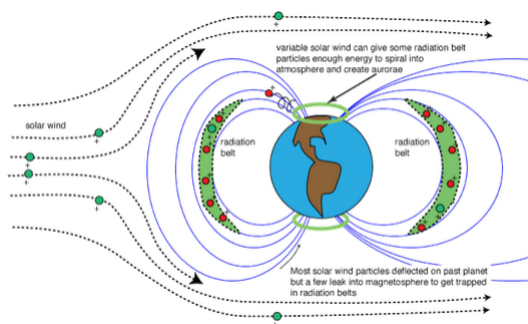


Figure 1: Van Allen Belts.

The Van Allen belts starting from the upper layers of the atmosphere and extend up to a distance of about 12 times the radius of the earth (76.000 km). This zone consists of two bands, internal and external. The first zone is composed of high-energy protons (10÷100 MeV) created by collisions

between the particles of cosmic rays with the atoms of the atmosphere. The second zone is composed of low energy electrons (MeV). The electrons have a low range of penetration, and for this reason are easily shieldable from the walls of the spacecraft, hence, they do not contribute to the dose absorbed by astronauts. The high energy of the protons allows them to penetrate inside the vehicle and to generate reactions that lead to the formation of secondary particles extremely damaging for the crews. The greatest contribution to the dose absorbed during space mission LEO¹ derives from protons. To be taken into account particularly during missions in LEO is the so-called The South Atlantic Anomaly, a region on the coast of Brazil, where the inner part of the Van Allen belts extending up to the part high of atmosphere, about 200 km altitude. Here, the radiation is very intense and therefore dangerous for astronauts, due to of its protons trapped in this area. This behavior is due to the fact that the axis Magnetic Earth is inclined by 11° in the direction of North America compared to axis of rotation and its center has moved 500 km to the Pacific Western.

1.2 Galactic Cosmic Rays

In the space environment there are many kind of energetic particles of different origin. The dominant radiation at energies above 30-50 MeV/nucleon is constituted by the Galactic Cosmic Rays (GCR). It consists of particles of charge from hydrogen ($Z=1$) to uranium ($Z=92$) arriving from outside the heliosphere. These particles continuously enter the solar cavity and are isotropically distributed. Cosmic rays originate as primary cosmic rays. Primary cosmic rays are composed of protons (87%), alpha particles (12%), with a small amount of heavier nuclei (~1%).

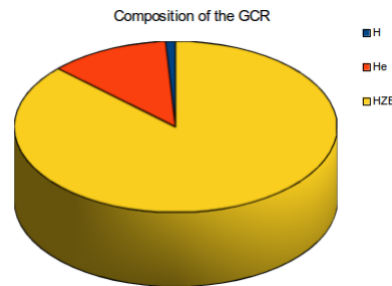


Figure 2: Composition of GCR.

Although, the galactic cosmic radiation is composed mainly of protons, they do not provide the main contribution in terms of absorbed dose.

¹Low Energy Orbit

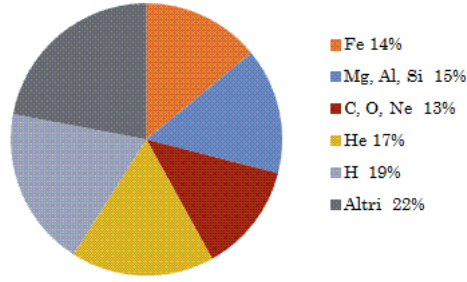


Figure 3: Percentage contribution of heavy ions.

Following is shown the percentage contribution for fluence, dose and equivalent dose of the different elements present in the GCR calculated with the code HZETRN by NASA.

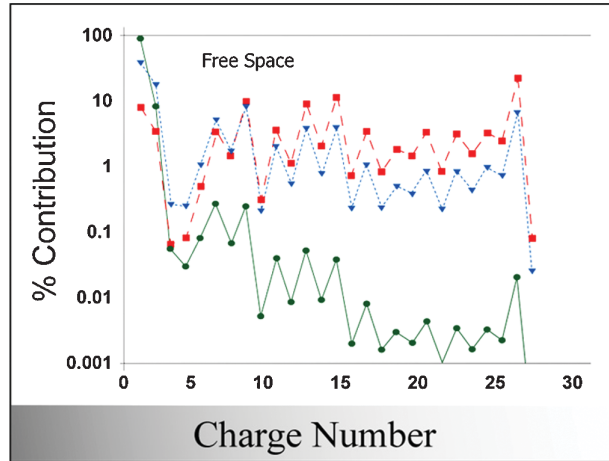


Figure 4: Code HZETRN by NASA.

It is evident that the risk of radiation in space is mainly linked to exposure to particles HZE. Although iron ions ($Z = 26$) are about ten times less abundant than carbon ions ($Z = 6$) and oxygen ($Z = 8$) and one thousand times less abundant protons their contribution to the equivalent dose is predominant. Secondary cosmic rays, caused by a decay of primary cosmic rays as they impact an atmosphere, include neutrons, pions, positrons and muons. The energy spectrum of CGR is described by the differential intensity or differential flux $\phi(E)$ which gives the number the particles with energy between E and $E + dE$, observed per unit surface, time, solid angle and energy i.e.:

$$\phi(E) \equiv \frac{dN}{dSdt d\Omega dE} \quad (1)$$

The GCR is over 80% effective dose for the crews on the International Space Station because of its greater penetration power, until to organs more interior, and the high values of the quality factors. The galactic cosmic rays flux is not constant and is strongly affected by solar activity. The figure shows the differential energy spectra for major ions for solar minimum (1977) and solar maximum (1959) (Badhward and O'Neill, 1992).

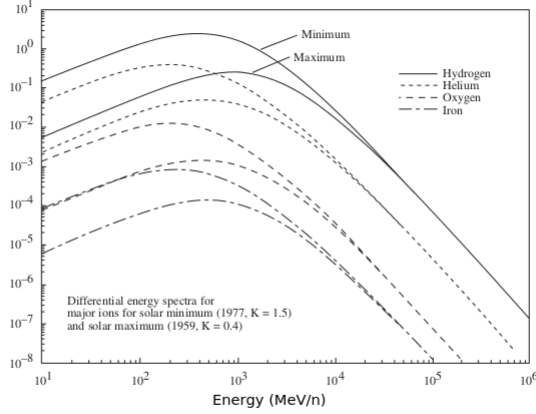


Figure 5: The differential energy spectra for major ions for solar minimum (1977) and solar maximum (1959)

The solar wind modulates the component of the GCR low energy ($< 1\text{GeV}/n$), with a regular cycle of about 11 years. During the phases of high solar activity, i.e. when it is the greater the intensity of the solar wind, the cosmic ray flux decreases by a factor between 3 and 4 with respect to phases of minimum solar activity, corresponding to weaker solar winds. The figure 5 also shows that the increase of solar activity maximum curve shifts from hundreds of MeV/n towards higher energies. For an energy of $100 \text{ MeV}/n$ the flows of particles differ by a factor 10 between the conditions maximum and minimum solar activity, while around $4 \text{ GeV}/n$ the variation observed is only of 20%, to zero, and finally, to higher energies. In addition to galactic cosmic rays is also observed the so-called abnormal component [Anomalous Cosmic Rays (ACRS)]. The ACRS is composed of particles, originally neutral from interstellar gas, which is partially ionize after entering in heliosphere as a result of interactions with the solar radiation. These particles are then accelerated by the flow variables of the wind solar collision zones, penetrating more in the the solar magnetic field compared to cosmic rays totally ionized. The energies of these particles are low (about $20 \text{ MeV}/n$); therefore stops completely the small screens, making negligible their contribution in terms of radiation protection.

1.3 Solar Particle Events

The Sun, as a result of sudden explosions local (Solar Particle Events, SPE), releases from the surface, large quantities of energy in the form of gamma rays, X-rays and radio waves a wide frequency band. During these SPE intense currents and varying magnetic fields accelerate the material constituting the solar corona (the most Outside of the solar atmosphere). These are large flows of particles totally ionized (coronal plasma), more protons ($\approx 98\%$ of the composition in the flow) with a small fraction of heavier nuclei (McGuire et al., 1986).

The SPE consisting in the issue by the sun of a flow of charged particles (protons, helium and heavy ions) in the space. The duration of event varies from a few hours to a few weeks; the frequency and the intensity of the emission increase throughout the maximum of solar activity up to a fluence of $10^{10} \text{ particles/cm}^2$ with energy greater than 1 GeV/n. The main contribution to the equivalent dose, for the solar events is provided by protons ($\sim 90\%$) and the remaining is attributed to heavy ions ($\sim 10\%$) (Durante,2002). The solar particles events have a maximum intensity during maximum solar intensity and are the greatest danger to the crews if unprotected. Although it is known that the occurrence of the SPE is related to an increased solar activity, in particular to an increase in the number of solar spots, there is not now an effective model for predicting the arrival, the direction and intensity. The solar flares are intense, however, relatively rare, in fact, they are recorded on Earth as random events of low frequency, typically one month. For the radiation protection would be, therefore, important to be able to predict intensity, energy and duration of the SPE, especially for long-term missions. In general, the energy of the SPE is smaller than the GCR, and the shield to represent a possible solution. However, the solar flares more intense can put even in serious danger of living a crew unprotected or induce syndromes acute exposure to radiation (such as nausea), especially during extra-vehicular activity.

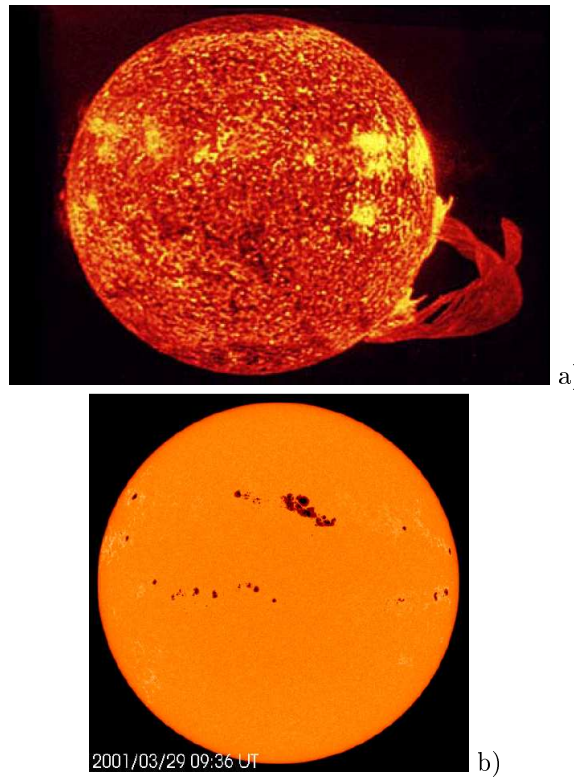


Figure 6: a) Solar eruption observed during the Skylab mission in 1996; b) Sunspots observed by NASA March 29, 2001.

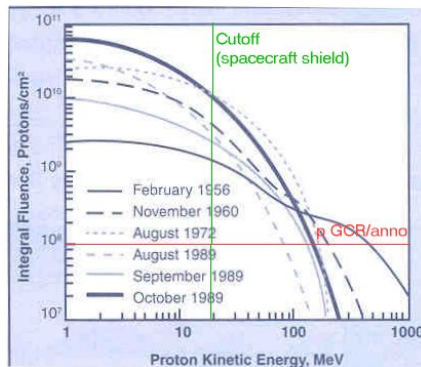


Figure 7: Integral energy spectrum of protons emitted during intense Solar Particle Events recorded in the 20th century (Kim et al., 2009).

The figure shows that the trend is $I = I_0 E^{-\gamma}$ where, I_0 represent the total number of the particles, insted the γ parameter decrease with increase of the time.

1.4 Radiation protection quantities

To define the radiation protection quantity of interest there are three fundamental parameters:

1. Energy deposition;
2. Quality of the incident radiation;
3. Radiosensitivity organs and / or tissues.

The first, the energy deposited is defined by Dose that is given by following relationship:

$$D = \frac{dE}{dm} \quad (2)$$

This formula represents the loss energy per unit of mass and the unit of measure is Gy.

The second parameter is defined by equivalent dose, that measures the dose D_{TR} (Gy) averaged over a tissue T by the tissue weighting fraction (ω_T) due to radiation R does not provide information about the biological response. An approximate scheme is to calculate the equivalent dose H_T (Sv) in the organ or tissue T using the following relationship:

$$H_T = \sum_R \omega_R D_T \quad (3)$$

where ω_R is the so-called radiation weighting factor, whose values are based on the review of biological information.

The third is the effective dose that is given by following relationship

$$E = \sum_T \omega_T H_T = \sum_T \omega_T \sum_R \omega_R D_{T,R} \quad (4)$$

where ω_T is the so-called tissue weighting factor. The unit of measure for the effective dose is Sv.

The ω_R and ω_T values reported in Table1 are provided by ICRP-103.

Radiation type	ω_R	Organ	ω_T
X and γ rays	1	Breast, bone marrow, lung, colon, stomach	0.12
Electrons and muons	1	Gonads	0.08
Protons and charged pions	2	Bladder, liver, esophagus, thyroid	0.04
α particles and heavy ions	20	Bone surface, brain, salivary glands, skin	0.01
Neutrons	2-20	Remainder	0.12

Table 1: Exposure of different organs or tissue is associated with different risks of stochastic effects.

For neutrons the weight factor, which depends on the radiation, is a continuous function of the energy of the neutron.

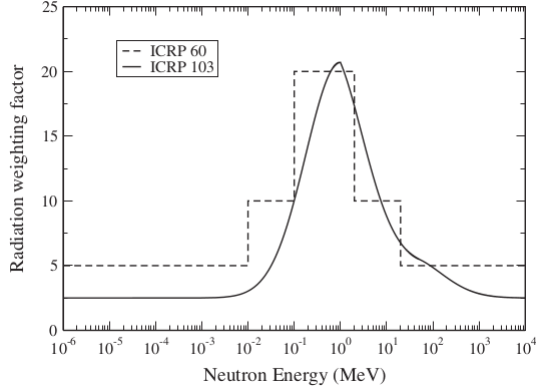


Figure 8: Weight factor for neutrons ω_R .

The step function is recommended of ICRP-60 (1991), and the continuous function concerns the recent recommendations of the ICRP-103 (2007).

Although it is less than the percentage of heavy ions, they give the largest contribution to the equivalent dose that has broad peak in the kinetic energy spectrum from 100 to 1000 MeV/n.

To estimate all possible stochastic effects, considering both uniform exposure that is not uniform, ICRP recommends the following relation which is independent of gender and age:

$$E = \sum_T \omega_T \left(\frac{H_T^M + H_T^F}{2} \right) \quad (5)$$

F and M are indices that refer to female and male.

The spectrum of the radiation space is a complex mixture of charged particles of the primary beam and the secondary beam characterized by various energies, for this reason NCRP recommended to evaluate the equivalent dose as follows:

$$H_T = \frac{1}{m} \int_m dm \int Q(L) F_T(L) L dL \quad (6)$$

In the formula 6, m is the organ mass, L (LET) is the linear energy transfer ($KeV/\mu m$), F_T represents the fluence of the particles through the organ T and Q is the quality factor (dimensionless). Unlike ω_R the quality factor Q is a continuous function of LET.

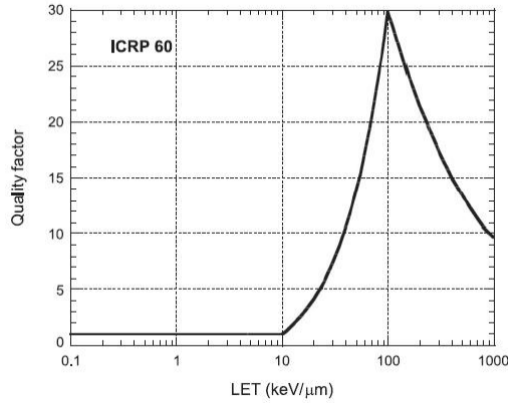


Figure 9: Graphical representation of the dependence of the quality factor from LET, in accordance with the recommendations of the ICRP.

1.5 Exposure limits

The term "risk" is the probability that the damage occurs. It is proportional to the effective dose by a suitable coefficient of risk assessed by organic effect, the exposure type (acute or late) of sex and age at which exposure occurs. The estimated risk coefficients have been possible because of epidemiological studies on the survivors of the atomic bombs Hiroshima and Nagasaki. The radiation protection quantity, effective dose E and equivalent dose H_T are used to fix the limits of exposure so that they are prevented tissue damage. The limits are updated regularly according to scientific developments. For exposed population on the earth the limits are provided by the ICRP and are based on the risk of cancer, because unlike the other effects occurs even at low doses. The limits of radiation exposure for astronauts are more than workers on Earth. In fact for the occupationally exposed workers the limit is $20mSv/year$ whereas for general population is $1mSv/year$. In the table there are the recommended limits of the equivalent dose for the astronauts, this value are provided by NCRP Report 132, 2000:

Age at Exposure	Equivalent Dose (Sv) Female	Equivalent Dose (Sv) Male
25	0.4	0.7
35	0.6	1.0
45	0.9	1.5
55	1.7	3.0

Table 2: Recommended limits of the equivalent dose, NCRP Report 132, 2000.

These values depend on the gender and age.

The table shows the effective dose E , for astronauts, during different space missions, previous and next (Durante, 2004). The values of maximum (calculated or measured) are shown in parentheses.

Program	Altitude	Number of astronauts	Dose rate ($\mu\text{Sv/day}$)	Total dose (mSv)
Gemini	454 (1370)	20	870 (4700)	0.53 (4.7)
Apollo	-	33	1300 (3900)	12.2 (33)
Skylab	381 (435)	9	120 (2100)	72 (170)
STS (alt. > 450 Km)	570	85	3200 (7700)	26.5 (78)
STS (alt. > 450 Km)	337	207	230 (400)	2.1 (7.1)
STS/MIR	341 (355)	4	720 (1000)	100 (140)
ISS	360 (450)	288	500 (1000)	80 (180)
Moon (190 days)	-	10 (60)	1300 (2000)	100 (195)
Mars (950 days)	-	4 (8)	1500 (2000)	400 (1200)
Callisto (5 years)	-	4 (8)	1500 (3500)	1600 (2500)

Table 3: The effective dose E , for astronauts, during different space missions.

The corresponding limits, recommended by NASA for astronauts involved in missions of the duration of 1 year in LEO, are reported in Table and compared with those of the other major space agencies (Cucinotta, Hu et al., 2010; Straube et al., 2010). Even NASA is based on the risk of 3% of cancer death induced by radiation exposure.

Space agency	Gender	Age at first exposure, (yr)			
		30	35	45	55
NASA (USA)	Female	0.47	0.55	0.75	1.1
	Male	0.62	0.72	0.95	1.5
JAXA (Japan)	Female	0.6	0.8	0.9	1.1
	Male	0.6	0.9	1.0	1.2
ESA		1.0	1.0	1.0	1.0
FSA (Russia)		1.0	1.0	1.0	1.0
CSA (Canada)		1.0	1.0	1.0	1.0

Figure 10: Exposure limits, in terms of effective dose. Recommended limits by different space agencies for astronauts during missions period of 1 year (Cucinotta, Hu et al., 2010; Straube et al., 2010).

The limits of effective dose E , expressed in Sv, is provided in relation to sex and age at which exposure occurs. The European Space Agency (ESA), Russian (FSA) and Canadian (CSA) not apply corrections according to sex and age but prefer to use a single limit value of 1 Sv. In this regard, the only agency that uses an approach similar to that NASA, is that Japanese (JAXA). These limits, however, are continuously reviewed and vary depending on the duration of the missions.

2 Shielding

The main aim of the radiation protection program in the space is to minimize the exposure of crew to ionizing radiation.

On the Earth, three parameters can be considered to limit the exposure to the radiation: exposure time, distance between source and target, shielding. Because the cosmic radiation is isotropic and because the mission has a fixed duration, the radiation protection in the space is a very complex problem so the only possibility to provide it is the shielding. The different radiation causes a high uncertainty on the estimated radiation health risk (including cancer and non cancer effects), and makes difficult the choice of a possible shielding. It should have important features: first of all, it has to be light, because very heavy shields are impractical on spaceships and especially must take into account the interaction of radiation with the materials, which produce secondary radiation that can be very harmful to the health of astronauts. In fact, since the radiation at high energies (order of GeV) is very penetrating, the use of large shields can result in an increase in the production of secondary particles at the expense of the effect of shielding. Protons and heavy ions, which make up the GCR and SPE, interacting with atomic nuclei of the shielding generating a wide variety of secondary products such as protons and neutrons, light fragments of the primary radiation, gamma rays and heavy nuclei of the target (the phenomenon of nuclear fragmentation). The fragmentation by changing the spectrum of the incident radiation and its distribution in LET, that are connected to the quality factor Q (figure 9), can induce an increase in the biological risk related to exposure.

The material mainly used for the realization of the walls of the spacecraft is the aluminum, with typical thicknesses of about 5g/cm^2 . This barrier is able to shield completely, all the protons of energy less than 65 MeV, resulting, therefore, effective in the case of exposure to radiation confined (LEO missions). In the absence of barriers, in fact, also the protons of a few MeV, can penetrate the layers of skin on our body and deposit their energy in the internal organs.

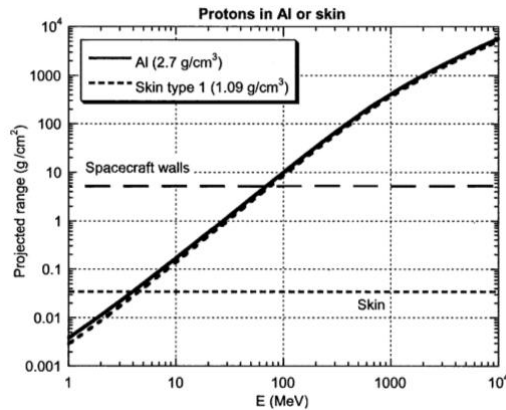


Figure 11: Energy-Range for protons in aluminum and human skin.

In the figure, the range is expressed in g/cm^2 . The horizontal dotted lines represent the typical thicknesses of the walls, in aluminum, spacecraft and human skin. The ranges were calculated with the simulation program SRIM2000 (Durante, 2002).

The spacecraft is also provided with small areas near the dormitories, with shields that about $20g/cm^2$ of aluminum, the '*storm shelter*'. These areas are designed to provide the crew an emergency shelter in case of intense SPE. However, the use of thicker shielding leads, inevitably, an increase of the total weight of the spacecraft. This complicates the implementation of appropriate protection systems with a consequent increase in costs of the mission. In conclusion, the study of the interaction of radiation with different materials is aimed at optimizing the shielding.

An interesting alternative to the passive shielding is the use of electromagnetic fields that deflect the charged particles so that it does not arrive on the space vehicle, the so-called active shielding. The basic idea is that a magnet can generate a strong field around the spacecraft to protect the crew from excessive exposure, as well as the geomagnetic field protects life on Earth from the dangers of galactic and solar radiation.

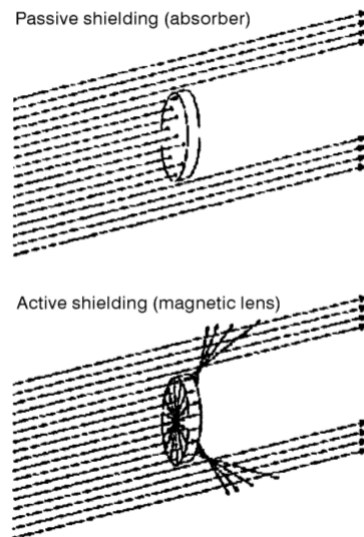


Figure 12: Passive (absorbing material) and active (magnetic lens) shielding (Durante, 2002).

However, the construction of magnetic shields is not yet a solution, feasible in practice, to the problem of radiation protection in space.

2.1 Interaction between radiation and matter

Charged particles were directly ionizing radiation as it interacts with matter, either directly ionize atoms and molecules of the medium. The passage of these particles through matter is characterized by two effects: loss of energy by the incident particle, and deflection of the particle itself from its initial direction.

The processes of interaction between charged particles and target depend on the energy of the particles and are:

1. ionization and excitation (inelastic collision);
2. nuclear reactions that cause fragmentation of particles involved in the collision.

Inelastic collisions are the main contribution of the loss energy into matter ($\sigma \sim 10^{-17} \div 10^{-16} \text{cm}^2$) and are usually divided into two groups (Leo, 1993):

- *soft* collision;
- *hard* collision.

In soft collisions, the interactions between the incident particle and the target occurs at large distances, when compared to atomic dimensions, resulting only to effects of excitation.

Following of the establishment of the orbital electrons in the various energy levels of the atoms involved are observed the photons or Auger electrons emissions. In the case of molecules excited take place more complex processes that may end with the breaking of chemical bonds, often chemically reactive. In hard collisions, however, the interaction concerns so directed one electrons of the peripheral orbital, that receiving energy greater than that of the bond is released, causing the ionization of the atom involved. Following the ionization process is the formation of couples electron and positive ion that, in general, tend to recombine, unless the electron released has not sufficient kinetic energy to move away from the track of the primary particle and generate events of secondary ionization (δ rays). The energy threshold of processes of excitation and ionisation are of order of several eV in the case electron less bound. The collisions are inelastic phenomena of stochastic nature, which occur in large numbers for paths macroscopic and give the fluctuations in the total energy loss so small you easily work with the average values.

Linear stopping power S , the energy loss of a particle undergoes, through the matter, per unit of path is defined by this relationship:

$$S = -\frac{dE}{dx} \quad (7)$$

The stopping power initially calculated by Bohr using classical arguments, was later reworked by Bethe and Bloch on the basis of quantum perturbation theory, getting the relationship:

$$-\frac{dE}{dx} = 2\pi N_a r_e m_e c^2 \rho \frac{Z}{A} \frac{z_{eff}^2}{\beta^2} \left[\ln \left(\frac{2m_e \gamma^2 \nu^2 W_{max}}{I^2} \right) - 2\beta^2 - \delta - 2\frac{C}{Z} \right] \quad (8)$$

r_e	Electron radius
N_a	Avogadro's Number
$m_e c^2$	Energy at rest of the electron
I	Ionization potential
Z	Atomic Number
A	Atomic mass Number
ρ	Density of the absorber material
β	v/c of the ion incident
z_{eff}	Effective charge of the incident particle
γ	$1/\sqrt{1-\beta^2}$
W_{max}	Maximum energy transferred in a single collision
C	Shell correction
δ	Density correction

Table 4: Parameters of the Bethe-Bloch formula.

The maximum energy transferred W_{max} in a single inelastic interaction is the one produced in a head-on collision.

The quantity δ and C are important corrective terms to the formula of Bethe and Bloch, respectively, in the limits of high and low energies.

The correction δ to the effect of density is only relevant when the kinetic energy of the projectile is comparable to or higher than its rest mass energy: in this case, the electric field of the ion incident polarized atoms of the medium in the proximity of its trajectory. Due to the polarization induced in this way, the electrons far from the path of the particle will be shielded from total intensity of the radiation field and, consequently, inelastic collisions with these electrons will contribute to a lesser extent to the total energy loss than expected of formula of Bethe and Bloch.

The greater the density of the material, greater importance is this effect. The shell correction term C assumes importance in the case where the velocity of the projectile is comparable or less than the orbital velocity of the electrons bound to the atoms of the medium. As the speed of the particles moves away from relativistic energies, collisions particles-electrons require a more detailed assessment of the bonding orbitals of each electron-target in order to obtain more accurate values of stopping power. In order to extend the formula of Bethe and Bloch in the low energy limit $v \sim 0.05c$ it is necessary to replace the initial charge z with effective charge of the incident particle z_{eff} .

The reduction of the effective initial charge z , as a function of the residual velocity of the ion accident, makes that the stopping power decreases rapidly and is expressed by the formula Barkas:

$$z_{eff} = z \left(1 - e^{-\beta z^{-\frac{2}{3}}} \right) \quad (9)$$

From the formula of Bethe and Bloch is possible to obtain the trend of the energy deposited in the material per unit of the path as a function of penetration depth. The corresponding curve is known as Bragg curve and shows how the heavy charged particles lose most of their energy at the end of their path as shown in figure 13.

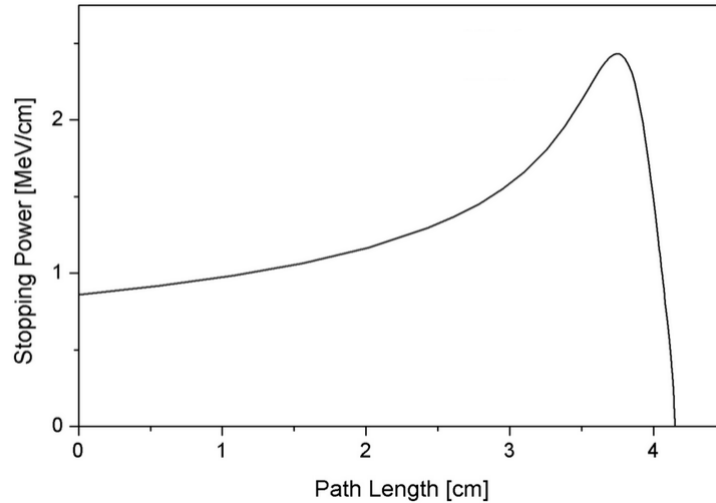


Figure 13: The Bragg peak shows the variation of dE/dx as a function of depth of penetration of the particle in the matter. It is very ionizing the end of its path.

The increase of ionization, that is the number of ion-electron pairs produced by the passage of the radiation, towards the end path can be explained by the dependence of the stopping power from the inverse square of the speed.

When the particle slows the ionization produced that increases then decreases rapidly because the residual energy is less than the ionization potential of the medium. One of the most important parameters in the formula of Bethe-Bloch is the ratio Z/A . This ratio gives information about the different absorber materials.

The table shows the values Z/A for some materials:

Materials	Z/A
Hydrogen (H)	1
Carbon (C)	0.5
Alluminum (Al)	0.48
Lead (Pb)	0.40

Table 5: Values Z / A for some materials.

The best absorber materials is the Hydrogen (H).

In the case of light particles (electrons and positrons), due to their reduced mass, are of great importance for energy losses by irradiation, already at energies of order of tens of MeV ('bremsstrahlung' radiation), the emission electromagnetic radiation resulting from the diffusion in the electric field of the atomic nucleus. The total electrons and positrons energy loss is, therefore, composed of two parts:

$$\left(\frac{dE}{dx}\right)_{tot} = \left(\frac{dE}{dx}\right)_{rad} + \left(\frac{dE}{dx}\right)_{coll} \quad (10)$$

where the ratio:

$$\frac{\left(\frac{dE}{dx}\right)_{rad}}{\left(\frac{dE}{dx}\right)_{coll}} \simeq \frac{ZE}{700} \quad (11)$$

The unit of measure for E is MeV.

For each material, can be defined the critical energy E_c at which the radiation losses are equal those collisional inelastic, then become the dominant contribution to $E > E_c$. An approximate value of E_c , expressed in MeV, is given by the formula:

$$E_c \simeq \frac{800}{Z + 1.2} \quad (12)$$

In collisions of hard type instead the main feature is represented by the process of pure fragmentation to the passage in the field of high-energy ions. A precise and accurate description of the transport of such particles in the field is, therefore, essential to understand the effects of the field of space radiation on humans (Zeitlin et al., 1997).

2.2 Fragmentation of heavy ions

In space missions is important to the description of the fragmentation of heavy ions to understand the effects of high Z component of GCR on living tissue. Very important is also the study of radiation damage in microelectronic circuits.

The shielding for photons is known and effective while the GCR due the high energy of the particles and nuclear fragmentation of heavy ions is more complex. Charged particles crossing a medium, are slowed down by interactions with atomic electrons. The protons and ions present in the GCR and in the SPE can interact with the atomic nuclei of the shield and, depending on the primary particles and of their energy, can be produced a great variety of secondary particles which include protons and neutrons, light fragments of the primary radiation, γ rays and heavy nuclei of the target.

Different models have been developed for the study of the fragmentation of heavy ions, such as the model of Bowman et al. 1974 at Langeley, known as abrasion-ablation model. This model schematizes the interaction between projectile and target as the two stage process. In the first step the projectile

collides with the target and the nuclear volumes that overlap the bump removes them while the remaining volume of the projectile (pre-fragment) continues to travel along the original trajectory with the same speed it had before the collision. The removal of nucleons caused by the interaction alters the stability of the nuclei which interact.

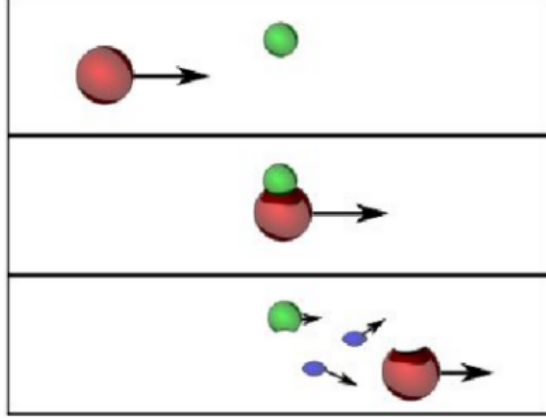


Figure 14: Abrasion-Ablation model.

Fragmentation changes the spectrum of the incident radiation and shift in the distribution of the LET. The cross section of the projectile fragmentation σ_P (cm^2/g) per unit mass of the target atomic weight of A_T can be approximated by the relation(Schimmerling et al., 1983)

$$\sigma_P \approx N_0 \pi r_0^2 \frac{(\sqrt[3]{A_P} + \sqrt[3]{A_T})^2}{A_T} \quad (13)$$

where N_0 is Avogadro's number, r_o effective radius of the nucleon and A_P atomic mass number of the projectile.

σ_P increases with A_T . It is very interesting to note that targets more lightweight fragment of heavy targets for the same mass. The shift of the spectrum in LET towards lower values is caused by a great fragmentation of heavy ions, as the fragments of the projectile have approximately the same speed of the primary ion and therefore lower LET.

From the formula 13 is known that the interaction probability σ_P increases both to growing of A_P , massive projectiles, which, for a given mass, for light targets, small values of A_T . The hydrogen, then, is the material which causes the greater fragmentation of heavy projectiles, as HZE of GCR. A high fragmentation of heavy ions move the spectrum of the LET towards lower values, since the fragments of the projectile, as already noted above, have approximately the same speed but the primary ion Z minor.

The different efficacy of the shields (figure 15) is a consequence of the relative attenuation of the components of the GCR, to vary the LET, the different materials. The spectrum of the GCR transmitted through the screens is generally shifted toward lower values of LET, compared to free space: the components of high LET are attenuated and those of low LET amplified. The threshold value of LET, which divides the component attenuated by the amplified, depends exclusively by the material of which is composed of the screen.

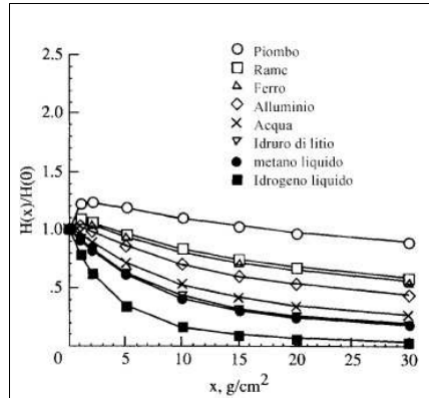


Figure 15: Relative attenuation of equivalent dose H , for a exposure period of a year during a minimum of solar activity, as a function thickness x [g/cm^2] for screens with different material (Wilson et al., 1995). The transport of the GCR is calculated with the code HZETRN.

2.3 Interaction protons - matter

Already in 1930 were observed cascades of particles as a result of the interaction of cosmic rays with matter. In those years, several studies were conducted on the thermal neutron flux density, induced by cosmic protons interacting with the atmosphere, the Earth's surface. The concept of nuclear spallation was born in 1937 by Glenn T. Seaborg that in his doctoral thesis described the inelastic scattering of neutrons (Seaborg, 1937).

The spallation is a process that occurs when a 'light' projectile (proton, neutron, or a nucleus of low Z), with a kinetic energy between the hundreds of MeV and several GeV, interacts with a 'heavy' nucleus (eg. Lead) causing the emission of a large number of hadrons (more neutrons) or fragments. This process consists of two phases:

- Intra-nuclear cascade (INC);
- De-excitation.

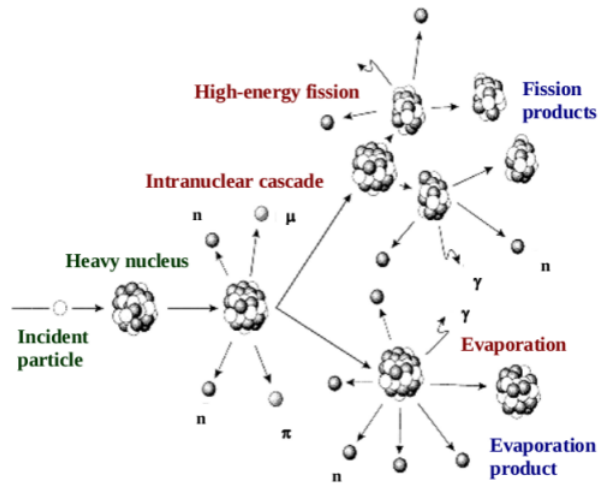


Figure 16: The spallation process.

2.3.1 Intra-nuclear cascade (INC)

The intra-nuclear cascade (INC) is the first and direct phase, the spallation process which is realized in a very short time Δt ($\Delta t \sim 10^{-22}s$). The intra-nuclear cascade is a succession of independent elastic collisions where projectile loses part of its energy, giving it to the nucleons, generating a cascade.

The INC is a process not clearly separated, in time, from the next decay phase to the achievement of the equilibrium state. In fact, for high energy beam ($E \sim 1GeV$) and especially in collisions involving heavy ions are possible emissions of pre-equilibrium. Following each interaction between the nucleons-target and the particle-projectile or those generated during the cascade, can be issued either fast particles, such as neutrons and protons with maximum energies similar to those of the incident beam, and fragments of relatively small charge, products 'multifragmentation'. The products of this stage are said particles of pre-equilibrium. Such particles have energies higher than those produced in the next phase of excitation and emitted mainly 'forward', that is, in the direction of the incident beam.

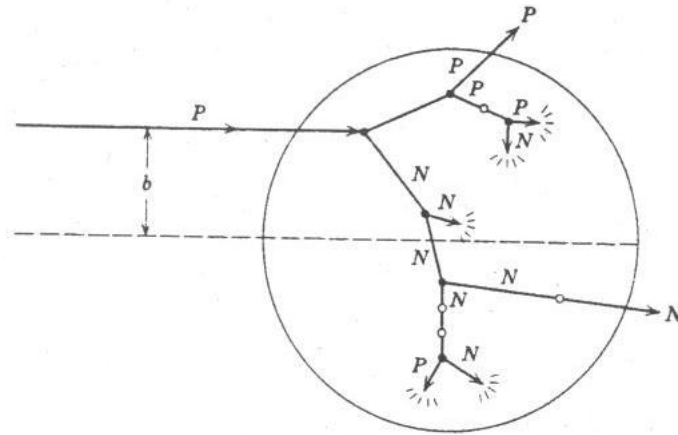


Figure 17: The scheme of the Intra-nuclear cascade.

2.3.2 De-excitation

The de-excitation is the second phase of the spallation process which is realized in a time Δt ($\Delta t \sim 10^{-16} s$).

This time, when compared with that of the Intra-Nuclear Cascade, is several orders of grandeur larger. For this reason, is often referred to 'slow' phase.

The target-nuclei are in highly excited states and energy excitation is equally distributed within them. The excitation occurs, through two mechanisms:

- evaporation;
- fission.

During the evaporation the excited nucleus transfers the excess energy to fragments light loads (e.g. p , d , t , α) and neutrons which, in contrast to the INC, are emitted isotropically (figure 18), compared to the center of mass of the system, with maximum energies of $\approx 40 MeV$, equal to the depth of the barrier of the nuclear potential.

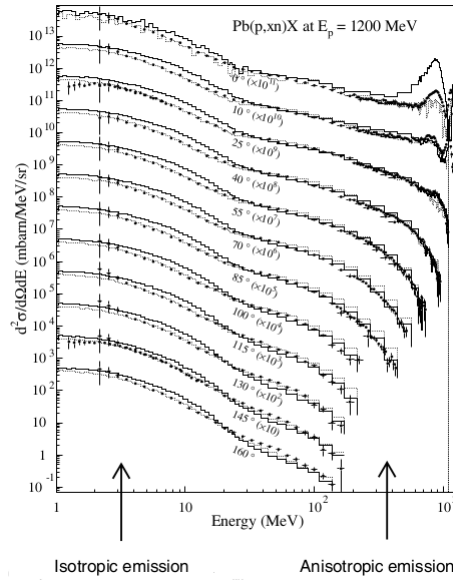


Figure 18: Differential cross sections in energy and angle for the production neutron reactions of protons from 1.2 GeV to on Pb target.

The figure 18 shows the differential cross sections in energy and angle for the production neutron reactions of protons of 1.2 GeV on Pb target (2 cm thick). The dots represent experimental values (measured with accelerator SATURN), the histograms represent the numerical values obtained with the model Bertini INC (continuous line) and the model INCL (dotted line) (Ledoux et al., 1999).

The fission carries the excited nucleus to split into two fragments with a similar number of protons. In their turn, the fission products, in relation to their excitation energy, may be subject to evaporation. Another de-excitation channel, is the emission- γ . When the nucleus, unstable, has not more enough energy for additional emission of neutrons, because its excitation energy is below the threshold of binding energy of nucleons (figure 19), it is de-excitation through the channel γ .

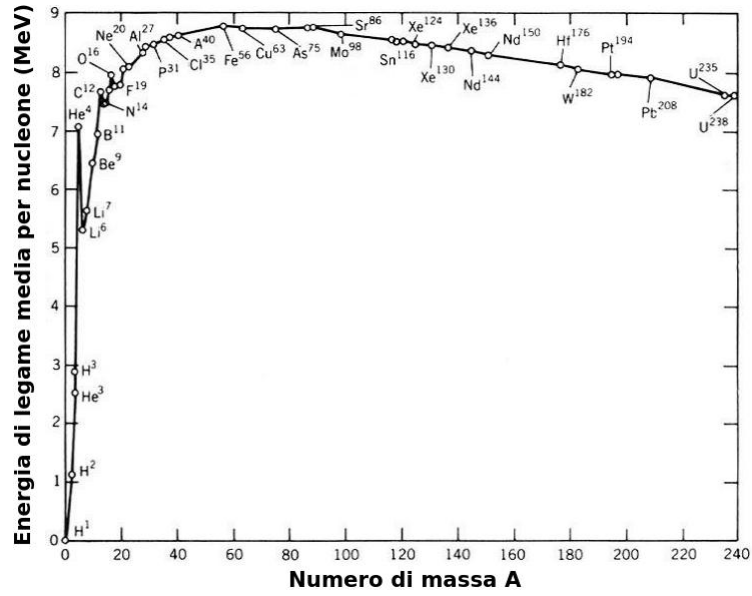


Figure 19: Binding energy per number of nucleons.

At the end of de-excitation through the transition γ , the daughter nucleus is generally β -active and decays to the stable state. In the end the main products in spallation reactions are the nuclei 'residues' and neutrons, the spallation neutrons.

2.4 Products spallation

The 'residues' nuclei are distributed on the nuclide chart, mainly in two regions as shown in figure 20.

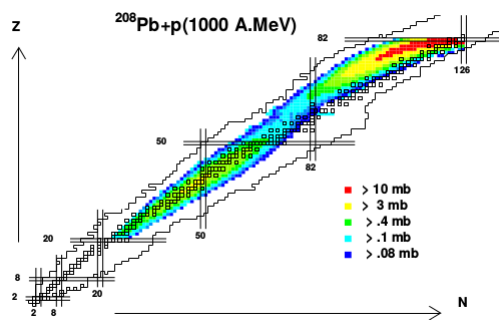


Figure 20: Cross sections for the production of residues nuclei in the reaction $^{208}\text{Pb} (1 \text{ GeV} / n) + p$.

The figure shows the distribution of the produced isotopes, where black open squares represent the

stable nuclei. Have been identified about 900 isotopes for a total section of impact of the reaction equal to $\sigma_{tot} = (1.87 \pm 0.23)b$ (Enqvist et al., 2001; Armbruster et Benlliure, 2001).

The upper right corresponds to the nuclei heavy residues, rich in protons, the evaporation products (products of spallation-evaporation) while the central part represents the residues of average mass due to the channel fission (spallation-fission products). The two areas of the paper of nuclides are separated by a zone of minimum cross section ($\sigma \sim 0.1mb$) for about $Z = 58$.

The spallation neutron can be characterized based on 3 factors: energy, spatial distribution and multiplicity.

The first two aspects (see figure 18 and figure 21), indicate that the emission spectrum of spallation is in the range of neutron energy, from tens of keV to energies close to those of the incident beam (about 1GeV), and is composed of an isotropic and an anisotropic part.

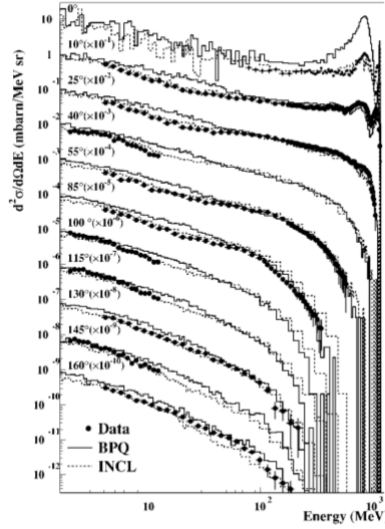


Figure 21: Differential cross sections in energy and angle for the production neutron reactions of protons of 1.2 GeV on Al target.

The figure 21 shows the differential cross sections in energy and angle for the production neutron reactions of protons of 1.2 GeV on Al target (3 cm thick). The dots represent experimental values (measured with accelerator SATURN) and are compared with numerical results obtained using the transportation code LAHET with model Bertini INC + pre-equilibrium (continuous line) or INCL (dotted line) (Leray et al., 2002).

The isotropic emissions, due to the channel de-excitation through evaporation are in the first part of the spectrum in the energy ($E < 100$ MeV), while those anisotropic, that characterize the emissions of pre-equilibrium, dominate at small angles, next to the direction of incidence of the beam ($\theta \sim 0$) and at high energies ($100 \text{ MeV} < E \lesssim 1\text{GeV}$).

The multiplicity is the average number of neutrons produced by spallation from a single projectile

particle. In the case of a large target, due to secondary reactions, the number of neutrons produced, for incident particle, is higher than in a spallation microscopic, or equivalently in a slim target (figure 22). The high-energy particles, which are able to escape from the nuclei-target during the INC, can induce further spallation reactions and give life to the inter-nuclear cascade. This process concerns more neutrons, which does not lose energy by ionization and can penetrate deeper into the target generating more neutrons by reactions of the type (n, xn) . Experiments carried out with protons of different energies, to varying of materials and size of the target, showing that the multiplicity increases with the energy of the incident beam, is greater for heavy nuclei-target and saturates at a given thickness.

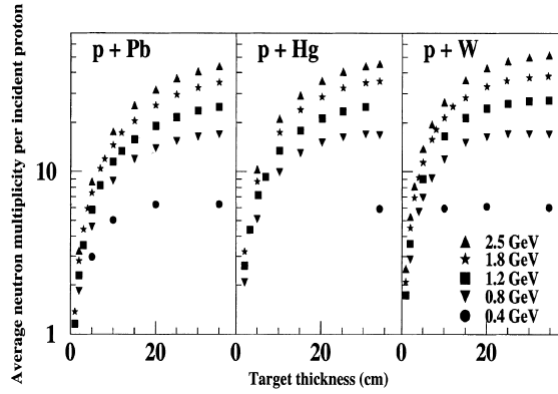


Figure 22: Average multiplicity of neutrons for incident proton as a function the thickness of the target (in cm) and of beam energy for lead (Pb), mercury (Hg) and tungsten (W).

The figure shows that the experimental data (measured at accelerator COSY) are correct for the fund and detection efficiency. All targets are cylinders 15 cm in diameter (Letourneau et al., 2000).

For example, the thickness of saturation of a target of lead for protons from 1 GeV is approximately 100 cm. Within this thick, almost all primary protons interacting are extinguished for spallation. In contrast, the charged fragments produced in the INC, emerging from a target often decrease because stopped in its interior because of the losses of ionization energy.

3 Geant4 -GEometry ANd Tracking

3.1 Simulation

Simulation is a powerful tool that allows us to study the temporal evolution of a real system through the observation of a computational model. A model is defined as a set of assumptions on a system for the only purpose of representing it. It can discern the static model, in which the assumptions concern a system at rest, from the dynamic model, in which they describe a system that evolves over time. The simulation is executable whenever the system concerned is describable through a model. It is mainly applied in the field of research because it allows to extract data and information that would be impossible to obtain for real experiments, difficult to implement. In science, simulation is a valid support for the experiments because it allows not waste time and money. The detailed results of the simulations can be available before the experiment is actually performed. The simulations allow to know, in a shorter time compared to the real case, the effects caused by the variations of the parameters which determine the different configurations of the simulated system.

The importance of the simulation is also be a powerful tool for analysis and verification of the system under observation. Neglecting all the effects considered not significant, it is possible to simplify the complexity of the system, allowing you to focus exclusively on the effects of primary interest (Hartmann, 1996).

3.2 Monte Carlo Method

The birth of the Monte Carlo method dates back to the period of the Second World War, when a collaboration between scientists, engineers and technicians gave life to one of the first electronic calculators *Electronic Numerical Integrator And Computer*, ENIAC. To developments of the ENIAC, completed in 1946, was attended by among the major scientific figures of era as Enrico Fermi, Nicholas Metropolis, Edward Teller and Stanislaw Ulam. Own latter, with the collaboration of John Von Neumann and Nicholas Metropolis, understood the power and utility of computers, gave birth to the Monte Carlo method based on statistical techniques fallen into disuse due to the complexity in the calculations.

The Monte Carlo method includes the class of computational algorithms acts to the resolution of complex systems, not easily approachable analytically, which can be described by a probability density function (PDF²).

The system can be so studied through decisions based on the probability distribution of the phenomenon to be examined, in order to generate the evolution of a possible scenario, statistically valid, extrapolating the effects of main interest.

²In probability theory the pdf (probability density function) of a continuous random variable is a function that describes the probability of taking a particular value. The probability that the value assumed by the random variable is on in a particular range is given by the integral of the pdf of the variable in this range. The probability density function is non-negative and its integral over all space is equal to one.

Note the PDF describing the system, we proceed to their random sampling using a uniform distribution of random numbers, including in interval $[0,1]$, which are generated by the computer through a suitable algorithm. In reality, it is pseudo-random numbers, in fact, if the generation algorithm always starts from the same starting point, the sequence of numbers generated will be identical. This is an advantage as it makes the experiment 'reproducible', which is essential so that we can repeat exactly the same simulation, identifying any errors related to the writing of algorithm (Hammersley, 1975). The application of Monte Carlo method is not limited only to the study of stochastic phenomena but can also be extended to deterministic systems, where there is the possibility to describe them in terms of the PDF.

The Monte Carlo method, based on the law of large numbers, allows to obtain significant results by setting a large number of events in the context of single simulation, so that the average value of the quantity considered is comparable to real within the statistical error.

The name Monte Carlo was inspired to homonymous the neighborhood of the Principality of Monaco, home to the casino, just for the analogy between the generation of random numbers and the game of roulette.

3.3 State of Art

Several software are based on the Monte Carlo method:

- **EGS:** (*Electron Gamma Shower*), it is a general purpose package for the simulation of the transport of pairs of electrons and neutrons. This toolkit is written in Mortran3. It was developed by A. James Cook and LJ Shustek at the Stanford Linear Accelerator Center (SLAC).
- **FLUKA:** (*FLUktuierende KAskade*), it is an integrated code for simulating the transport and interaction of particles and nuclei. It is used in the field of elementary particle physics, radiation protection, cosmic ray physics, dosimetry and medical physics. It is developed in FORTRAN language and is available as an object library, pre-compiled for some computing platforms. The software is distributed and maintained by INFN and CERN that they own the copyright.
- **MCNP:** (*Monte Carlo N-Particle Transport Code*), it is a package for the simulation of nuclear processes, such as fission. It is developed by the Los Alamos National Laboratory and is distributed in the United States by the Radiation Safety Information Computational Center and in the international level by the Nuclear Energy Agency. The areas of application include radiation protection, dosimetry, medical physics, projects fusion reactors, etc.

Another simulation software based on the Monte Carlo method, the most used in the field of scientific research, is Geant. Of this software will be discussed in more detail below.

3.4 Development of the Geant project

Geant is a Monte Carlo code open source, therefore, available free, created in 1974. It simulates the passage of elementary particles through matter. It was initially created to experiments at high energies, and today it is applied in other fields, for example in the medical, biological, spatial and radiation protection.

The first version of Geant is a basic system that allows the transport only of a small number of particles through the detectors characterized by a simple design.

Over the years there have been several updates to the software getting so very different and mutually incompatible versions.

At the end of 1994 was born Geant4, a project proposed by the *Detector Research and Development Committee (DRDC) at CERN*. This version is completely new compared to previous because the base language programming is C ++, instead of Fortran, and is used the *object-oriented* technology.

The first prototype dates from the end of 1995 and the first alpha version in the spring of 1997. The software was developed and maintained by a collaboration between different experimental groups³ and subsequently revised and corrected by the *DRDC project RD44* (Giani, 1995) during the tests of alpha and beta versions.

The Geant4 code and documentation are available, with the *Geant4 Software License*, on the website <http://geant4.web.cern.ch/geant4/support/download.shtml>. The latest version of the software, currently only available in beta format is Geant4 10.1, released June 27, 2014.

3.5 Object-Oriented Programming

Geant4 is based on the Object Oriented Programming (OOP) in C++, a technique suitable for the development of a software subject to constant changes and updates. The object-oriented programming is a paradigm of the programming that brings together in small areas of the code (classes) the declarations of the data structures and procedures that operate on them. Geant4 is a versatile and powerful toolkit to simulate the particles passage through matter. It includes a large variety of functionality for each type of particles in the energy range from few eV to several TeV. The main Geant4 components are: the kernel, the description of setup experimental and physics processes.

The basic concepts of object oriented programming are:

- **object;**
- **class;**
- **message;**
- **encapsulation;**

³SLAC, CERN, CEA, KEK, INFN, University of Manchester STFC, etc.

- **inheritance**;
- **polymorphism**.

With **object** in the context of programming shall mean in a more general way a region of allocated memory.

An object is defined by:

- variables and / or constants that define the characteristics or properties (attributes), resulting in one of the possible conditions of existence (state);
- actions that can be done and / or suffer (methods).

Each object is independent of the others, because it has its own variables that are not shared with the outside. This allows you to not alter the properties if you work on other parts of the code. However, this does not prevent an object to communicate with others.

A **class** is an abstract structure in which they are contained similar objects, including attributes and methods. Each object represents, therefore, an instance of a class.

The **messages** allows objects to communicate with each other by making available the results obtained after the execution of a task encoded in a method.

The **encapsulation** is the property for which the data that define the internal state of an object are accessible only to methods of the same object, unless they have not been made.

The mechanism, which allows a derived class (subclass or child class) to maintain the methods and attributes of the classes from which it is derived, is called **inheritance**. By modifying a feature in class mothers, the change will be inherited by all child classes.

The **polymorphism** is the ability to originate behaviors and different results using the same methods with different objects.

3.6 General structure of the software Geant4

Geant4 provides a wide range of useful functions for the simulation of the interaction of radiation with matter:

- allows you to define the geometry of the system, the materials, the primary beam and the physical processes;
- allows tracking the motion of the particles in the material even in the presence of electromagnetic fields;
- allows to obtain the response of the sensitive components of a detector;
- allows the graphical display of the experimental setup and of the particle trajectories.

The general structure of a complete code provides:

- A directory 'include', which contains the header files. In this directory are defined objects with their attributes and methods, and classes of belonging;
- A directory 'src', containing the source files. In this directory are implemented the attributes and methods of the objects defined in the include directory.

An application in Geant4 is based on the derivation and implementation of concrete classes from abstract classes provided by the kernel of the toolkit, eight user classes.

These classes are of two types:

- Three mandatory user classes;
- Five optional user classes.

The three mandatory user classes, which allow you to user to define the elements required for the development of application, are:

- **G4VUserDetectorConstruction**, to define the geometry and properties (i.e. materials) of the elements present in the simulation, the volumes of sensitive detectors and view attributes;
- **G4VUserPhysicsList**, to define the particles involved in the simulation, the physical processes and parameters of cut-off⁴ associated.
- **G4VUserPrimaryGeneratorAction**, to define the properties of the primary beam (i.e. energy, the direction of the moment, vertex, geometry of the beam source, etc.).

The first two are of the user initialization classes, used in the initialization phase of application, the other is a user action class, used during the run.

For these three user classes, Geant4 does not provide a default behavior, in fact the user has the possibility to define in accordance with its needs concrete classes.

The optional user classes allow the user to modify the default behavior of Geant4, are all user action classes, and are derived from the following abstract classes:

- **G4UserRunAction**, allows you to set actions to be performed at the beginning and end of each run;
- **G4UserEventAction**, allows you to implement the actions to be performed at the beginning and end of each event;
- **G4UserStackingAction**, allows you to manage access to the stack, which contains the information of every track;

⁴The cut-off is a threshold value, defined for the particles involved in the simulation, typically represented by a distance (or range), converted into energy. Represents the threshold below which no secondary particles are generated. Must be set in the initialization phase within the method SetCuts () of the class G4VUserPhysicsList (Geant4, 2013).

- **G4UserTrackingAction**, allows you to set actions to be performed during the creation of each track;
- **G4UserSteppingAction**, allows you to manage and customize the actions to be carried out before and after each step.

The three mandatory user classes and the optional user classes used must be recorded to provide the information necessary to configure the run to class *G4RunManager*. It is defined class manager, because responsible for checking the flow of the simulation through the management of events within each run. It is also responsible for initializing the parameters of the simulation. The main is the file where the class is instantiated *G4RunManager*.

3.7 The main Geant4 components

The software Geant4 uses a system of categories. They are the set of classes that working on this aspect of the simulation and are connected to each other if they perform similar functions. This modular architecture and hierarchical (figure 23) is highly flexible, as it allows each user to achieve the desired configuration using only the components it needs, provided by the software. For these characteristics Geant4 is considered a general-purpose toolkit.

The main categories are:

- Kernel;
- Geometry;
- Materials;
- Particles;
- Processes;
- Run;
- Event;
- Tracking;
- Hits;
- Visualization;
- User interfaces;

Kernel

The kernel is the core of Geant4, it is possible to distinguish some basic concepts for the simulation.

Geometry

The geometry is defined by a number of volumes. The larger volume is called the *World Volume* and it must contain all other volumes that define the system to be simulated. Each volume is created describing the shape and physical features. To describe the form of a volume using the concept of *solid*. A solid is a geometric object that has a specific shape and size. In order to describe all the properties of a volume using the *logic volume* that includes the geometric properties and the material that constitutes the volume. The location of the volume is defined by the *physical volume*.

Materials

In Geant4 the materials are defined by elements and isotopes using three important classes:

- *G4Element* that describes the properties of atoms: the atomic number, the number of nucleons, the atomic mass etc.
- *G4Material* that describes the macroscopic properties of matter: density, state of aggregation, temperature, pressure etc.
- *G4Isotope* that defines the different isotopes in the atomic number and the mass of one mole.

All of these classes provide a table for each material used sections of shock and energy for many particles.

Particles

Geant4 provides the definition of ordinary particles such as electrons, protons, photons, etc. using the three main classes:

- *G4ParticleDefinition*: this class allows us to characterize the particles for the name, mass, charge, spin, and other features. These features, with the exception of the average life and the boards of decay, can not be changed.
- *G4Particle*: the class allows you to define other particles, and each of it has its own class that defines the properties.

- *G4ParticleTable*: this class is the “dictionary” of particles currently known and allows you to get all of the most important properties of the same.

The classes that represent the different particles are statistical objects and define a single particle object.

The following is the classification of particles in Geant4:

- Stable particles such as electrons, protons, neutrons and gamma;
- Average long-lived particles ($> 10^{14}$ s) such as muons and charged pions;
- Particles with the short average life;
- Optical photons: Cerenkov and scintillation light;
- Geantino and Geantino charged particles that are not real and no interaction, designed by the developers of Geant4 to test the system.

Processes

The *Processes* Category manages all physical processes, which describe the interaction of particles with matter, by the base class *G4VProcess*. From *G4VProcess* can be instantiated subclasses, each corresponding to a single physical process as *G4PhotoElectricEffect*, *G4ComptonScattering*, etc., which must be attached to the particles in question by invoking methods of the class *G4ProcessManager*.

Run

In Geant4 a Run is the largest unit of simulation. It is a collection of events with the detector under the same condition, in fact, inside it can not be changed the geometry definitions nor the set of physical processes implemented.

Event

An event is the set of primary particles. These, when starting a simulation are placed in a stack. The class that represents an event is *G4event* that contains the methods to obtain the information, for example, the characteristics of the particles generated, the identification number of the event processed etc.

Tracking Step

The Tracking manages the evolution of the state of the tracks determined by physical interactions. A Step is the interval defined by two spatial points and is represents by the class G4Step. Associated with the concept of steps there are several information accessible from the methods of G4Step as the length, energy lost during step etc.

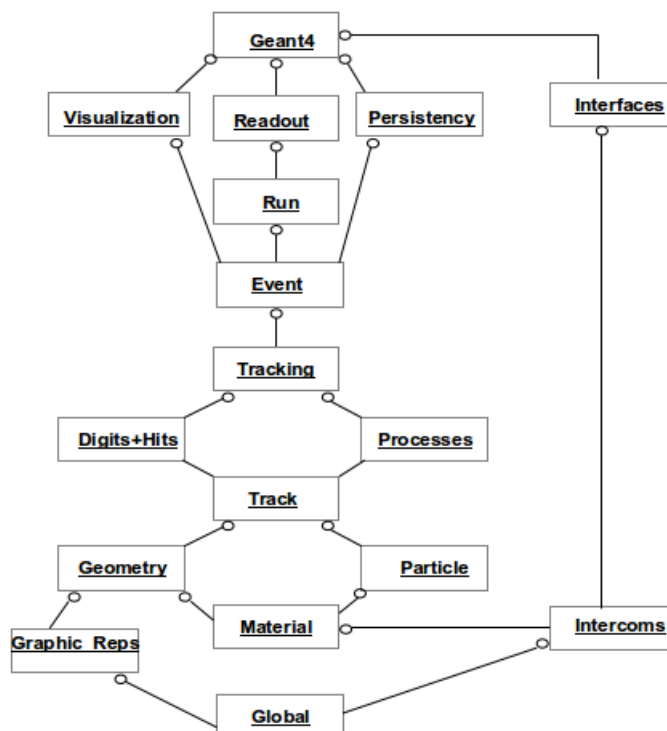


Figure 23: Diagram of the categories of Geant4. The circle in conjunction lines represents a relationship, the category adjacent to the circle using the joint category.

Hits

A Hit is a snapshot of the interaction of a track or collection of interactions in sensitive regions of the detector. The object Sensitive Detector creates the hits using the informations accessible by other classes, for example at the level of step or event.

Visualization

In Geant4, you can view all the experimental setup, the geometry of the system, the traces of the

primary particles and secondary and any hit that take place within of the target and of the detector. The toolkit is compatible with drivers of different graphics systems, such as OPENGL, OPAC and DAWN that allow you to monitor the implementation of the geometry with the use a user interface.

User interface

- Geant4 allows you to run an application mode “hard coded” that is through the direct use of Geant4 classes, defining the steps to run the simulation directly in the *C++* code, or in “batch mode” reading commands from the appropriate file, called “macro file”. However, to avoid an excessive amount of lines of code and make the interactive application, the intercoms category provides the abstract class *G4UISession* that allows the user to interact with the application through the use of controls already implemented in the toolkit. The latter are divided into directories based on the capabilities assigned to them, shall be made available to the user from the group interfaces, through textual and graphical interfaces.

Some of the directories of commands provided by the toolkit are:

- **/run/**: contains commands related to the run as "initialize" to initialize the kernel of Geant4, "BeamOn," for the starts of run defining the number of events, "verbose", to indicate the information to be displayed;
- **/tracking/**: contains commands related to the trajectory of the particle and the step. For example, the command "abort" and "resume" allow, respectively, to stop and restart the current process *G4Track* and "verbose" means the level of information on particle tracks that the user want to display;
- **/particle/**: contains commands related to the particles of the primary beam incident. "Select" allows you to select a particle, "list", printing the list of particles available in Geant, "find", is a type of particle among those available, etc .;
- **/vis/**: contains the commands of the graphic display. You can define the graphics system (ie OPENGL), the size of the graphics window, zoom, view angle, colors, etc .;
- **/gun/**: contains commands to define the incident beam, ie the type of particle, the direction of the moment, the vertex, the kinetic energy, etc. The command "list" prints the list of available particles, "number" defines the number of particles (default is 1) to be generated in any event, etc .;
- **/gps/**: contains commands for the control of extended sources. In addition to the features already described for / gun / you can, for example, by the type command to define the type of source (ie, point, plane, surface, volume), "shape" to determine the shape of the source (ie

circular, square, spherical , cylindrical, etc.), "center" to define the center of the coordinates (X, Y, Z) of the source, the default (0, 0, 0), etc.

Geant4, also, given its flexibility, allows the user to define their commands, not implemented by default, through the class '*Messenger*'.

4 SPACE ENVIRONMENT INFORMATION SYSTEM SPENVIS

SPENVIS is an interactive tool it was carried out by European Space Agency (ESA) and provides information on the space environment. SPENVIS consists of an integrated set of models that facilitate its use in the space environment. Project concept is the core of SPENVIS. A project is a set of input and output obtained from a series of related runs. A project is a subdirectory on the hard disk of the system hardware on which it is running Spenvis. In the subdirectory, all input and output files generated by the system are stored. For this reason and because each users has a permanent personal account, there is no need enter the parameters for input again on each study. All operations such as creating, modifying or deleting are performed directly on the project page that you can reach through the link. The initial menu which appears access within the program is shown in figure 24.

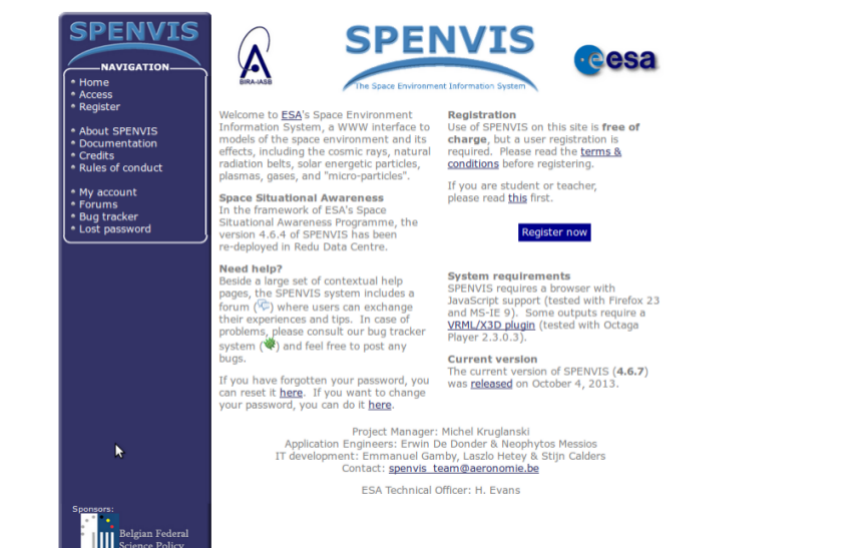


Figure 24: Graphical Interface of the SPENVIS access.

4.1 Generator of orbits

The models implemented in SPENVIS require as input a complete set of points that uniquely identify the trajectory of the spacecraft. In SPENVIS, there are two different ways to assign these conditions:

- Generator of orbits
- Generator of the coordinate grid

Each trajectory or coordinate grid that has been generated, it can be used by different models. The first point defines the orbit of the satellite in approximated trajectories using the method of numerical integration, "Runge-Kutta". This can be used for low-altitude orbits and orbits with high

eccentricity. The generator of the coordinate grid produces a series of geographic positions (grid) used as input.

1. A single geographic point: the profile can be generated in terms of the input parameters of the model;
2. A profile altitude-latitude-longitude or time (universal or local) with the other coordinates fixed;
3. A map of the world for a specific altitude with a time (universal or local) considered fixed.

The result of the coordinate grid is a file containing a table that describes the satellite's orbit.

4.2 Radiation Sources

Characterized a particular mission profile, it is necessary to evaluate the environment, with particular attention to the radiative, determining the influence of the particles at various energy levels.

The radiation sources can be divided into:

- Radiation in Van-Allen belts;
- Radiation generated by solar flux;

For the simulation, the software SPENVIS gives the possibility to choose among three different models to represent the flow of protons and electrons, which take account of the dynamics present in the Van-Allen belts. The models considered are "*AP-8*" for protons and "*AE-8*" for the electrons, which are available in two profiles: solar maximum and solar minimum. These models were formulated by NASA and are based on long-term measurements of particle fluxes. Data were collected by revelations made by satellites in the 60s. These models must be continuously updated. They contain static or quasi-static averages of satellite measurements, failing to simulate the temporal evolution of the radiation belts. In addition to the Van-Allen belts should be taken into account in the modeling also the flow of particles from the sun. In this case it is not sufficient to consider the flow "constant" because it depends on the cycle of solar activity, for this reason it is difficult to estimate the intensity and duration. The models used for these studies are:

- King
- JPL
- ESP

King model takes into account the flows that arrive on the ship during long periods of time. This model is built on data obtained during the years of the solar cycle, between 1966 and 1972. This solar cycle is taken into account because unlike previous has a greater frequency and intensity. In the database of the model of King, there are two classes of events: of major importance and ordinary. According to these data to update the model using statistical approaches: by defining the probability P as the

probability of having the fluence f of protons with energy E during a mission of duration t . The model of King, however, turned out to be questionable, for this reason was formulated an alternative model "JPL model" using a set of data which, in the first version (JPL85) included observations between 1956 and 1963 (during the solar cycle 19). The main innovation of the new model was the show that you could take into consideration only one part of the solar cycle that is just the part where the activity is more significant (duration 7 years). The JPL model therefore considers only the flow of protons from the sun during the seven years, excluding those of quiet. A newer version of the model is the JPL91 that bases its observations between 1963 and 1988 The data set contains JPL91 continuous recordings of the average daily flow greater than a predetermined limit value. The King and JPL models are useful for determining events for the long term, but have limitations:

- The energy level of the protons is confined to a range of values;
- Neither of the two models include high-quality data on three separate cycles: in fact, each cycle can be very different from the previous or next.

4.3 Radiation Protection

The effects of the radiation field has on the satellite does not depend only on the flow of protons and electrons along the orbit, but also on the type of shielding present on the spacecraft. Also in this case the features of the models can be schematized.

The models for evaluating the danger of ionization of the material are the SHIELDOSE and the SHIELDOSE2.

The first is a computer code capable of calculating the radiation dose absorbed as a function of the depth of the material chosen, established the flow of protons and electrons in orbit. The code processes the effects of using data as the thickness of the material and energy flow. The incident radiation is considered to be uniform on the surface. The SHIELDOSE calculated for an arbitrary flux of protons and electrons can be evaluated as to the structure in different ways:

- The structure is considered as a semi-infinite plane with the radiation, represented by a parallel beam, which intersects this (a);
- The structure is considered as a finite plane with the radiation, represented by a parallel beam, which intersects this (b);
- The structure is considered as a solid sphere with flux coming from all directions (c).

4.4 Multi-layer protective: MULASSIS

MULASSIS is a Geant4-based tool that provides a general one-dimensional space radiation analysis for a multi-layered, shield. MULASSIS is a complex tool, so please consult the help page before using it. The current version of MULASSIS is v1.23. If you want to use the previous v1.19 interface click [here](#).

Status	Settings	Remarks
defined	Source particle macro	mono-energetic, proton, GPS macro file
defined	Geometry	Planar slab, 1 layer
defined	Analysis parameters	Total ionizing dose
Advanced settings		
defined	Material definition	3 material defined
defined	Cuts-in-range	No cuts-in-range

Create macro

Tool developed by

Figure 25: Interfaces Spenvis for Mulassis.

The MULASSIS is a module of Geant4 for the study and simulation of the effects of radiation in space environment on the shielding. All aspects of the simulation are included in the Geant4 toolkit and allow management:

- Geometry of the system;
- Materials of interest;
- Particles;
- Generation of events;
- Tracking the particle in matter;
- Responses of sensitive components;
- Saving events;
- Displaying events and particle trajectories.

The interface takes as input the definition of the geometry of the target, providing the possibility to choose between a flat plate and a sphere, specifying in both cases the number of layers that compose. For each thickness, the user can choose the type of material (as connected to the NIST) and the required thickness. However, if the material is not in the list, the software allows you to "create"

specifying the name, chemical formula and density. Defined material input in assigning the incident particles, the energy spectrum and the angular distribution. To assign the spectrum you can proceed in different ways:

- In the mono-energetic distribution must be assigned in input only two values: the energy expressed in MeV (default value is $100 MeV$) and intensity expressed in $cm^{-2}s^{-1}$ (default value is $1 cm^{-2}s^{-1}$).
- In the “linear” distribution expressed by the relation:

$$\frac{dF}{dE} = AE + B$$

where you must specify the gradient A, the intercept B ($cm^{-2}MeV^{-2}s^{-1}$), the minimum and maximum energy in MeV to determine the range.

- In the “power law” distribution expressed by the relation:

$$\frac{dF}{dE} = AE^\alpha$$

where you must specify the A ($cm^{-2}MeV^{-2}s^{-1}$), the constant α , the minimum and maximum energy.

- In the “exponential” distribution expressed by the relation:

$$\frac{dF}{dE} = Ae^{-E/E_0}$$

where you must specify the A ($cm^{-2}MeV^{-2}s^{-1}$), the minimum and maximum energy E_0 .

- Finally, the distribution defined by the user is necessary enter the data of energy and flow. You should also assign the type of interpolation among linear, exponential, power-law and spline.

The physical models can be implemented in SPENVIS and are reported in Table 6.

Particles	Energy Range	Physical models
Proton	< 10 GeV	Standard EM or Low-Energy EM - G4Binary
Proton	> 10 GeV	Above + G4QGSM
Ion	< 10 GeV/n	Standard EM or Low-Energy EM - G4BinaryforLightIons
Neutron	thermal -20 MeV	G4Neutron_hp or G4Binary
Neutron	> 20 MeV	G4Binary + G4QGSM
Electron/Gamma	< 1 keV	Low-Energy EM
Electron/Gamma	> 1 keV	Standard EM or Low-Energy EM
Others		G4LEHEP

Table 6: Physical models implemented in SPENVIS for each particles.

The last step is "the analysis of the parameters" in particular you can choose between four different types:

- Fluence analysis;
- Non-ionizing dose;
- Energy deposition and total ionizing dose;
- Pulse-height spectrum analysis.

Fluence analysis This analysis allows the user to control the spectra fluence of particles at the boundaries among the different layers. The units of fluence used in the MULASSIS output may be selected as *particles/cm² – bin* or *particles/m² – bin* according to the selection box: *cm²* or *m²*. The type of fluence measurement can be selected as *omni* or *planar*:

- The omnidirectional fluence includes a modification to the weight of the boundary-crossing particle according to the $\cos\alpha$, where α is angle of incidence, and is applicable to determination of dose using stopping powers and NIEL coefficients.
- Planar fluence is based purely on the number of boundary crossing events and is applicable to count rates in planar detectors, for example.

Non ionizing dose (NID) The non ionizing dose can be calculated in units of:

- rad;
- MeV/g;
- Gray.

It is the users responsibility to select the appropriate set of coefficients for the material and layer under investigation.

Energy deposition/total ionizing dose (TID) Energy deposition can be calculated for each of the layers in units of :

- eV and multiple;
- Gray;
- rad.

Pulse-height spectrum analysis The energy depositions from each incident particle and its secondaries can be logged as a function of layer to determine the pulse-height spectra of energy deposition events.

Results The output files produced by MULASSIS reported in Table:

File Name	Description
spenvis_mlr.txt	Report file
spenvis_mlp.txt	Log File
spenvis_mlo.txt	Outputs for the selected analysis type
spenvis_mul.wrl	VRML representation of the geometry
spenvis_mul.eps	Cross section view of the geometry

Table 7: Output files generated by MULASSIS.

To generate plots, select the plot type(s), options and graphics format, and click the "plot" button. The current page will be updated with the newly generated plot files.

4.5 Analysis of microdosimetry: GEMAT

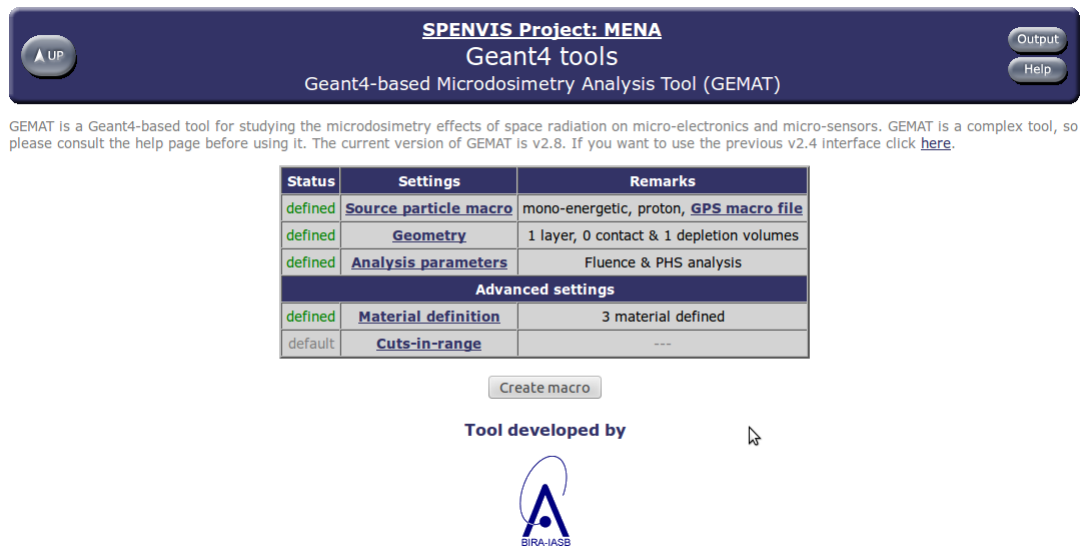


Figure 26: Interfaces Spenvis for Gemat.

Gemat content in Geant4 is a tool for the study of the effects of space radiation. In Gemat is necessary to define the geometry. The simulation geometry is constructed in terms of layers, contact volumes (CV) and volume depletion (DV). By default the geometry is loaded placing 6 layers including 2 CV and 4 DV. For each layer of material is possible to define a different type of material and represent with different colors. The preassigned materials are aluminum, silicon, vacuum and air, but you can define

other materials entering the chemical formula. For volumes, we must also determine the shapes of contact volumes and emptying, which can be represented by cylindrical, cubic L or U shape. Defined geometry, the user can select the type of the incident particle, the energy and angular distribution. It can also be specified in the expected number of particles to simulate correctly with the Monte-Carlo method. Similarly to MULASSIS there are four different types of analysis:

- Fluence analysis;
- Energy deposition pulse height spectrum;
- Path length distribution;
- Coincidence rates among volume.

Fluence analysis The analysis fluence allows the user to measure the number of particles that enter each depletion volume and record the spectrum of an energy. The user can specify the particle type to be included in the fluence analysis: protons, neutrons, electrons, gamma rays and charged pions.

Energy deposition pulse height spectrum At the end of the execution, the pulse height spectrum of energy deposition in each depletion volume is obtained.

Path length distribution Regardless of the energy, the path length is calculated in μm .

Coincidence event rates The trigger energy threshold of each depletion volume can be set by the user. This type of analysis is only performed when more than one depletion volume were defined.

Results For the output GEMAT produces the files, as reported in Table 8 .

File name	Description
spenvis_ger.txt	Report file
spenvis_gep.txt	Log file
spenvis_geo.txt	Outputs for the various analysis type
spenvis_gem.wrl	VRML representation of the geometry

Table 8: Output files generated by GEMAT.

To generate plots, select the plot type(s), options and graphics format, and click “plot” the button.

The current page will be updated with the newly generated plot files.

4.6 Sector Shielding Analysis Tool (SSAT)

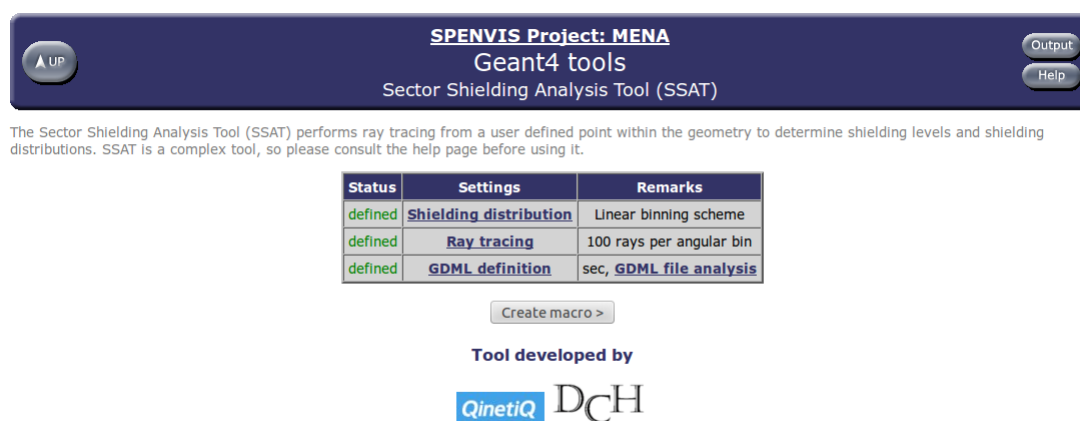


Figure 27: Interfaces Spenvis for SSAT.

The Sector Shielding Analysis Tool (SSAT) performs a ray tracing inside the geometry to determine the levels of shielding. SSAT can accept an external geometry defined in the Geometry Definition Markup Language (GDML), format library of objects C++ that can read an XML file.

This interface allows you to enter information about the shielding in three ways:

- the first step is a set of default bins, corresponding to the SHIELDDOSE bins;
- the second step is a set of bins spaced equidistantly, with this option, the minimum and maximum thicknesses and the number of bins have to be specified;
- the third step is arbitrary, defined by a series of bin-edges provided by the user; the minimum and maximum thicknesses have to be specified.

The shielding units have to be specified, with the latter two options.

The location of the source is specified considering Cartesian coordinates. In case you are using a file GDML in which the geometry is described, can also be defined the source and the detector location. Instead, in SSAT using polar coordinates to specify the position and orientation of the shieldings.

In addition SSAT allows you to check the definition of the geometry. The output is written to the log file. SSAT produces a VRML representation of the geometry input GDML. The user has the

possibility to include the display of the traces. This option is available only if selected viewing more calculation.

When all inputs are defined is generated a macro.

Results As a result, SSAT generates the files listed in table 9:

File name	Description
<i>spenvis_ssp.txt</i>	Log file
<i>spenvis_ssa.gdml</i>	GDML description of the geometry
<i>spenvis_sso.txt</i>	2-D and 1-D shielding distributions
<i>spenvis_ssa.wrl</i>	VRML representation of the GDML geometry

Table 9: Output files generated by SSAT.

4.7 Geant Radiation analysis space (GRAS)

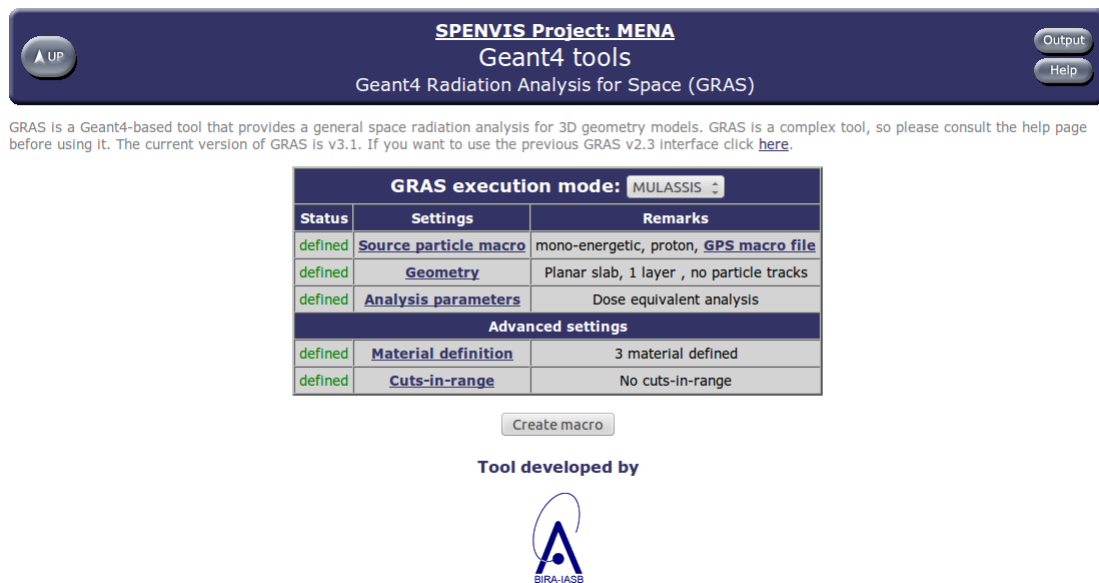


Figure 28: Interfaces Spenvis for GRAS.

GRAS is a tool that provides a general analysis of the space radiation for 3D geometries. It is based on the use of Geant4. In particular GRAS allows the definition of a more complex geometry using multiple volumes and the source of the incident particle. By using the Geant4 toolkit, GRAS simulates the transport of radiation through the geometry and electromagnetic and nuclear interactions. Because

the model is based on Monte Carlo simulation, the execution time can be very long. The execution is limited to ten minutes of CPU time on the simulation server. If the simulation exceeds the time available, it will be terminated and the user can view intermediate results.

Furthermore GRAS can be implemented in two ways:

- GDML;
- Mulassis;

The interface GRAS allows a user to specify the incident particle, the energy spectrum and angular distribution. The source of particles can be of different type:

- Point;
- Disk;
- Sphere.

The default geometry source is a point source located inside the volume “world volume” at $x = 0, y = 0, z = 100 [mm]$ pointing at the centre of “world volume”.

The analysis that can be performed with concerns GRAS:

1. Fluence;
2. Non-ionizing energy loss (NIEL);
3. Energy deposition and total ionizing dose (TID);
4. Dose equivalent;
5. Equivalent dose analysis.

The user can select only one analysis type at a time.

Fluence The parameters in the fluence analysis allows the user to control the spectral fluence of particles at the boundaries among the different volumes.

The results are recorded as:

- Total (cumulative) fluence at the selected boundaries.
- Individual energy spectra for the particle types requested by the user.

Non-ionizing energy loss (NIEL) The NIEL can be calculated in this units:

- 95 MeV mb ;
- $\text{MeV cm}^2/\text{g}$;
- $\text{MeV cm}^2/\text{mg}$;
- $\text{keV cm}^2/\text{g}$;
- 10 MeV p .

It is the users responsibility to select the appropriate set of coefficients for the material and volume under investigation.

Energy deposition and total ionizing dose (TID) The total energy deposition can be calculated for each of the selected volumes in units of:

- rad ;
- MeV ;
- Gray .

Furthermore, the TID analysis also calculates the energy deposited at each event in order to allow the user to get the event pulse height spectrum (PHS).

Dose equivalent This analysis allows to obtain the total equivalent dose in a selected volume. It is available in:

- rad ;
- MeV ;
- Gray .

For the calculation of this quantity, the software takes into account the Relative Biological Effectiveness (RBE) of radiation as a function of particle type and energy using the Quality Factor (QF) [ICRP 60, 1990].

Equivalent dose analysis For the calculation of this quantity, the radiation weighting factor, ω_R , is used and the user can choose among the values adopted in ICRP 60 [ICRP 60, 1990] or the updated factors given in ICRP 92 [ICRP 92, 2003].

Results The output files produced by GRAS reported in Table 10:

File name	Description
spenvis_gras.g4log	Log File
spenvis_gras.g4mac	Macro File
spenvis_gras.csv	Outputs for the selected analysis type
spenvis_gras_aida.root	Output root file for the selected analysis type
spenvis_gras.wrl	VRML representation of the geometry
spenvis_gras.eps	Cross section view of the geometry
spenvis_gras_aida.ps	Output preview of GRAS results (PS)

Table 10: Output files generated by GRAS.

5 Geant4 Results

Application Development STP and Dose For the development of the applications have been implemented six of the eight user classes provided by the kernel of the toolkit Geant4. In addition to the three mandatory user classes, the optional user classes have been instantiated, from abstract classes G4UserRunAction, G4UserEventAction G4UserSteppingAction and, respectively, the concrete classes RunAction, EventAction and SteppingAction. Because the topic of interest, in both applications, is the study of interaction matter - proton beam of energy of order of GeV, the physical processes involved are the same. Therefore, the mandatory user classes, G4UserPhysicsList, has been so derived a only time in the concrete class, ordinary, *PhysicsList*.

5.1 PhysicsList

Physical processes can be divided into three basic classes:

- processes 'at rest', in which the particles involved do not vary their position spatial, as in the case of the decay;
- processes 'continuous', in which the interactions are distributed in space and time, as in the case of the loss of energy for excitation and ionization;
- processes 'discrete', in which the interactions retain their character, point by point, in space and in time, as in the case of photoelectric and Compton effect.

In Geant4, every process of interaction is described by most models, each valid for a specific energy range from a few eV up to TeV, and is characterized by its own cross section σ . This depends on the energy of the incident particle and the characteristics of the medium and is obtained by means of theoretical models or based on experimental data libraries implemented in the toolkit. All physical processes, in Geant, involve two distinct phases:

- the calculation and the use of the total cross section;
- the generation of the final state.

and physical nature are divided into two broad categories:

- electromagnetic interactions;
- hadronic interactions.

Below, are given for each category, the processes implemented in proposed applications, STP and dose, with the names of their respective classes.

5.1.1 Electromagnetic Interactions

Photons

- Photoelectric Effect - *G4PhotoElectricEffect*;
- Compton Effect - *G4ComptonScattering*;
- Conversion range or production couples - *G4GammaConversion*;
- Elastic Scattering (or Rayleigh) - *G4RayleighScattering*.

Electrons and Positrons

- Bremsstrahlung emissions - *G4eBremsstrahlung*;
- Ionization and production of δ -rays- *G4eIonisation*;
- Multiple scattering - *G4eMultipleScattering*;
- Annihilation of positrons - *G4eplusAnnihilation*.

Hadrons and Ions ($Z \geq 2$)

- Multiple scattering - *G4hMultipleScattering*;
- Ionization and production of δ -rays, valid for hadrons - *G4hIonisation*;
- Ionization and production of δ -rays, valid for ions - *G4ionIonisation*.

5.1.2 Hadronic Interactions

Protons

- Elastic scattering of protons and nuclei target - *G4HadronElasticProcess*;
- Inelastic scattering of protons and nuclei target - *G4ProtonInelasticProcess*.

Neutrons

- Elastic scattering of neutrons and target nuclei - *G4HadronElasticProcess*;
- Inelastic scattering of neutrons and target nuclei - *G4NeutronInelasticProcess*;
- Process of capture of neutrons by nuclei of the target - *G4HadronCaptureProcess*.

Deuteron and Triton

- Elastic scattering between isotopes of hydrogen H and target nuclei - *G4HadronElasticProcess*;
- Inelastic scattering between nuclei Tritium H_3 and target nuclei - *G4TritonInelasticProcess*;
- Inelastic scattering between nuclei of deuterium H_2 and target nuclei - *G4DeuteronInelasticProcess*.

Ions ($Z \geq 2$)

- Elastic scattering between ions and target nuclei - *G4HadronElasticProcess*;
- Inelastic scattering between ions and target nuclei - *G4HadronInelasticProcess*;
- Inelastic scattering of particles α and target nuclei - *G4AlphaInelasticProcess*.

Details of the energy range of validity and the models associated with each process are available in *Physics Reference Manual* to address: <http://geant4.web.cern.ch/geant4/UserDocumentation/UsersGuides/PhysicsRe>

5.1.3 Determination of the interaction point

The simulation of the transport of a particle is made, as already said, through a sequence of steps each of which is associated with a particular physical process. Note the total cross section of a given process $\sigma(Z, E)$ by atom, the free walk across or interaction length in a composed medium is:

$$\lambda(E) = \left(\sum_i [n_i \sigma(Z, E)] \right)^{-1} \quad (14)$$

where \sum_i is referred to all the elements that compose the medium and n_i represents the number of atoms per unit volume of i -th element.

$$n_i = \frac{N_a \rho \omega_i}{A_i} \quad (15)$$

where N_a is Avogadro's number;
 ρ is the density of the medium;
 ω_i is the mass fraction of the i -th element;
 A_i is the atomic mass of the i -th element;

$\sum_i [n_i \sigma(Z, E)]$ is the macroscopic cross section.

The values of the total cross sections for atom and mean free paths are tabulated by the software in the initialization phase. At each step, all physical processes implemented and applied to the particle concerned can help to determine the step length, to generate secondary and change the state of the track. The total number of mean free paths λ that the particle carries before arriving at the point of interaction is sampled at the beginning of step as:

$$n_\lambda = -\log(\eta) \quad (16)$$

where η is a random number uniformly distributed in the interval (0,1) . If you with n_r denotes a random variable is shown that applies the function of distribution:

$$P(n_r < n_\lambda) = 1 - e^{-n_\lambda} \quad (17)$$

Finally, the process is selected which is associated with the step length less:

$$s(x) = n_\lambda \cdot \lambda(x) \quad (18)$$

The description concerns the differential approach for the transport of the particles. In this approach, each process, both discrete and continuous, imposes a limit on the size of the step because of the dependence of σ from the energy of the particles. The step must be, therefore, small enough to consider constant cross sections. Very small step allow to have very accurate simulations at the expense of the time needed to computation, which increases with decreasing size of the step. Order to remedy this problem, Geant4 provides for each process one 'step limit' of which the most important are those due to the conditions of edge and the continuing loss of energy. In the passage of a particle from a volume to another the size of the step is limited by the boundary surface so that the points of start and end step are always contained in a single volume. Continued loss of energy imposes, however, that the size of one step are never stopping such that the range of a particle decreases more than 20% ($step_{max}/Range \sim 0.2$). This condition gives good results for kinetic energies $> 1MeV$, but at low energies implies a significant increase in computational time as the steps in size significantly reduced. The problem is solved with the introduction of a final range ρ_R , the value of remaining range of a particle from which the ratio $step_{max}/Range$ takes the value 1.

5.2 STP

The application STP (STopping Power) was developed with the only purpose to 'validate' the physical processes of the category of electromagnetic interactions. The validation process of physics, implemented in an application of Geant4, consists in test the correct operation of the code in relation to the physical processes that take place during the simulation. To do so, choices some significant values, comparing the data obtained with those available in the literature. The validation is a prerequisite for use of any application. In this specific case, were compared to values of stopping power electronics with those provided by the NIST database PSTAR.

5.2.1 Experimental Setup

The geometry simulated in the application **STP** is constituted by a point source of protons with energies from 800MeV to 1.2GeV , placed at 30cm from the center of the target, in vacuum. The target is a slab of aluminum ($\rho = 2.7\text{g/cm}^3$) in the shape of a parallelepiped, of mass thickness 20g/cm^2 in the direction of incidence of the primary beam ($z = 7.4\text{cm}$) and with the dimensions of $30 \times 30\text{cm}^2$. The thickness of the target, typical of storm shelters, has been chosen in relation the range of the protons. To compare the values of electronics stopping power is necessary that the energy of the primary beam does not vary appreciably in through the target condition ensured by a small thickness (i.e. order of %) compared to the range. In the case presented here, in reference to the tables in the database PSTAR, the thickness of aluminum is 5% of projected-range⁵. Average value of the depth at which a charged particle penetrates in the course of slowing down to a stop. This quantity is measured along the initial direction of the incident particle of the protons, which varies from $\sim 300\text{g/cm}^2$ to $\sim 530\text{g/cm}^2$ in energy range $800\text{MeV} \div 1.2\text{GeV}$.

5.2.2 G4hIonisation

In Geant4, the processes that simulate the interaction of particles with matter calculate also the energy loss. In **STP** application, for the calculation of energy loss by ionization and excitation of the protons in aluminum is the class used *G4hIonisation*. This last, for the secondary products below a predetermined energy threshold T_{cut} , summarizes the energy loss as a continuous process, while above simulating the 'discrete' ionization, or the explicit production of secondary particles, the rays δ . For a charged particle of energy E , which interacts with a medium, atomic number Z , the differential cross section for the secondary emission of a particle that has kinetic energy T is:

$$\frac{d\sigma(Z, E, T)}{dT} \tag{19}$$

⁵ Average value of the depth at which a charged particle penetrates in the course of slowing down to a stop. This quantity is measured along the initial direction of the incident particle (<http://physics.nist.gov//PhysRefData/Star>).

The production of secondary, with kinetic energy $< T_{cut}$, called 'soft', is simulated as an energy loss due directly to the primary particle, through a continuous process of slowing down. This last is characterized by the average rate of loss of energy:

$$\frac{dE_{soft}(E, T_{cut})}{dx} = n_{at} \int_0^{T_{cut}} \frac{d\sigma(Z, E, T)}{dT} T dT \quad (20)$$

where n_{at} is the number of atoms per unit volume of the medium.

If several processes are responsible for the loss of energy for a given particle, the total of the continuous part is obtained from the sum:

$$\frac{dE_{soft}^{tot}(E, T_{cut})}{dx} = \sum_i \frac{dE_{soft,i}(E, T_{cut})}{dx} \quad (21)$$

The total cross section, by atom, the emission of a particle secondary of kinetic energy $T > T_{cut}$, however, is given by:

$$\sigma(Z, E, T_{cut}) = \int_{T_{cut}}^{T_{max}} \frac{d\sigma(Z, E, T)}{dT} dT \quad (22)$$

with T_{max} maximum energy transferable to a secondary particle, given by following relation:

$$T_{max} = \frac{2m_e c^2 (\gamma^2 - 1)}{1 + 2\gamma(m_e/M) + (m_e/M)^2} \quad (23)$$

where m_e is the mass of the electron and M is the mass of the incidence particle. The values of the continuous losses of energy dE_{soft}/dx and total cross section, relative to the different materials implemented, are calculated by Geant4 during the initialization phase and stored in appropriate tables, used during the next phase of the run.

5.2.3 Continuous energy loss

For the continuous process of energy loss the integration of 12 leads to the restricted formula of Bethe-Bloch (Yao et al., 2006), as it contains various corrective terms (Ahlen, 1980).

$$\frac{dE}{dx} = 2\pi r_e^2 m c^2 n_{el} \frac{z^2}{\beta^2} \left[\ln\left(\frac{2m c^2 \beta^2 \gamma^2 T_{up}}{I^2}\right) - \beta^2 \left(1 + \frac{T_{up}}{T_{max}}\right) - \delta - 2\frac{C_e}{Z} + F \right] \quad (24)$$

where:

r_e is the classical radius of electron $e^2/(4\pi\epsilon_0 mc^2)$;

mc^2 is the mass energy of electron;

n_{el} is the electron density in the material: $n_{el} = \sum_i Z_i n_{ati} = \sum_i Z_i \frac{N_a \omega_i \rho}{A_i}$;

I is the average energy of excitation in the material;

Z is the atomic number of the material;

z is the charge of hadron incident in the unit charge of electron;

γ is E/mc^2 ;

β^2 is $1-(1/\gamma^2)$;

T_{up} is $\min(T_{cut}, T_{max})$;

δ is the correction term for density effect;

C_e is the correction term due to shell;

F is the correction term of higher order.

The values of average energy of excitation I for all the elements are tabulated in agreement with those recommended by International Commission on Radiation Units & Measurements (ICRU) (Allisy et al., 1984). For low energy values of the particles ($T_{lim} \sim 2MeV$), the Bethe-Bloch formula is characterized by a less precision because of increase of the various corrective terms. For $T > 10MeV$ accuracy is guaranteed $\sim 2\%$, while for energies $T \sim 1keV$ is 20%. To remedy this problem, the values of stopping power, in the range of low energies, are obtained using parameter values tabulated in the report ICRU49 (Allisy et al., 1993) and the database of PSTAR - NIST (Geant4 Physics Reference Manual).

5.2.4 δ -rays

The differential cross section for the “discrete” production of the δ -rays implemented in the *G4hIonisation* class is (Yao et al. 2006):

$$\frac{d\sigma}{dT} = 2\pi r_e^2 mc^2 Z \frac{z_p^2}{\beta^2} \frac{1}{T^2} \left[1 - \beta^2 \frac{T}{T_{max}} + \frac{T^2}{2E^2} \right] \quad (25)$$

The total cross section for atom σ is obtained by integrating 17 from T_{cut} (default $\geq 1keV$) to T_{max} .

$$\sigma(Z, E, T_{cut}) = \frac{2\pi r_e^2 Z z_p^2}{\beta^2} mc^2 \left[\left(\frac{1}{T_{cut}} - \frac{1}{T_{max}} \right) - \frac{\beta^2}{T_{max}} \ln \frac{T_{max}}{T_{cut}} + \frac{T_{max} - T_{cut}}{2E^2} \right] \quad (26)$$

where the last term is only valid in the case of spin $\frac{1}{2}$ (Geant4 Physics Reference Manual).

5.2.5 STP Results

The validation of electromagnetic processes with software Geant4 was performed comparing the data obtained by the software in output with those provided by the NIST database PSTAR. It is presented below is a screenshot of the home screen of PSTAR (figure 29):

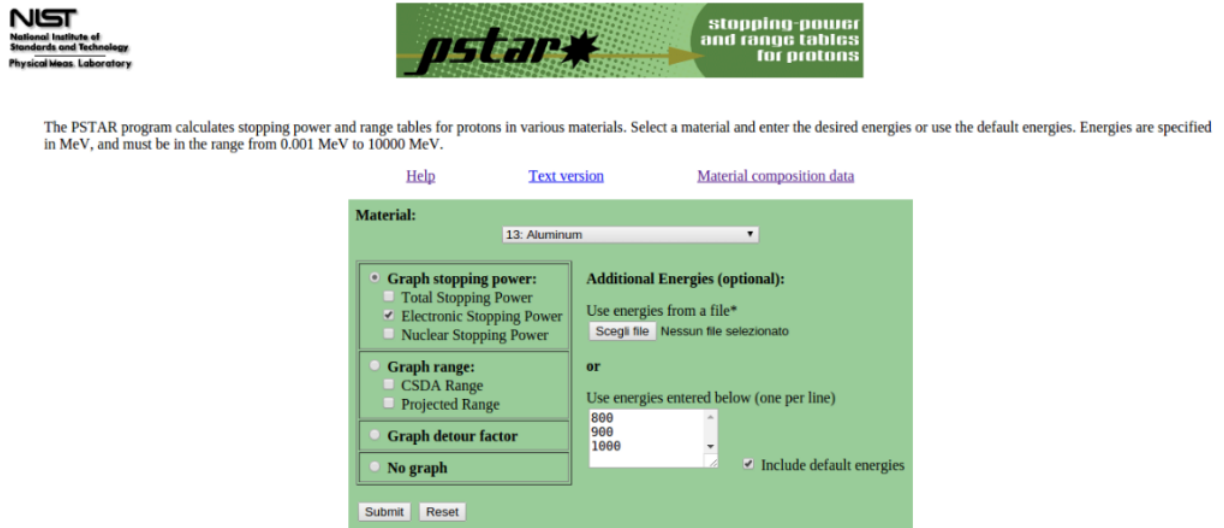


Figure 29: Screenshot of the initial screen of the database PSTAR -NIST.

and the calculated curve (figure 30) of the electronic stopping power, expressed in $MeV\ cm^2/g$, of protons in aluminum in the energy range $1\ keV \div 10\ GeV$:

PSTAR : Stopping Power and Range Tables for Protons

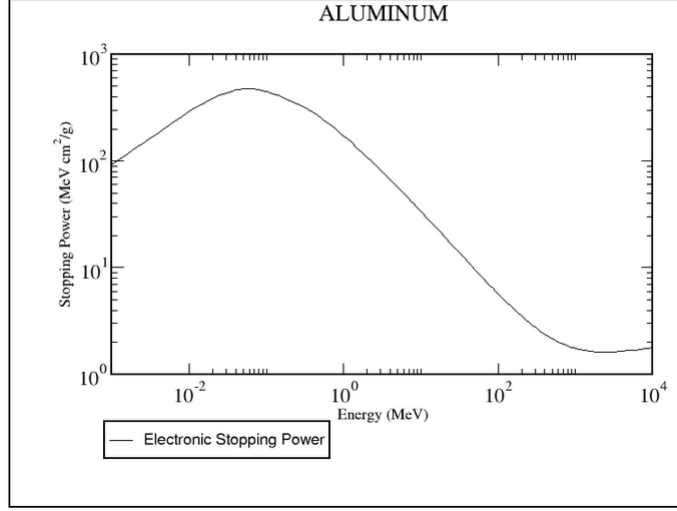


Figure 30: Electronic stopping power of protons in aluminum calculated from PSTAR.

In Table 11, for the same energy of the primary beam, there are respectively, the values of the electronic stopping power obtained using the STP application, with its uncertainty, and those calculated by PSTAR:

Energy (MeV)	PSTAR ($MeV\ cm^2/g$)	STP ($MeV\ cm^2/g$)	σ_x ($MeV\ cm^2/g$)
800	1.845	1.861	0.093
825	1.830	1.845	0.095
850	1.816	1.829	0.095
875	1.803	1.815	0.094
900	1.790	1.801	0.098
925	1.779	1.792	0.097
950	1.768	1.783	0.100
975	1.759	1.773	0.100
1000	1.749	1.760	0.101
1025	1.741	1.755	0.102
1050	1.733	1.744	0.100
1075	1.725	1.739	0.105
1100	1.718	1.729	0.104
1125	1.711	1.724	0.106
1150	1.705	1.725	0.106
1175	1.699	1.711	0.107
1200	1.693	1.704	0.110

Table 11: Comparison between electronic stopping power values obtained with the STP application and those calculated by PSTAR.

Each value of the stopping power of the application STP, varying the input energy of the primary beam, was obtained by averaging over a run of 500000 events, for better statistics. The output file, .out format was processed on an Excel worksheet, to obtain the values of average and standard deviation of the mean $\sigma_{\bar{x}}$. In figure 31 the trend of the stopping power of protons in aluminum, in the range $800 \div 1200 \text{ MeV}$, for the application STP and the database PSTAR is showed.

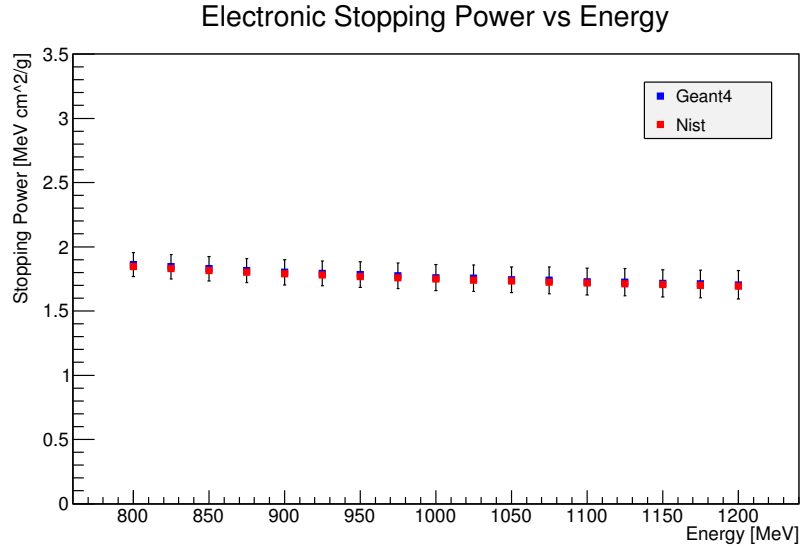


Figure 31: Comparison between experimental data NIST-PSTAR.

5.3 Dose

The application *Dose* has been developed to validate the physical processes belonging to the category of hadronic interactions and to evaluate the trends of the dose of a primary beam of protons by 1 GeV , before and after the target of various materials. The validation process was performed by comparing the values of simulated dose, obtained in output from *Dose* application, with those measured during the experiment conducted at the NASA Space Radiation Laboratory (NSRL), Brookhaven National Laboratory, USA (Mancusi et al., 2007).

5.3.1 Experimental Setup

The geometry simulated in the application *Dose* is constituted by circular source ($r = 10 \text{ cm}$) of protons with energies 980 MeV , placed at 30 cm from the center of the target, in air. The target is a slab of

aluminum ($\rho = 2.7g/cm^3$), Nomex ($\rho = 1.15g/cm^3$) or PMMA ($\rho = 1.19g/cm^3$) in the shape of a parallelepiped, of mass thickness $\sim 20g/cm^2$ in the direction of incidence of the primary beam ($z_{Al} = 7.9cm$; $z_{Nomex} = 17.4cm$ and $z_{PMMA} = 16.8cm$) and with the dimensions of $60 \times 60 \text{ cm}^2$. The value of the dose was obtained by simulating the presence of a equivalent tissue ionization chamber ($\rho = 1.13g/cm^3$), produced by the Far West Technology, Inc. IC-17 (<http://www.fwt.com/detector/ic17ds.htm>), suspended, using an aluminum support, with the center along the axis of the primary beam.

5.3.2 *G4ProtonInelasticProcess*

The transport of ions in matter has stimulated the interest for the simulation of inelastic hadronic interactions. An important input for the simulation of these processes is the determination by reaction total cross section σ_r defined as:

$$\sigma_r = \sigma_T - \sigma_{el} \quad (27)$$

where σ_T is the total cross section and σ_{el} is the elastic cross section for nucleus-nucleus reaction. In Geant4, σ_r implemented are the result of several studies, both theoretical and experimental, from which have developed more than one parameter empirical. The model, implemented in Geant4, for the study of inelastic scattering hadron-nucleus is based on a redesign of the code INUCL (Titarenko et al., 1999), which to generate the final state of the interaction simulates the model proposed by Bertini for the intra- nuclear cascade. To study the collisions, in this model are added to the excitons models⁶ (Griffin, 1966), the pre- equilibrium, the nuclear explosion, fission and evaporation. In the model of Bertini, which solves the average equation of Boltzmann transport, the nucleus-target is modeled as a set of concentric shells, for a maximum of six, as an approximation of the flux density distribution of the material to internal of the nucleus. The cascade begins when the incident particle hits a nucleon in the target nucleus and produces secondary particles. These secondary particles can interact in turn with other nuclei or be absorbed. The cascade ends when all the particles, with sufficient energy, escape from the nucleus. In dealing with the evolution of the cascade is applied relativistic kinematics. This model is in agreement with the experimental data for nuclear reactions that involve long-lived hadrons, such as protons, neutrons and pions, with energies between $100MeV$ and $10GeV$ (Geant4 Physics Reference Manual). The intranuclear cascade model, implemented in Geant4, can be schematized as follows (Heikkinen et al., 2003):

1. the space point where the incident particle enters the nucleus is selected uniformly over the projected area of the nucleus,
2. the region-depenent nucleon densities and total particle-particle cross sections are used to select a path length for the projectile,

⁶The excited states of nucleons are represented by the number of bound states particle - pit, called excitons.

3. the type of reaction and the four-momenta of the reaction products are determined, and
4. the exciton model is updated as the cascade proceeds,
5. If $E_{particle} > E_{cutoff} = 2MeV$ and the Pauli exclusion principle allows, step (2) is performed to transport the products.

At the end of the intra-nuclear cascade, the excitation energy of the residual nuclei produced is used as input for the models of de-excitation listed above. In the initialization phase is also fixed the nuclear radius of the nucleus - target, modeled as concentric spheres, for a maximum of three, means of parameter setting function of the mass number A. In particular, the reaction total cross section σ_r of protons on nuclei, tabulated in Geant4 libraries, is calculated by the empirical formula proposed by Letaw (Letaw, 1983), function of the incident energy of the projectile and the mass number A of the target. For the study of the cascade and of the reaction products, the cross sections nucleon-nucleon interactions of individual, supposed free, experimental data are obtained by assigning parameters to change of the energy (Barashenkov et al., 1974).

5.4 Dose Results - Al Target

The validation of hadron process with Geant4 was performed by comparing the values obtained in output from application dose, and those measured during the experiment carried out at the laboratories of NASA. As first step was performed an analysis of the secondary particles that are generated from interaction of a point source of protons of $1GeV$ into a target of aluminum of $\sim 20g/cm^2$, placed at $z = 30cm$ from the target, in air. In this phase has been set a run of 1000000 events. Below are graphs, obtained by processing the output of application Dose, with software ROOT.

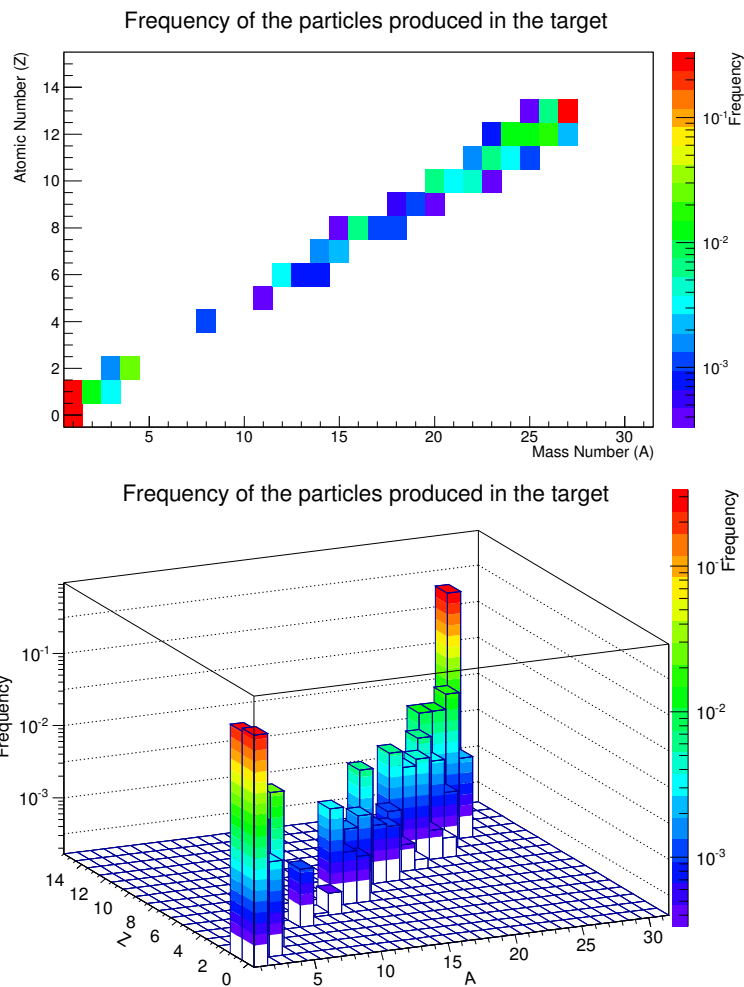


Figure 32: Normalized distribution of secondary particles produced in the Al target.

The figure 32 shows that the spectrum of the secondary particles produced are in a range in Z which varies from the value $Z = 1$, for protons, $Z = 13$ for aluminum ions. In the graph, were also included neutrons, to which was assigned the symbolic value $Z = 0$, as in the following graphs. From bars of frequency, expressed in logarithmic scale, can be seen that the evidence produced more frequent ($\geq 10\%$) are protons, neutrons and aluminum ions.

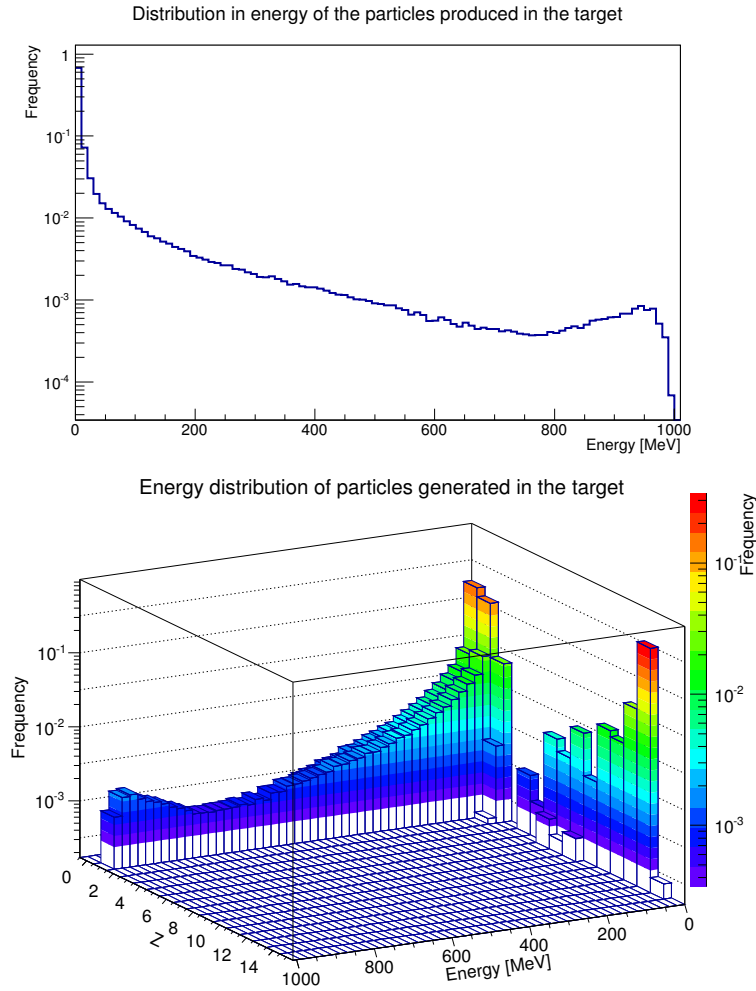


Figure 33: Normalized energy distribution of secondary particles produced in aluminum target.

Figure 33 shows that the spectrum in the energy of the secondary particles, generated in the target, is in the energy range 0 to 1000 MeV, where the upper bound corresponds to the energy of the primary beam incident. The Energy - Frequency graph, in semi-logarithmic scale, shows a strongly decreasing initial trend with the increase of energy and to remain about values less of $\sim 1\%$ for energies $E \sim 800 \text{ MeV}$.

Particular attention is given to the first portion of the curve $0 < E \lesssim 50 \text{ MeV}$, and the last $800 < E < 1000 \text{ MeV}$. The energy range, $0 < E \lesssim 50 \text{ MeV}$, contains more than 70% of total secondary particles produced. By the frequency distribution, differentiated with respect to Z of the atomic species considered, it is possible to note that this portion is populated by all the ions produced with $Z \geq 1$ and by the neutrons, the products of 'evaporation'. The final portion of the curve shows, instead, a slight increase due to the production of secondary protons in collisions frontal type, 'head-

on'. Subsequently, was performed an analysis on the particles, both primary and secondary, outgoing from the surface of the target, opposite to the input of the primary beam.

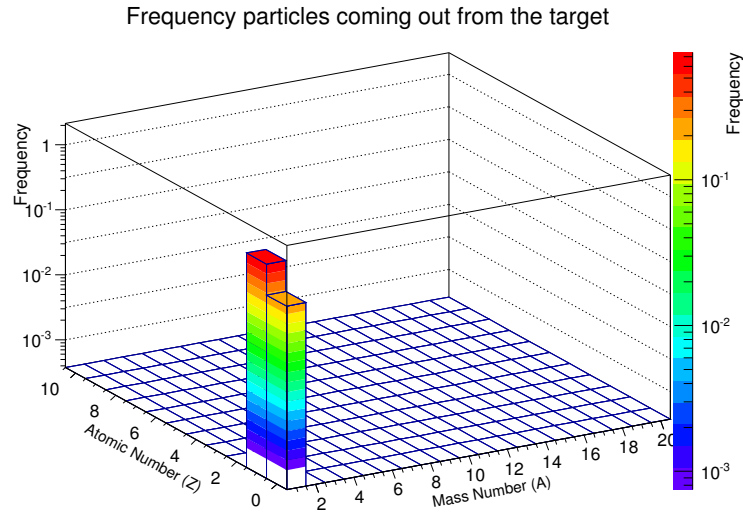


Figure 34: Normalized distribution of outgoing particles from the aluminum target.

It is clear that the only particles, outgoing from the surface of target, are neutrons and protons with frequency values, respectively, of $\sim 20\%$ and $\sim 80\%$. Not recorded ions $Z > 1$ since, being characterized by low values of energy $E \leq 50$ MeV (figure 33), not allowed to emerge from the target (figure 34).

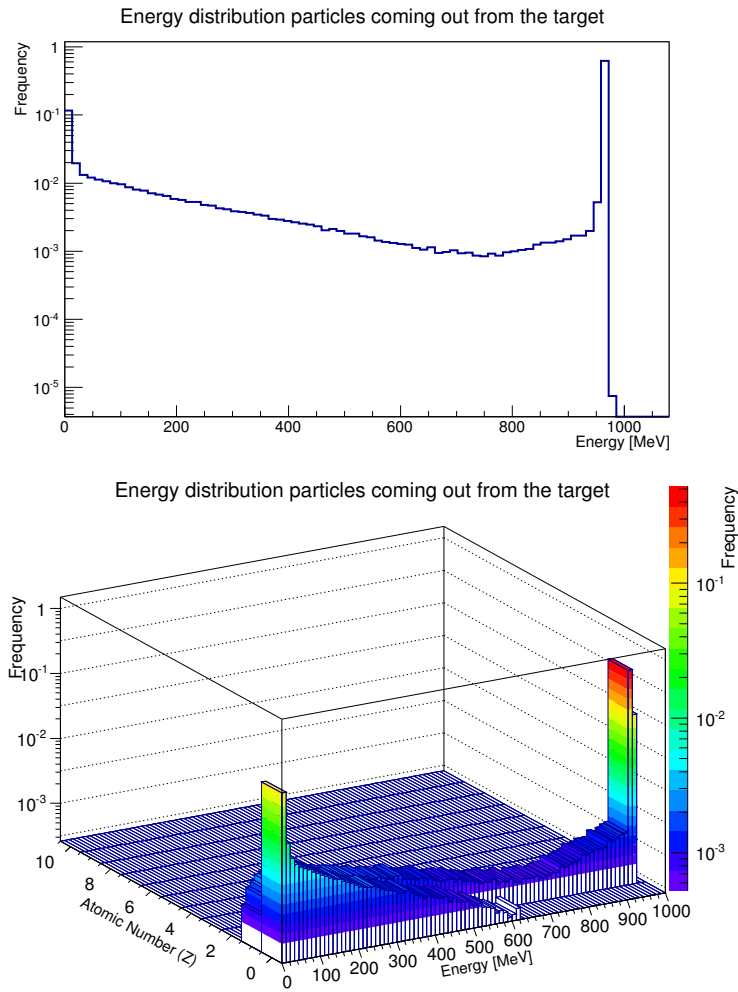


Figure 35: Normalized energy distribution of the particles coming out from the aluminum target.

Figure 35 shows that the spectrum in the energy of the particles, primary and secondary, outgoing from the target, is in an energy range from 0MeV up to $\approx 1000\text{MeV}$.

In this case the upper extreme corresponds to the output energy primary beam, slowed after of interactions with target atoms.

The Energy-Frequency graph in semi-logarithmic scale, shows an initial decreasing trend as a function of increased energy, and to remain at 1‰ for energies $E \approx 700\text{MeV}$.

Particular attention is given to the first part of the curve, $0 < E \lesssim 50\text{MeV}$, and to last $900 < E < 1000\text{MeV}$. In the energy range, $0 < E \lesssim 50\text{MeV}$, are contained $\sim 10\%$ of the total spectrum of the outgoing particles from the target. From the frequency distribution, differentiated respect to Z of the atomic species considered, it is noted that such tract is populated mainly by neutrons, produced of 'evaporation'. It is also possible to note a small contribution, the lower the 1%, due to protons of low

energy, they also produced the '*evaporation*'. The final part of the curve presents, however, a strong increase, frequency $\sim 70\text{-}80\%$, due to the primary protons, not subject to nuclear reactions in the target, and those secondary products in frontal collisions, '*head-on*'.

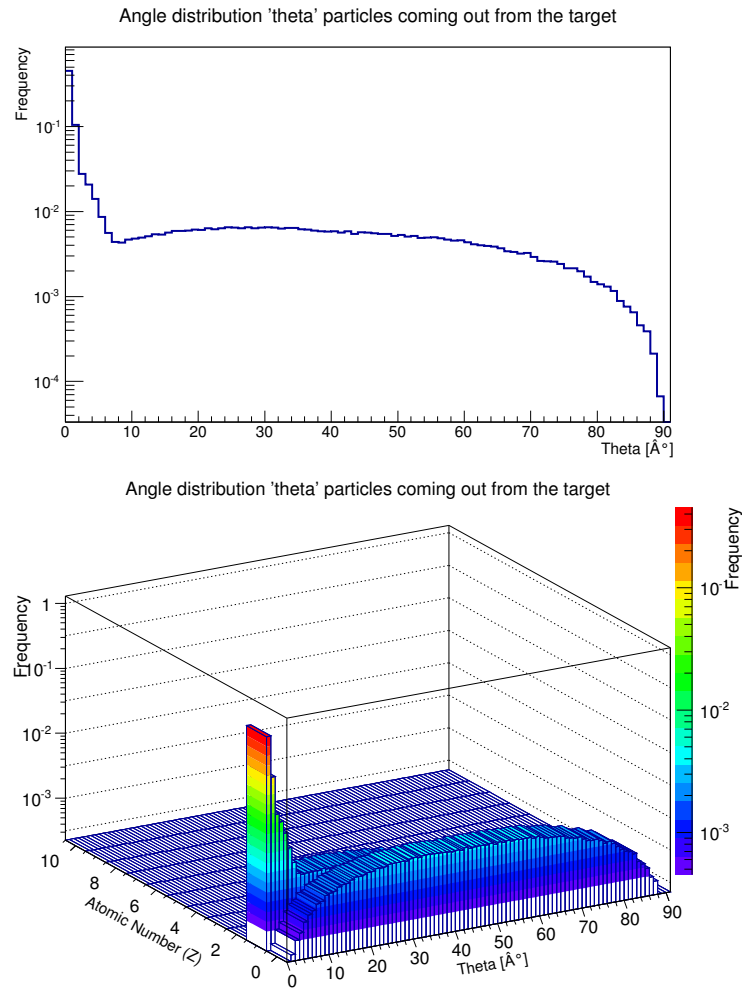


Figure 36: Normalized angular distribution in θ [$^\circ$] respect to the direction of incidence of the primary beam, of the outgoing particles from the aluminum target.

Figure 36 shows that the distribution in angle frequency in the range $0^\circ < \theta < 10^\circ$, has a peak which contains more than 70% of the outgoing particles from the target. From the distribution, differentiated with respect to the atomic number Z , we note that the spectrum of such particles is composed, mainly, by protons. These latter, as noted previously, are both primary protons, that in through the target are near to the direction of incidence of the beam, and secondary, emitted '*forward*', after of '*head-on*' collisions.

For angles $10^\circ < \theta < 80^\circ$ the frequency curve shows a continuous trend, with values less than 1%, then brusquely to zero for $\theta = 90^\circ$. From the distribution, differentiated in Z , it is clear that, in this range, the spectrum of the particles is composed, mainly, by neutrons and with a minor contribution of protons. These particles are the reaction products of evaporation, as described in chapter 2, are characterized by isotropic emission, at low energies. In the second phase was varied the size of the source, to evaluate whether and how, the latter may affect results.

We considered three cases:

- Point source;
- Circular source $r = 4$ cm;
- Circular source $r = 10$ cm;

and was performed an analysis of the profile of the beam be output from a target of aluminum of $20g/cm^2$, placed in vacuum. In all three cases, the source of protons of 1 GeV, is placed at $z = 30$ cm from the center of the target. In this phase of the simulation, the run is 1000000 events.

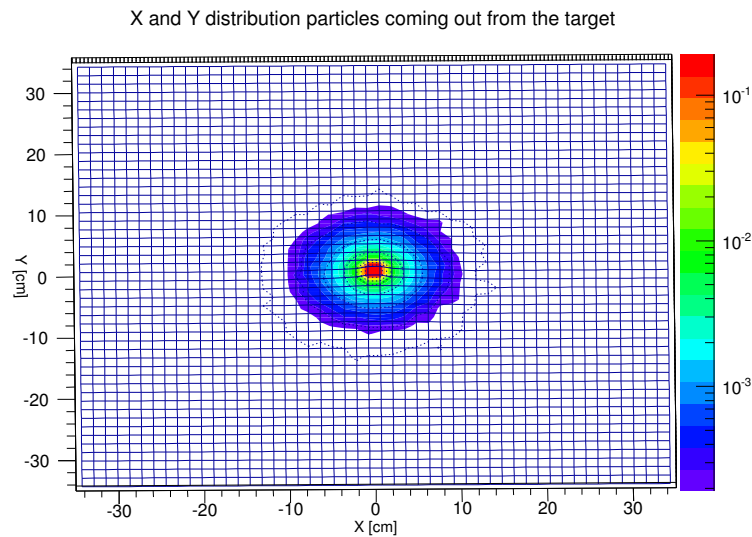


Figure 37: Normalized distribution in x and y of the particles, both primary and secondary, outgoing from the target surface of aluminum, in the case of point source.

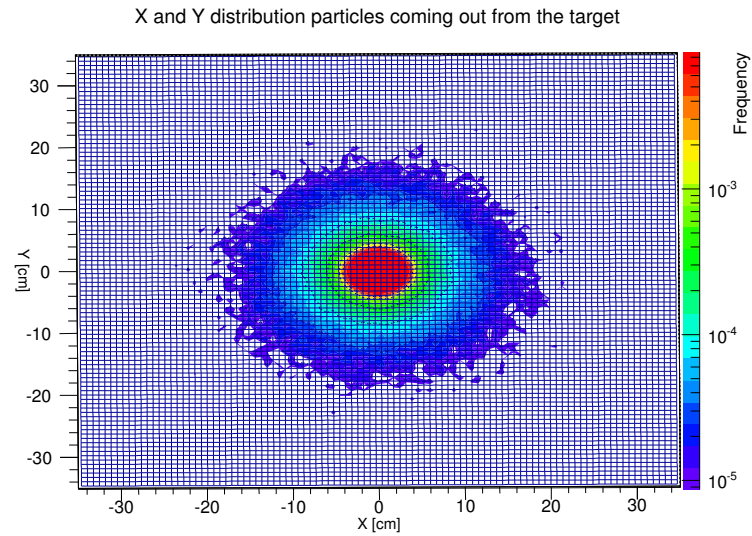


Figure 38: Normalized distribution in x and y of the particles, both primary and secondary, outgoing from the target surface of aluminum, in the case of source circular with a radius $R = 4$ cm.

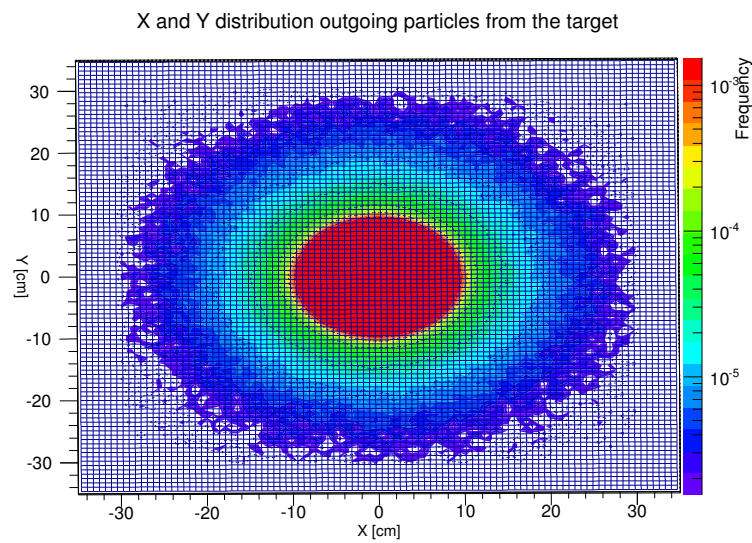


Figure 39: Normalized distribution in x and y of the particles, both primary and secondary, outgoing from the target surface of aluminum, in the case of source circular with a radius $R = 10$ cm.

Subsequently, it was performed a comparison between the trends simulated dose for point source, circular with $R = 4$ cm and a circular with $R = 10$ cm, in the regions before and after the target. Since it is only a preliminary simulation, for each point, were simulated run of the individual, 500000 events. This, at the moment, has not allowed the development of an appropriate statistical analysis

of the data.

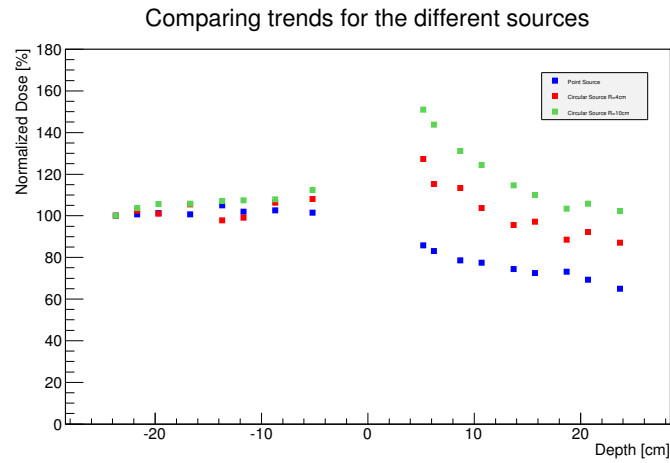


Figure 40: Comparing the trends simulated dose, normalized with respect to the reference position $z=-23.7$ cm of the center of the World Volume, for point source, circular source $R=4$ cm and $R=10$ cm. The dose values are expressed in %.

The table 12 shows the values of the points on the graph shown in figure 40.

Depth (cm)	Dose point source (%)	Dose source circular $R=4$ cm (%)	Dose source circular $R=10$ cm (%)
-23.7	100	100	100
-21.7	100.70	102.38	103.76
-19.7	101.28	100.98	105.74
-16.7	100.72	105.45	105.86
-13.7	105.00	97.79	107.04
-11.7	101.92	99.12	107.47
-8.7	102.57	106.35	107.83
-5.2	101.48	108.07	112.37
5.2	85.74	127.35	151.02
6.2	83.00	115.26	143.78
8.7	78.66	113.34	131.12
10.7	77.41	103.78	124.37
13.7	74.45	95.56	114.58
15.7	72.48	97.14	110.06
18.7	73.09	88.49	103.41
20.7	69.35	92.19	105.90
23.7	65.05	87.12	102.37

Table 12: Dose values simulated, normalized with respect to the reference position $z = -23.7$ cm of the center of the World Volume, expressed in%.

The figure 40 shows that, among the three simulated trends, the case of circular source of radius $R = 10$ cm has a greater increase in the dose normalized. For this reason it was considered appropriate a detailed analysis of the spectra of the particles, both primary and secondary, that arrive on the walls of the ionization chamber, contributing to increase, registered, of the simulated total dose . In this phase of the simulation, the run is 1000000 events.

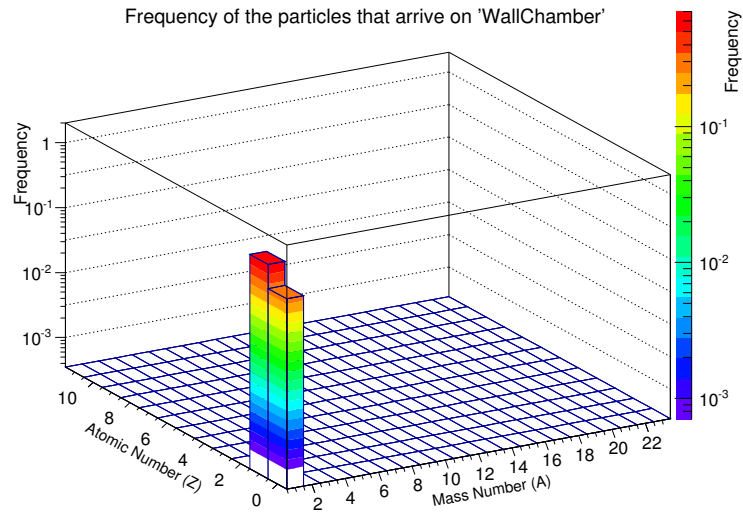


Figure 41: Normalized distribution of particles that arrive on the Wall Chamber. Circular Source $R=10$ cm.

The spectrum of the particles that arrives on the ionization chamber consists of neutrons and protons. In particular, the higher frequency values concern protons, $\sim 80\%$.

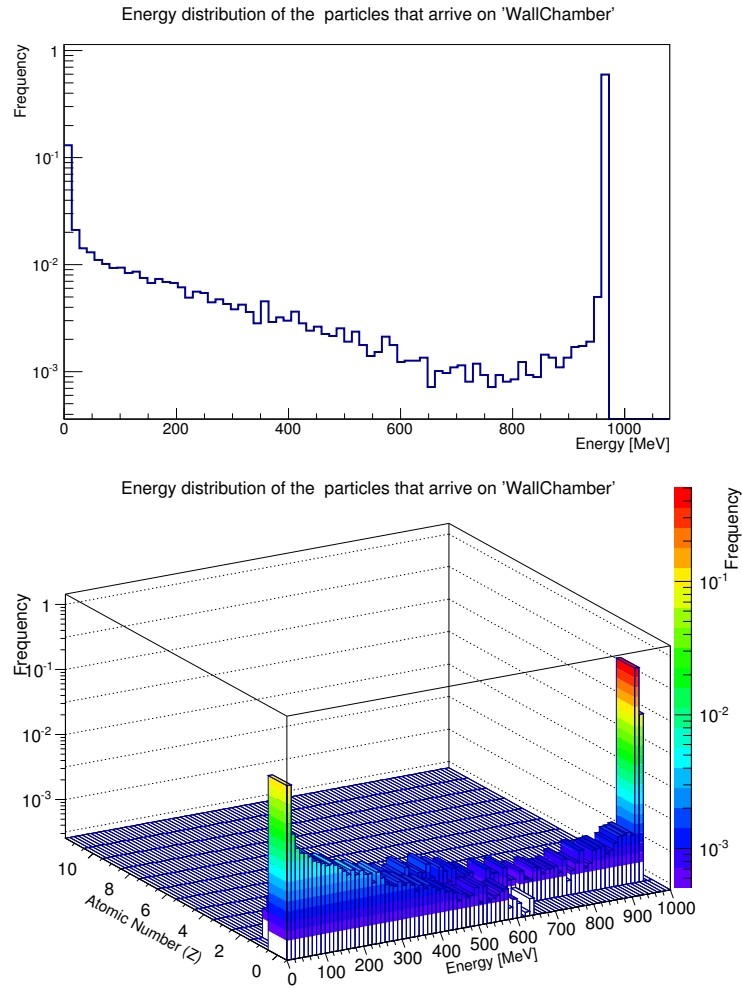


Figure 42: Normalized energy distribution of the particles coming out from the aluminum target and that arrive on the Wall Chamber. Circular Source $R=10\text{cm}$.

The figure 42 shows that the spectrum in the energy of the particles that arriving on the walls of the ionization chamber is in an energy range from 0 MeV up to ~ 1000 MeV.

The upper extreme corresponds to the energy output of the primary beam, slowed due to interactions with the target. The Energy-Frequency graph, in semi-logarithmic scale, shows a trend of decreasing initial function of increased energy, and then fixed in 1% for energies $E \sim 800\text{MeV}$.

Of great interest is the first part of the curve $0 < E \lesssim 50\text{MeV}$ and the portion in the range of energy $900 < E < 1000\text{MeV}$. The range $0 < E \lesssim 50\text{MeV}$ comprises about 20% of the total spectrum of the particles in question, and by the frequency distribution, differentiated respect to Z , it is possible conclude that it is mainly of neutrons, products of 'evaporation'. The final portion of the curve is characterized by the presence of a peak, frequency $\sim 70 - 80\%$. From the comparison with the

performance of the frequency distribution, differentiated with respect to Z , it is clear that the peak is populated by protons, both primary and secondary, are not subject to nuclear reactions in the target, products of frontal collision, 'head-on'.

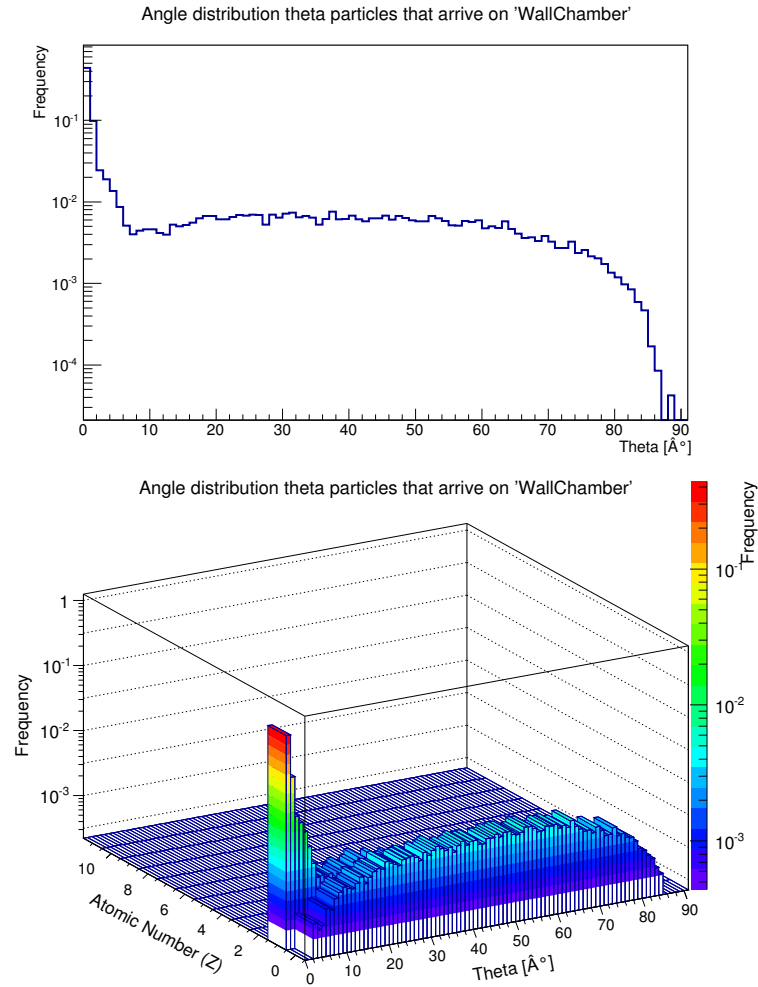


Figure 43: Normalized angle distribution, the primary and secondary particles, produced in the aluminum target, that arrive on the walls of ionization chamber (Chamber Wall). Circular source $R = 10$ cm.

The figure 43 shows that the distribution in angle θ has a peak frequency in the range $0^\circ < \theta < 5^\circ$, in which are contained $\sim 60\%$ of the particles that arrive on the walls of the ionization chamber. From the distribution, differentiated respect to the atomic number Z , we note that the spectrum of such particles is composed, mainly, by protons. These latter, as previously observed in figure 42 are both primary protons, that when they pass through the target are near to the direction of incidence of the beam, that secondary protons emitted forward, as a result of collisions 'head-on'.

For angles of $5^\circ < \theta < 80^\circ$, the frequency curve shows a trend continuous, with values $\lesssim 1\%$, and then quickly zero for $\theta = 90^\circ$. From the comparison with the distribution, differentiated in Z, and with the distribution energy (figure 42) it is deduced that, in this range, the spectrum of the particles is composed, mainly, by low-energy neutrons ($E \sim 50$ MeV). The latter are the reaction products of 'evaporation'. These neutrons represent a risk to the health of astronauts since, being human tissues rich in hydrogen, may interact causing the issuance of free protons of low energy, in the internal organs.

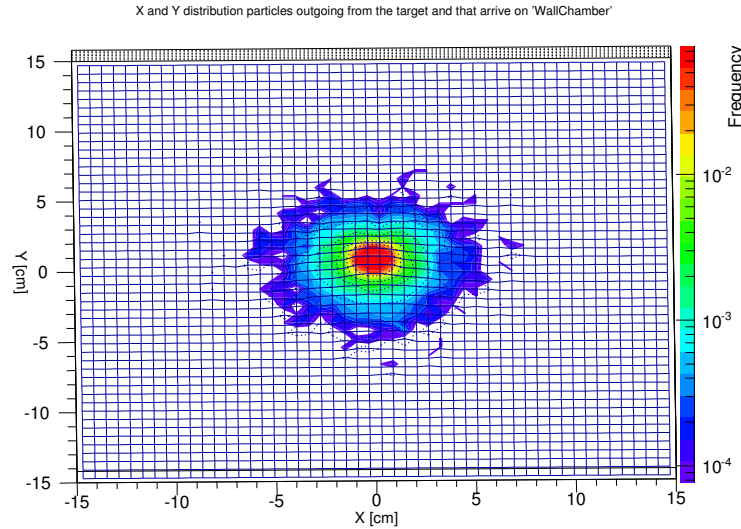


Figure 44: Normalized X and Y of the particles coming on the walls of the ionization chamber (Chamber Wall). Circular source $R = 10$ cm.

The figure shows, in agreement with the data distribution in θ (figure 43), that the particles coming on the walls of the ionization chamber are, mainly, those closest to the direction of incidence of the primary beam.

The circular area of red color, figure 44 has a diameter of ~ 2 cm, comparable to the ionization chamber, $R = 1.12$ cm.

Following the preliminary study has been performed validation process.

In order to compare the simulated data with the experimental ones (figure 45), the dose values obtained in output from application have been normalized with respect to the value of the position $z = -27.4$ cm.

This last value is evaluated in relation to the target surface opposite to the input of the primary beam. The dose values normalized simulated are expressed in % and were obtained by performing run of 1500000 events. In order to obtain a better statistical each run, during the processing and analysis of output data, has been divided into ten groups each of 150000 events. The output file format .out, were analyzed on Excel spreadsheets to calculate the mean and standard deviation of the mean $\sigma_{\bar{x}}$.

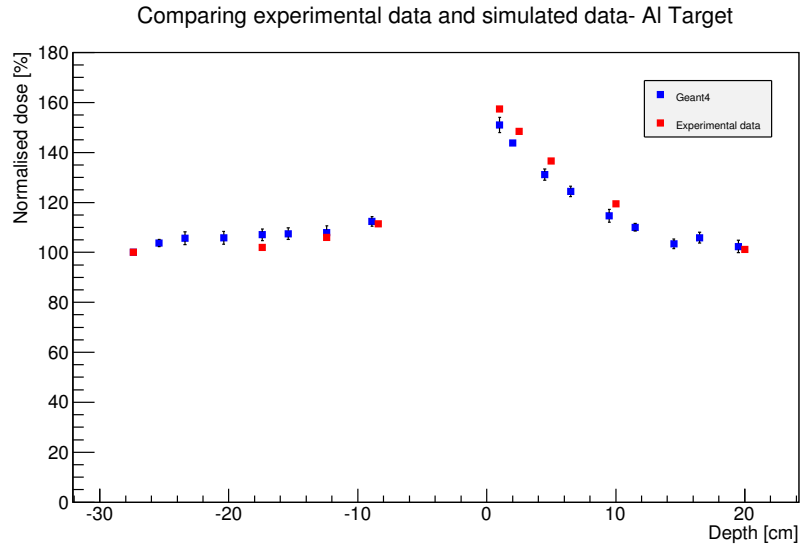


Figure 45: Comparison between simulated and experimental dose values for Al target.

In tables 13 and 14 are shown the values of the points shown on the graph of figure 45:

Depth (cm)	Experimental Dose (%)	Uncertainty (%)
-27.4	100.00	0.01
-17.4	101.93	0.01
-12.4	105.95	0.01
-8.9	111.43	0.01
1.5	157.40	0.01
2.5	148.50	0.01
5.0	136.60	0.01
10.0	119.50	0.01
20.0	101.24	0.01

Table 13: Experimental dose value-Al Target.

Depth (cm)	Simulated Dose (%)	Uncertainty (%)
-27.4	100.00	1.17
-25.4	103.76	1.41
-23.4	105.74	2.56
-20.4	105.86	2.53
-17.4	107.04	2.36
-15.4	107.47	2.32
-12.4	107.83	2.75
-8.9	112.37	1.92
1.0	151.02	2.99
2.0	143.78	1.19
4.5	131.12	2.19
6.5	124.37	2.12
9.5	114.58	2.56
11.5	110.06	1.52
14.5	103.41	1.90
16.5	105.90	2.12
19.5	102.37	2.43

Table 14: Simulated dose value-Al Target.

The figure 45 shows that the performance trends were comparable, both before and after the target. In the region before of the target, there is an increase of 12% of the simulated dose comparable with an increase of 11% of the experimental dose. In the region after the target there is a trend of decreasing exponential type in agreement with the experimental data, caused by the presence of air which favors the attenuation of the beam. For small distances $\sim 1\text{cm}$ is observed great increase of the simulated dose $\sim 51\%$, unlike the increase of $\sim 57\%$ experimental dose. Following the validation process, was made the comparison of the performance of the simulated dose with a target of different materials, aluminum, Nomex and PMMA.

5.5 Dose Results- Nomex Target

In agreement with the company I have identified a new material Nomex, that is a meta-aramid fiber. This is a good materials for the shield because has a two fundamental features:

- High mechanical resistance to traction (3.0 - 4.5 GPa);
- High resistance to flame.

In table 15 the composition of this material is reported:

Element Composition	Percentage %
H	4
C	54
N	9
O	10
Cl	23

Table 15: Percentage elements in Nomex material.

First step was performed an analysis of the secondary particles that are generated from interaction of a point source of protons of 1 GeV into a target of Nomex of $\sim 20\text{ g/cm}^2$, placed at $z = 30\text{ cm}$ from the target, in air. In this phase has been set a run of 1000000 events.

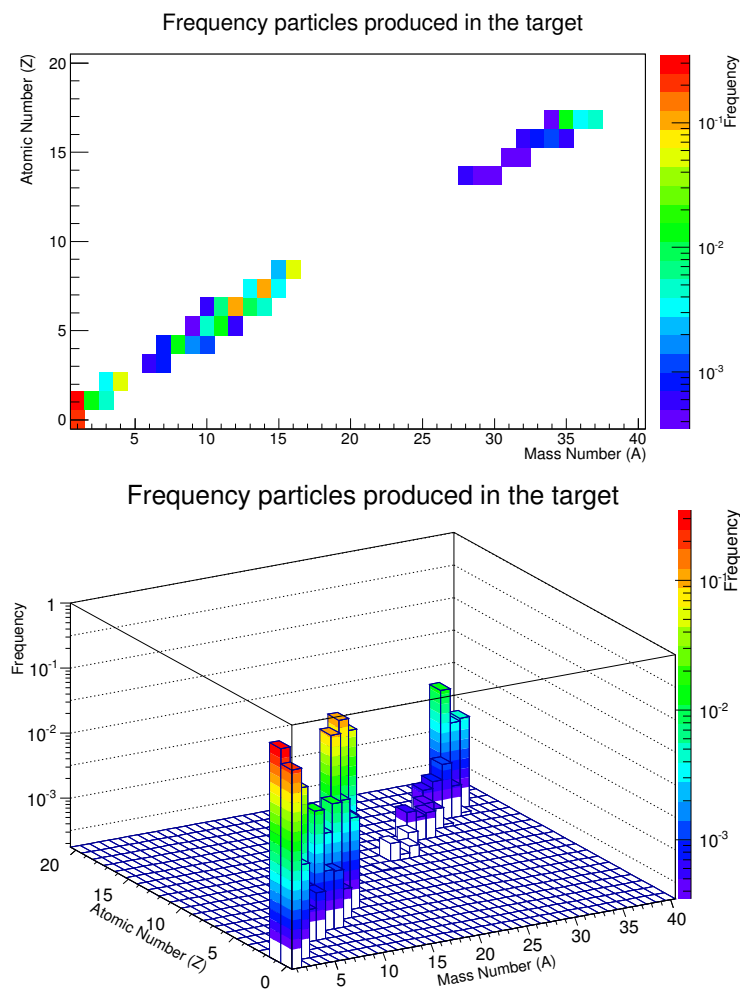


Figure 46: Normalized distribution of secondary particles produced in Nomex target.

The graph shows that the spectrum of the secondary particles is in a range from $Z = 1$ to $Z = 17$, chlorine ions. By frequency bars, expressed in logarithmic scale, can be seen that the evidence produced more frequent ($\geq 10\%$) are protons and neutrons, instead for the frequency $\sim 10\%$ are, carbon $Z=6$, nitrogen $Z=7$ and oxygen $Z=8$ ions. In lower quantity, there are the chlorine ions, this is a good result because heavy ions provide the main contribution to the equivalent dose.

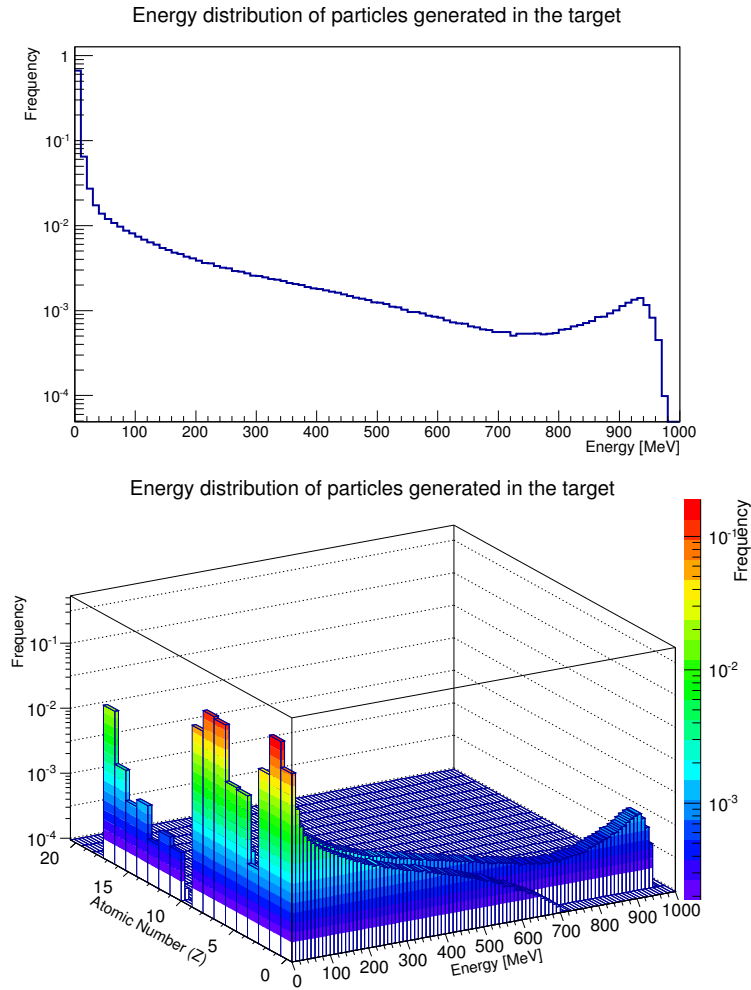


Figure 47: Normalized energy distribution of secondary particles produced in Nomex target.

Figure 47 shows that the spectrum in the energy of the secondary particles, generated in the target is in the energy range 0 to 1000 MeV. The Energy-Frequency graph, in semi-logarithmic scale, shows a strongly decreasing trend with increasing energy, up to 1% for energy $\leq 900\text{MeV}$. Particular attention is given to the first portion of the curve $0 < E \sim 20\text{MeV}$, and the last $900 < E < 1000\text{MeV}$.

The energy range, $0 < E \sim 20\text{MeV}$, contains more than 70% of total secondary particles produced. From the frequency distribution, differentiated with respect to Z of the atomic species considered, it is noted that this portion is populated by all the ions produced with $Z \geq 1$ and by the neutrons, the products of 'evaporation'. The final portion of the curve shows, instead, a slight increase due to the production of secondary protons in collisions frontal type, 'head-on'. Subsequently, was performed an analysis on the particles, both primary and secondary, outgoing from the surface of the target, opposite to the input of the primary beam.

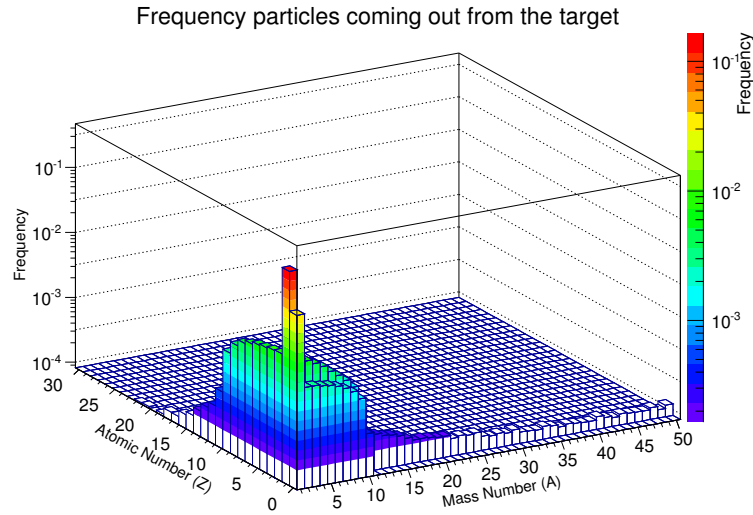


Figure 48: Normalized distribution of outgoing particles from the Nomex target.

It is evident that the particles, outgoing from the surface of target, with major frequency, are neutrons and protons with frequency values, respectively, of $> 20\%$ and $\geq 3\%$ (see figure 48).

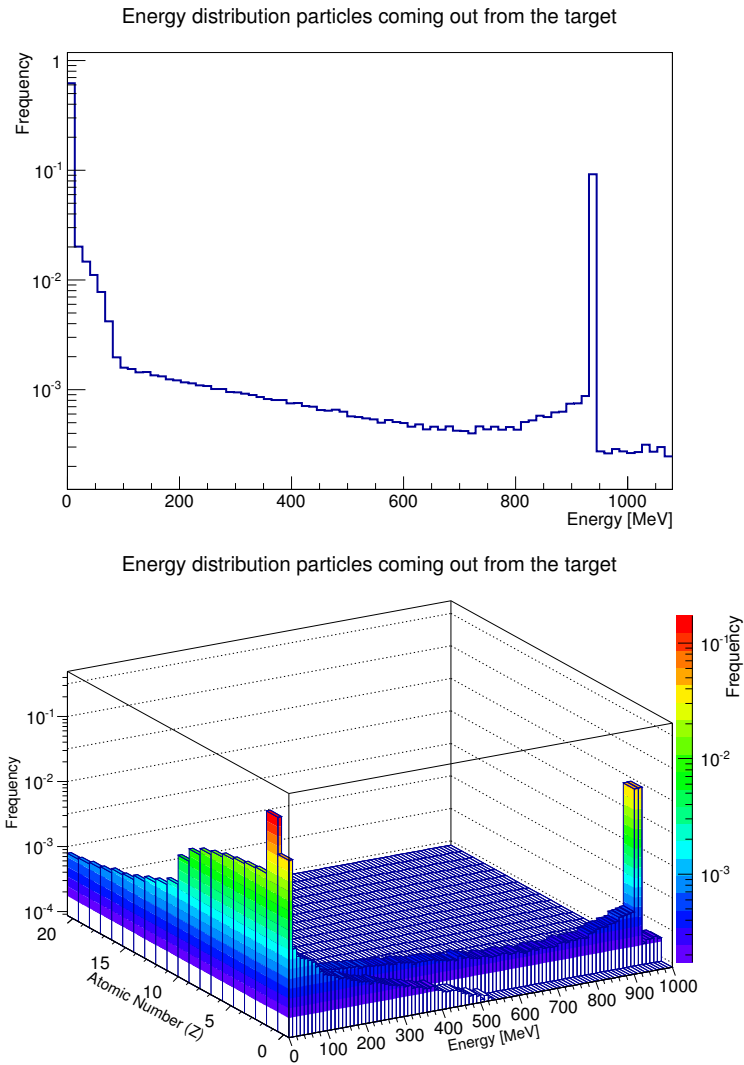


Figure 49: Normalized energy distribution of the particles coming out from the Nomex target.

It is also evident that the spectrum in the energy of the particles, primary and secondary, outgoing from the target, is in an energy range from 0MeV up to $\sim 1000\text{MeV}$ (see figure 49).

In this case the upper extreme corresponds to the output energy primary beam, slowed after of interactions with target atoms.

The Energy-Frequency graph in semi-logarithmic scale, shows an initial decreasing trend as a function of increased energy, and to remain at $\%_{00}$ for energies $E \geq 300\text{MeV}$.

Particular attention is given to the first part of the curve, $0 < E \lesssim 100\text{MeV}$, and to last $850 < E < 950\text{MeV}$. In the energy range, $0 < E \lesssim 100\text{MeV}$, are contained $\sim 60\%$ of the total spectrum of the outgoing particles from the target. By the frequency distribution, differentiated respect to Z of the

atomic species considered, it is noted that such tract is populated mainly by neutrons, produced of 'evaporation'. It is also noted a small contribution, the lower the 4%, due to protons of low energy, they also produced the 'evaporation'. The final part of the curve presents an increase, frequency $\sim 10\%$, due to the primary protons, not subject to nuclear reactions in the target, and those secondary products in frontal collisions, 'head-on'.

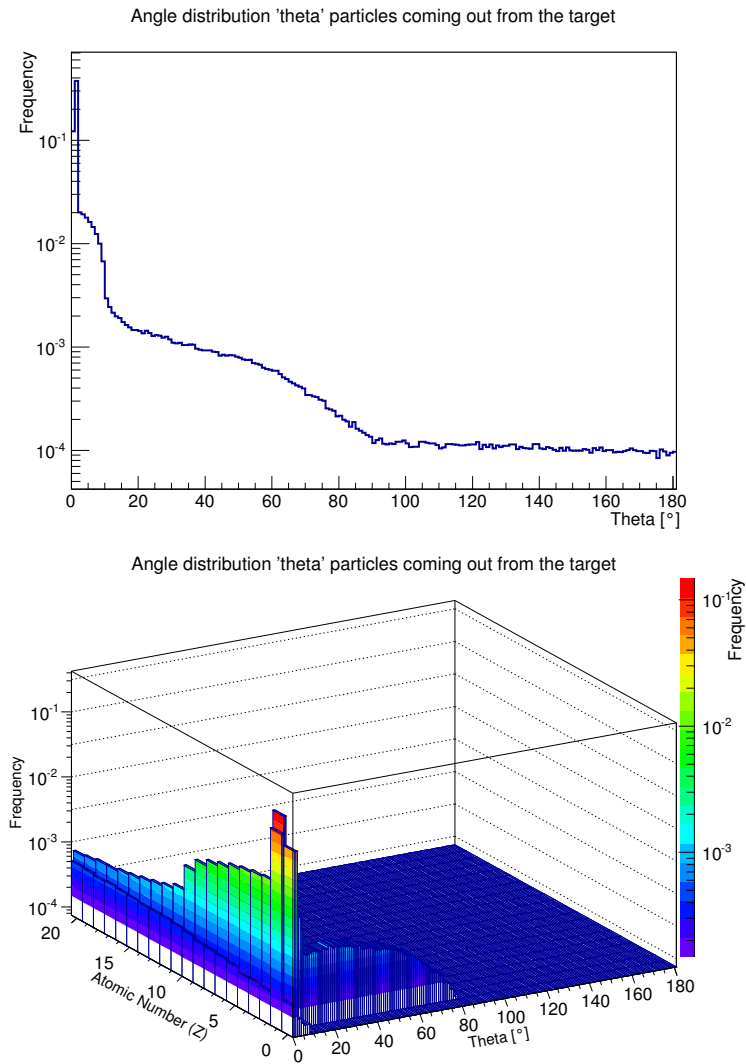


Figure 50: Normalized angular distribution in θ [°] respect to the direction of incidence of the primary beam, of the outgoing particles from the Nomex target.

In the figure 50 we observed that the distribution in angle frequency in the range $0^\circ < \theta < 5^\circ$, shows a peak which contains $\sim 50\%$ of the outgoing particles from the target. From the distribution,

differentiated with respect to the atomic number Z , we note that the spectrum of such particles is composed, mainly, by protons. These latter, as noted previously, are both primary protons, that in through the target are near to the direction of incidence of the beam, and secondary, emitted '*forward*', after of '*head-on*' collisions.

For angles $10^\circ < \theta < 40^\circ$ the frequency curve shows a decreasing trend, with values less than 1%. From the distribution, differentiated in Z , it is clear that, in this range, the spectrum of the particles is composed, mainly, by neutrons and protons of low energy, the reaction products of '*evaporation*'.

5.6 Dose Results- PMMA Target

The first step was performed an analysis of the secondary particles that are generated from interaction of a point source of protons of 1GeV into a target of PMMA of $\sim 20\text{g}/\text{cm}^2$, placed at $z = 30\text{cm}$ from the target, in air. In this phase has been set a run of 1000000 events.

The graph shows that the spectrum of the secondary particles is in a range from $Z = 1$ to $Z = 8$, oxygen ions. By frequency bars, expressed in logarithmic scale, can be seen that the evidence produced more frequent ($\geq 10\%$) are protons, neutrons and carbon ions. From a comparison between figure 32 and figure 51 it is observed that in the PMMA, being a hydrogen-rich material, the production of neutrons is lower than for the aluminum, as predicted by theoretical models.

It is evident that the spectrum in the energy of the secondary particles, generated in the target is in the energy range 0 to 1000 MeV, where the upper bound corresponds to the energy of the primary beam incident (see figure 52). The Energy-Frequency graph, in semi-logarithmic scale, shows a strongly decreasing initial trend with the increase of energy and to remain about values less of $\sim 1\%$ for energies $E \sim 800\text{MeV}$.

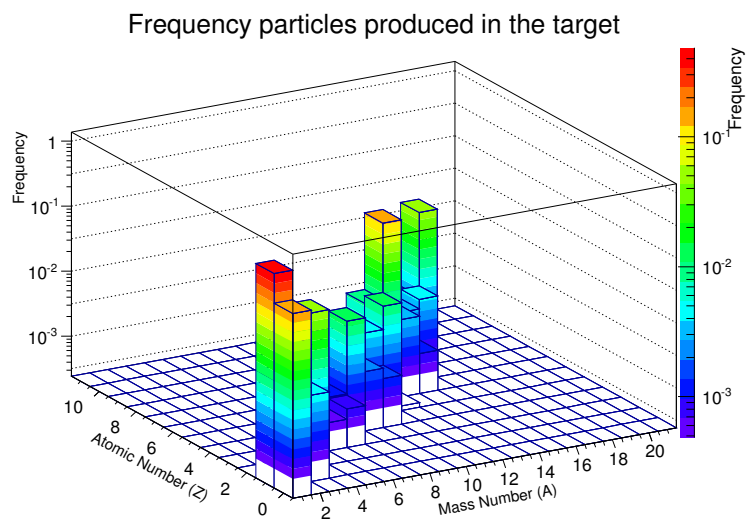
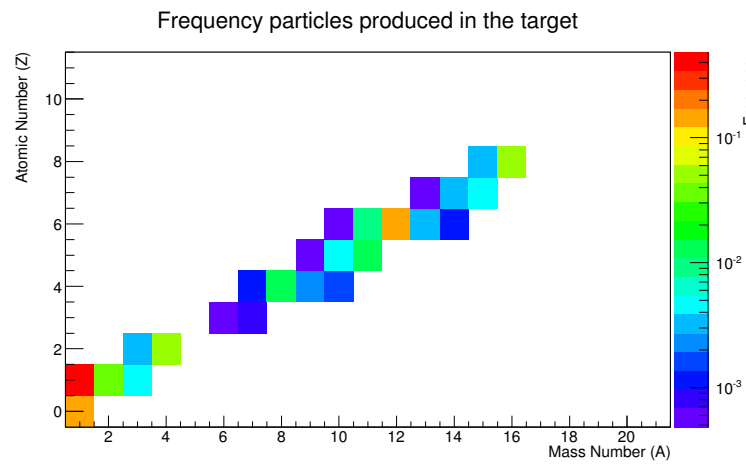


Figure 51: Normalized distribution of secondary particles produced in PMMA target.

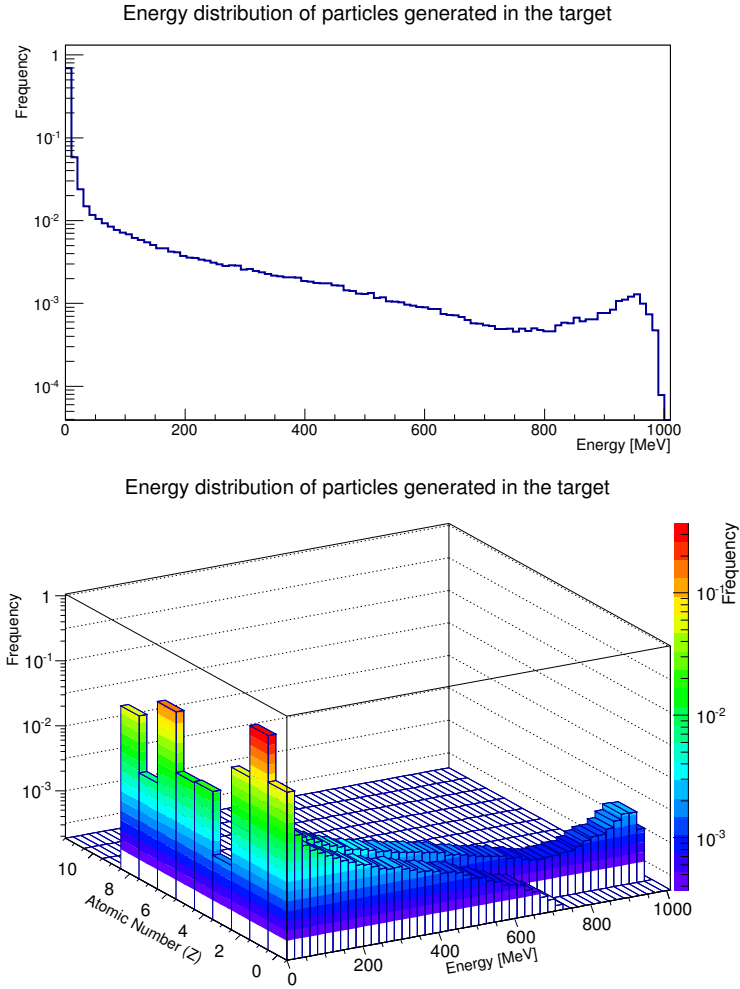


Figure 52: Normalized energy distribution of secondary particles produced in PMMA target.

Particular attention is given to the first portion of the curve $0 < E \lesssim 50 \text{ MeV}$, and the last $800 < E < 1000 \text{ MeV}$. The energy range, $0 < E \lesssim 50 \text{ MeV}$, contains more than 70% of total secondary particles produced. From the frequency distribution, differentiated with respect to Z of the atomic species considered, it is noted that this portion is populated by all the ions produced with $Z \geq 1$ and by the neutrons, the products of 'evaporation'. The final portion of the curve shows, instead, a slight increase due to the production of secondary protons in collisions frontal type, 'head-on'. Subsequently, was performed an analysis on the particles, both primary and secondary, outgoing from the surface of the target, opposite to the input of the primary beam.

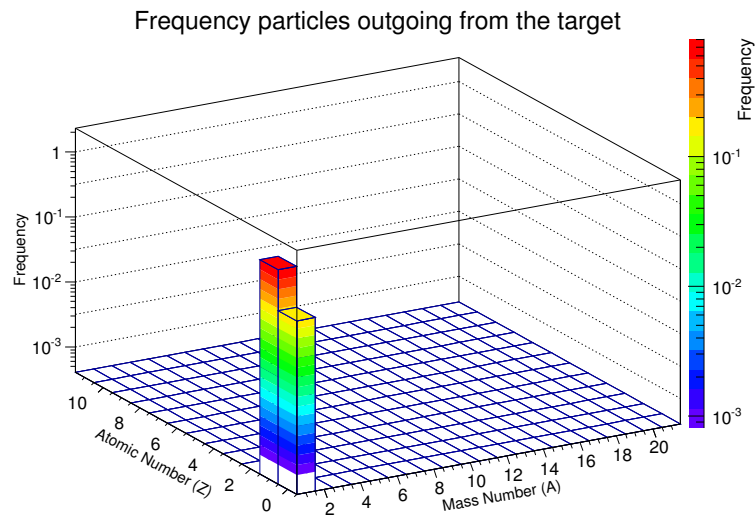


Figure 53: Normalized distribution of outgoing particles from the PMMA target.

The particles outgoing from the surface of target, are neutrons and protons with frequency values, respectively, of $< 20\%$ and $> 80\%$ (see figure 53). In comparison with figure 34, we note that the frequency of outgoing neutrons from the target PMMA, is smaller than that for to the target of aluminum. Not recorded ions $Z > 1$ since, being characterized by low values of energy $E \leq 50$ MeV (figure 52), not allowed to emerge from the target.

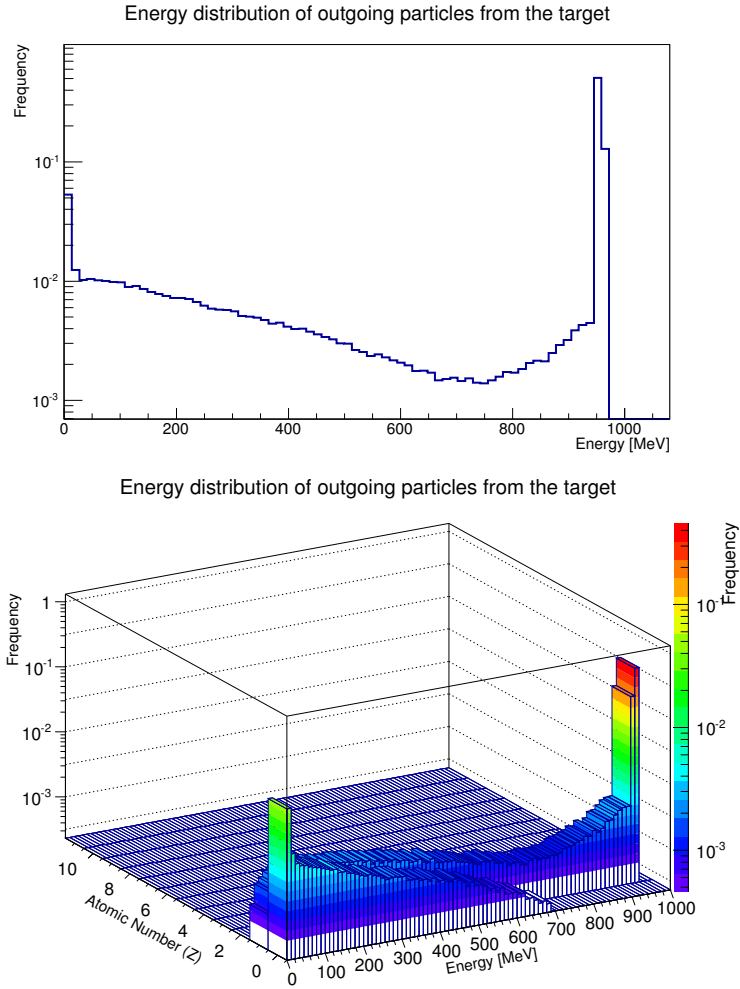


Figure 54: Normalized energy distribution of the particles coming out from the PMMA target.

The spectrum in the energy of the particles, primary and secondary, outgoing from the target, is in an energy range from 0MeV up to $\sim 1000\text{MeV}$ (see figure 54).

In this case the upper extreme corresponds to the output energy primary beam, slowed after of interactions with target atoms.

The Energy-Frequency graph in semi-logarithmic scale, shows an initial decreasing trend as a function of increased energy, and to remain at $\%_{00}$ for energies $E \approx 700\text{MeV}$.

Particular attention is given to the first part of the curve, $0 < E \lesssim 100\text{MeV}$, and to last $900 < E < 1000\text{MeV}$. In the energy range, $0 < E \lesssim 100\text{MeV}$, are contained $\sim 10\%$ of the total spectrum of the outgoing particles from the target. From the frequency distribution, differentiated respect to Z of the atomic species considered, it is noted that such tract is populated mainly by neutrons, produced of 'evaporation'. It is also noted a small contribution, the lower the 1%, due to protons of low energy,

they also produced the '*evaporation*'. The final part of the curve presents a strong increase, frequency $\sim 70\%$, due to the primary protons, not subject to nuclear reactions in the target, and those secondary products in frontal collisions, '*head-on*'.

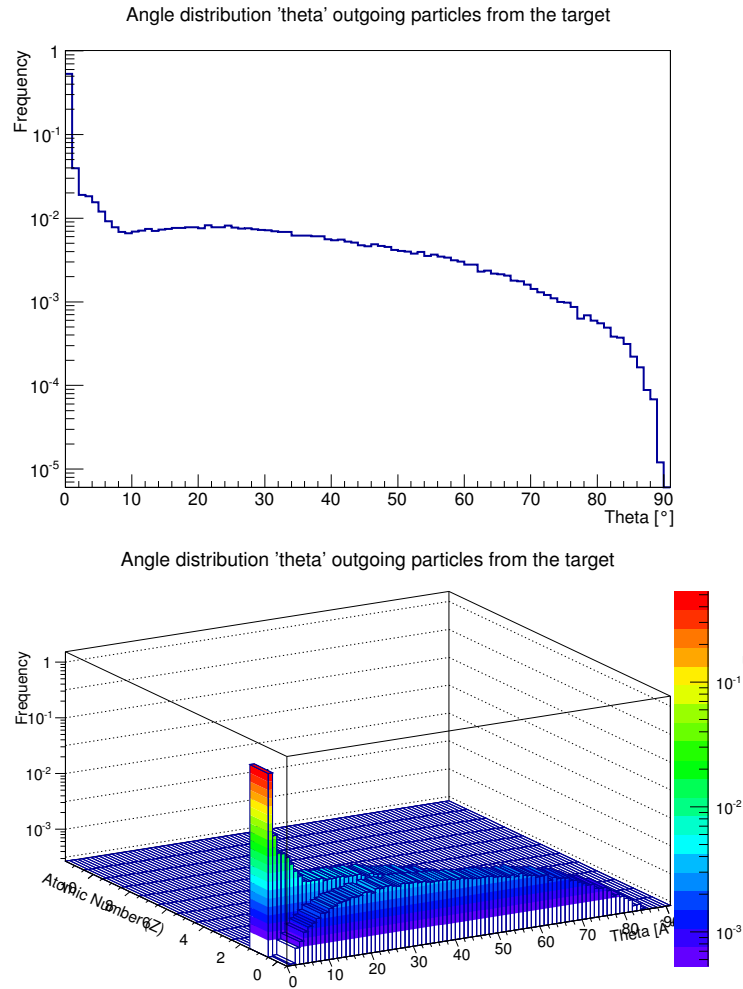


Figure 55: Normalized angular distribution in θ [$^{\circ}$] respect to the direction of incidence of the primary beam, of the outgoing particles from the PMMA target.

It was observed (figure 55) that the distribution in angle frequency in the range $0^{\circ} < \theta < 10^{\circ}$, shows a peak which contains $\sim 70\%$ of the outgoing particles from the target. From the distribution, differentiated with respect to the atomic number Z , we note that the spectrum of such particles is composed, mainly, by protons. These latter, as noted previously, are both primary protons, that in through the target are near to the direction of incidence of the beam, and secondary, emitted '*forward*', after of '*head-on*' collisions.

For angles $10^\circ < \theta < 80^\circ$ the frequency curve shows a continuous trend, with values less than 1%, then brusquely to zero for $\theta = 90^\circ$. From the distribution, differentiated in Z, it is clear that, in this range, the spectrum of the particles is composed, mainly, by neutrons and protons of low energy, the reaction products of 'evaporation'. The comparison between the figure 36 and figure 55 shows that for PMMA, unlike of the aluminum, the contribution of the protons is predominant compared to neutrons, also in this range of angles.

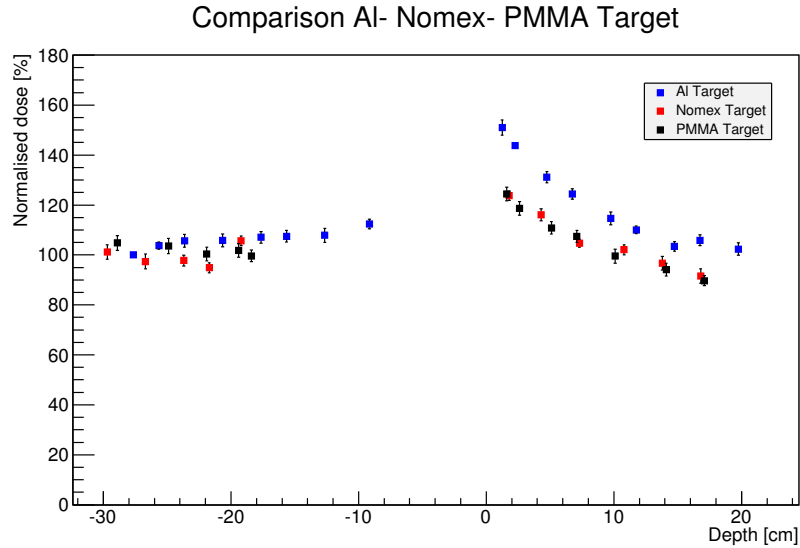


Figure 56: Comparison trends among three different materials.

This plot shows the comparison among the trends of three different materials tested with Geant4, Aluminum, Nomex and PMMA. The Nomex is the best material to be used as shielding material during the SPEs for technical features and response in terms of dose reduction (in particular in the region after the target).

6 Spenvis Results

During the intership “*Validation of the electromagnetic physical processes with software SPENVIS*” in the “Società Aerospaziale Mediterranea” it was used another software for the simulation. The company uses this software to simulate any space missions, in particular to design satellites orbiting, the orbit at low energy.

The validation of electromagnetic processes with software SPENVIS was performed in the same way of Geant4.

For the validation, was performed the comparing between the data obtained by the software with those available in the literature. The validation is, as previously said, is essential for the use of any application. Also in this case, the values of the electronic stopping power were compared with those provided by the NIST database PSTAR.

The interface used in this case is MULASSIS.

6.1 Experimental setup

The experimental setup adopted for the validation of the electromagnetic physical processes, is reported in 57. The simulated geometry is constituted by a point source of protons with energies from 800 MeV to 1200 MeV, in the vacuum. The target is a slab of aluminum ($\rho \sim 2.7g/cm^3$), in the shape of a parallelepiped, of a mass thickness $20g/cm^2$ in the direction of incidence of the primary beam ($z = 7.4$ cm) and with surfaces $30x30cm^2$. To compare the values of the electronic stopping power it is necessary that the energy of the primary beam does not vary appreciably in the target, condition assured by a small thickness. In this configuration, the thickness used aluminum is 5% of the projected-range of the protons, which varies from $300g/cm^2$ to $530g/cm^2$ in the energy range from 800 MeV to 1.2 GeV in referring to the tables in the database PSTAR (Berger et al., 2005).

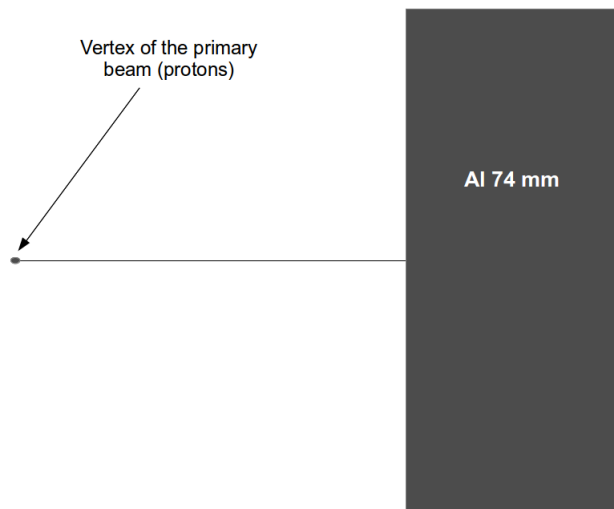


Figure 57: Experimental Setup: target is a slab of aluminum ($\rho \sim 2.7g/cm^3$) of a thickness 74 mm, in the direction of incidence of the primary beam.

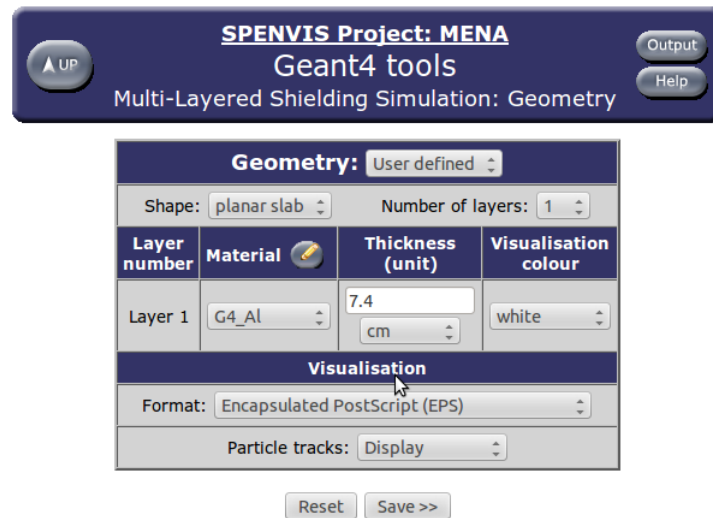
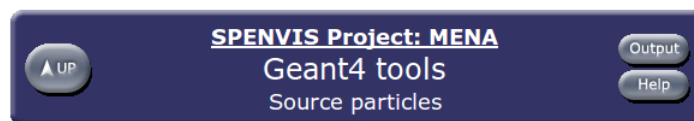
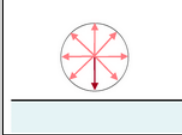


Figure 58: Interfaces for Spenvis Mulassis. In this picture you can see as you enter information about the geometry in Spenvis software.



These settings are used as an input by MULASSIS v1.23, GEMAT v2.8 and GRAS v3.1.

Source particle type and spectrum		
Environment:	User defined	mono-energetic
Number of primary particles to simulate:	100	
Incident particle type:	proton	
Incident energy spectrum		
Mono-energetic energy:	1200.0	[MeV]
Fluence/(Flux) intensity:	1.0	[(s ⁻¹)]
Angular distribution: point source		
Minimum angle:	0.0	[degrees]
Maximum angle:	90.0	[degrees]
		
<input type="button" value="Reset"/> <input type="button" value="Create GPS macro"/>		

Tool developed by

Figure 59: Interfaces for Spenvis Mulassis. In this picture you can see as you enter information about the source particles in Spenvis software.

6.2 Results Mulassis

The table 16 shows, for the same energy of the primary beam, respectively, the values of the electronic stopping power obtained using the application, with relative uncertainty, and those calculated by PSTAR:

Energy (MeV)	StoppingPower Spenvis($\text{MeV cm}^2/\text{g}$)	\pm	StoppingPower PSTAR ($\text{MeV cm}^2/\text{g}$)
800	1,89	0,05	1,85
850	1,85	0,05	1,82
900	1,83	0,05	1,79
950	1,78	0,05	1,77
1000	1,78	0,05	1,75
1050	1,77	0,05	1,73
1100	1,74	0,05	1,72
1150	1,69	0,05	1,71
1200	1,65	0,05	1,69

Table 16: Values of the electronic stopping power of the database PSTAR and the Spenvis software with error.

The following shows the graph, which reproduces the performance of the stopping power of protons in aluminum, in the range $800 \div 1200$ MeV, for the application and database PSTAR.

The results reported in Tab.16 show the expected trend of stopping power, which decreases with increasing energy. With the use of the software SPENVIS-MULASSIS, the stopping power and its relative uncertainty, were obtained from the output 'Energy deposition' that was normalized respect to the mass thickness. The values shown in the PSTAR database of the NIST are supplied without error because the tables of stopping power and range of protons are calculated in accordance with the Bethe Bloch formula.

As previously mentioned Spenvis is used online, this puts limits on the run due to the computational time. For this reason the run is 100 events.

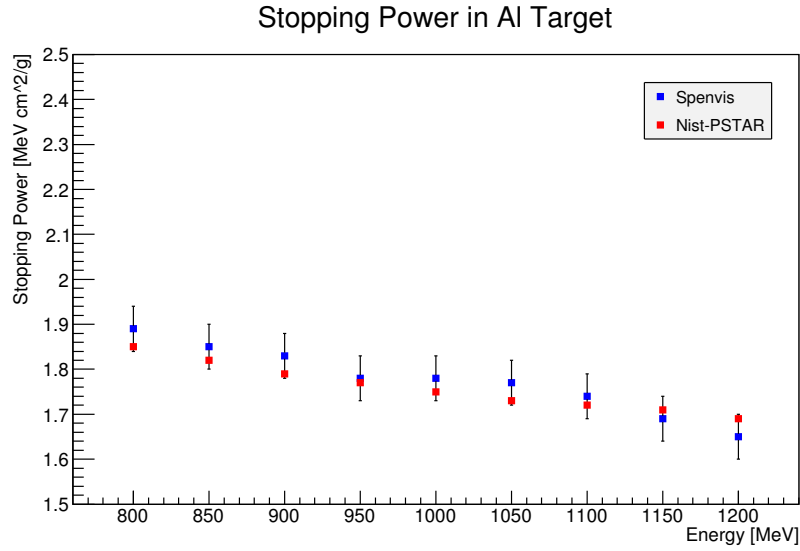


Figure 60: Comparison of the values of the electronic stopping power of the Spenvis software and database PSTAR, of protons in aluminum in the range 800 ÷ 1200 MeV.

It was later made the comparison with Geant4. Obviously, the simulation was performed in the same experimental conditions and considering for the both software same run. The following figure 61 shows the graph that compares the performance of the electronic stopping power of the database PSTAR, Spenvis software and Geant4 software.

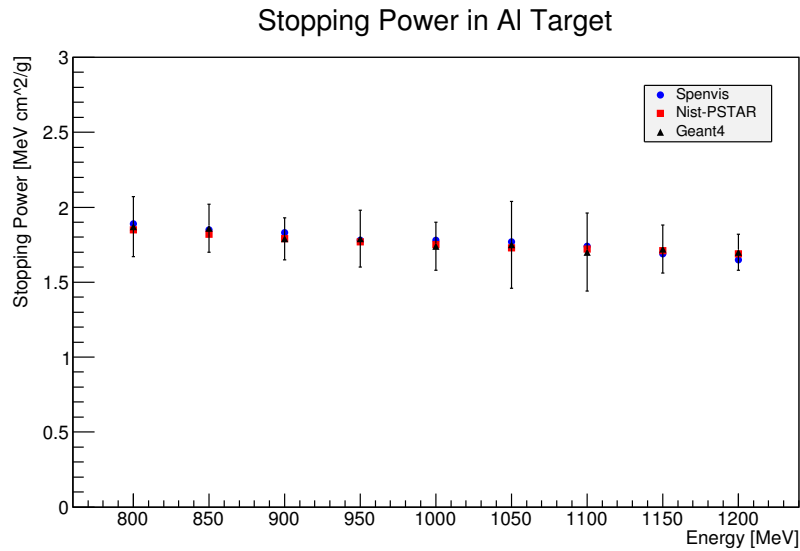


Figure 61: Comparison of the values of the electronic stopping power of the Spenvis software, Geant4 software and database PSTAR, of protons in aluminum in the range 800 ÷ 1200 MeV.

The graphs that show the trends of Stopping Power were obtained with the software ROOT (figure 61).

The blue circles represent the Stopping Power values obtained with the MULASSIS module, the red squares represent the values shown in the PSTAR database and the black triangles represent the values obtained with the Geant4 toolkit. The table and graph show that there is a good agreement between simulated data, with SPENVIS-MULASSIS and Geant4, and the tabulated data PSTAR-NIST because the tabulated value is in the range determined by the standard deviation.

Conclusions

The space radiation represents a serious risk for astronauts during space missions. The risk related to the space radiation exposure could involve acute and/or late effects.

My research project concerns the identification of materials of interest in the field of aerospace for the radioprotection of the astronauts during the space missions. This PhD work provides an important contribution to the study of the effectiveness of materials used as shielding for radiation, especially in view of new missions and of longer duration than previous. In particular this study was conducted in the case of exposure to Solar Particle Events for astronauts.

In this context, by using Geant4, the validation of the electromagnetic and hadronic physical processes were performed for energy characteristic of SPE.

This validation is an essential prerequisite for the use of any application.

The application STP (stopping power) for Geant4 was developed and validated by comparing values of electronics stopping power with those provided by the NIST database PSTAR.

The experimental setup consists of a source of proton with energy that varies in the range $800 \div 1200$ MeV and that interacts with an aluminum slab of mass thickness $20g/cm^2$.

These applications were developed to validate the electromagnetic physical processes. The results show a good agreement between simulated data and tabulated data, for this reason the electromagnetic physical processes is validated.

Instead, the DOSE application was developed to validate the hadronic physical processes and to evaluate the trends of the dose, due to a primary beam of protons. The experimental setup consists of a source of proton with energy 1GeV that interacts with aluminum slab, of mass thickness $20g/cm^2$ and the ionization chamber of the equivalent tissue (eggs chamber $r=1.6$ cm). In the region before the target, there is an increase of 12% of the simulated dose comparable with an increase of 11% of the experimental dose. In the region after the target there is a trend of decreasing exponential type in agreement with the experimental data, caused by the presence of air which favors the attenuation of the beam. For small distances (1 cm) is observed a great increase of the simulated dose 51%, unlike the increase of 57% experimental dose. The validation process was performed by comparing the values of the simulated dose with those measured during the experiment conducted at the NASA Space Radiation Laboratory (NSRL), Brookhaven National Laboratory, USA.

The first analysis concerns the validation using a thickness of aluminum and the results show a good agreement between simulated data and experimental data, so the hadronic physical processes is validated.

After validation with Dose Application other materials were tested, in particular were studied the trends of dose of these materials. The materials that were tested with Dose Application are PMMA

and Nomex (this material was supplied by SAM in collaboration with the engineers of the materials of the Salver of Brindisi).

The trends, in the regions before and after the target, are comparable.

In the first region of the target there is a slight increase in the dose simulated near the surface of the target. In the region after the target is recorded, for all materials, a trend of decreasing exponential type, caused by the presence of air which favors the attenuation of the beam. For small distances from the surface of the target, it is observed a strong increase of the simulated dose, approximately 51% for aluminum, and 24% for the PMMA and the Nomex.

The results show that among aluminum, PMMA and Nomex, for technical features (as well as high mechanical resistance to traction (3.0 - 4.5 GPa) and high flame resistance) and response in terms of dose reduction (in particular in the region after the target), the Nomex is the best material to be used as shielding material during the SPEs.

During PhD's period, I performed (from September to December 2014), an intership with the Società Aerospaziale Mediterranea company, "*Validation of the electromagnetic physical processes with software Spenvis*" using an other software, Spenvis- MULASSIS. The simulation was performed assuming a slab of $20g/cm^2$ as shielding, whose thickness characterizes the shelter used by the crew in case of emergency caused by intense SPE. The primary beam consists of protons of energy varying between 800 to 1200 MeV. There is a good agreement between simulated data, with SPENVIS-MULASSIS and Geant4, and the tabulated data PSTAR-NIST because the tabulated value is in the range determined by the standard deviation.

These validation applications can represent the universal key to test any materials subjected to irradiation with protons without long and expensive use of accelerators.

References

Ahlen, S.P., *Theoretical and experimental aspects of the energy loss of relativistic heavily ionizing particles*, Rev. Mod. Phys. 52, 121. 1980.

Allisy, A., et al., *ICRU Stopping Powers for Electrons and Positrons*. ICRU Report 37. 1984.

Allisy, A., et al., *Stopping Powers and Ranges for Protons and Alpha Particles*. ICRU Report 49.1993.

Armbruster, P., and Benlliure, J., *Basic Nuclear Data at High and Intermediate Energy for Accelerator-Driven Systems*. NU-PECC Nuclear Science: Impact, Applications, Interactions.2001.
[Online] Available: <http://www.nupec.org/iai2001/report/A6.pdf>.]

Badhwar, G.D., and O' Neill, P.M., *An improved model of galactic cosmic radiation for space exploration missions*. Nucl. Tracks & Radiat. Meas., 20, pp. 403-410. 1992.

Barashenkov, V.S., et al., *Inelastic interactions of high energy nucleons with heavy nuclei*. Nuclear Physics A Volume 222, Issue 1, pp. 204220. 1974.

Berger, M.J., et al., *ESTAR, PSTAR, and ASTAR: Computer Programs for Calculating Stopping-Power and Range Tables for Electrons, Protons, and Helium Ions (version 1.2.3)*. National Institute of Standards and Technology, Gaithersburg, MD. 2005.
[Online] Available: <http://physics.nist.gov/Star>.

Bowman, J.D., et al., *Abrasion-ablation of Heavy Ions*. Report LBL- 2908, Lawrence Berkeley Laboratory. 1973.

Durante, M. and Cucinotta, F. A., *Physical basis of radiation protection in space travel*. Reviews of Modern Physics, Vol. 83. 2011.

Cucinotta, F. A., Hu, S., et al., *Space radiation risk limits and Earth- Moon-Mars environmental models*. Space Weather 8, S00E09. 2010.

Durante, M., *Radiation protection in space*. Rivista del Nuovo Cimento, 25 , n. 8, 7-8. 2002.

Enqvist, T., et al., *Isotopic yields and kinetic energies of primary residues in 1 A GeV 208 Pb+p reactions*. Nuclear Physics A 686, pp. 481-524. 2001.

Far West Technology, Inc. IC-17 (<http://www.fwt.com/detector/ic17ds.htm>)

Geant4 User's Guide for Application Developer, 2013

[Online] Available: <http://geant4.web.cern.ch/geant4/UserDocumentation/UsersGuides/ForApplicationDeveloper/html/index.html>.

Geant4 Physics Reference Manual

[Online] Available: <http://geant4.web.cern.ch/geant4/UserDocumentation/UsersGuides/PhysicsReferenceManual>.

Giani, S., *Geant4: Simulation for the next generation of HEP experiments*. Chep95 Proceedings. 1995.

Griffin, J.J., *Statistical Model of Intermediate Structure*. Physical Review Letters 17, pp. 478-481. 1966.

Hammersley, J.M. and Handscomb, D.C., *Monte Carlo methods*. Fletcher ISBN 0-416-52340-4. 1975.

Hartmann, S., *The World as a Process: Simulations in the Natural and Social Sciences*. Theory and Decision Library. Dordrecht: Kluwer, pp.. 77-100. 1996.

Heikkinen, A., Stepanov, N., Wellisch, J.P., *Bertini intra-nuclear cascade implementation in Geant4*. CHEP03 March 24-28, 2003 La Jolla, California. arXiv:nucl-th/0306008. 2003.

ICRP, *Recommendations of the International Commission on Radiological Protection*. Annals of the ICRP, 21. Publication 60. 1991.

ICRP, *Recommendations of the International Commission on Radiological Protection*. Annals of the ICRP, 37. Publication 103. 2007.

Kim, M.Y.H., et al., *Prediction Of Frequency and Exposure Level of Solar Particle Events*. Health Physics: Volume 97, pp 68-81. 2009.

Ledoux, X., et al., *Spallation Neutron Production by 0.8, 1.2, and 1.6 GeV Protons on Pb Targets*. Physical Review Letters 82 4412-5. 1999.

Leo, W.R., *Techniques for nuclear and particle physics experiments*. Second revised edition, Springer-Verlag. 1993.

Leray, S., et al., *Spallation neutron production by 0.8, 1.2, and 1.6 GeV protons on various targets*. Phys. Rev. C 65, 044621. 2002.

Letaw, J. R., et al., *Proton-nucleus total inelastic cross sections - an empirical formula for E greater than 10 MeV*. The Astrophysical Journal Supplement Series, Vol. 51, pp. 271-275. 1983.

Letourneau, A., et al. *Neutron production in bombardments of thin and thick W, Hg, Pb targets by 0.4, 0.8, 1.2, 1.8 and 2.5 GeV protons*. Nucl. Instrum. Meth. B 170, pp. 299322. 2000

Mancusi, D., et al. *Comparison of aluminum and lucite for shielding against 1 GeV protons*. Advances in Space Research 40 581585. 2007.
[Online] Available: <http://www.sciencedirect.com>.

NASA, NASA/SP-2009-3405, 2009.

NCRP, *Radiation Protection Guidance for Activities in Low-Earth Orbit*. NCRP Report No. 132. 2000.

McGuire, R.E., et al., *The composition of solar energetic particles*. Astrophysical Journal, vol. 301, pp. 938-961. 1986.

Schimmerling, W. Rapkin, M., Wong, M. and Howard, J., Fragmentation cross sections. *Med. Phys.*, 13 212. 1983.

Straube, U., et al. Operational radiation protection for astronauts and cosmonauts and correlated activities of ESA Medical Operations. *Acta Astronaut.* 66, 963. 2010.

Titarenko, Yu. E., et al. *Experimental and Computer Simulation Study of Radionuclide Production in Heavy Materials Irradiated by Intermediate Energy Protons*. arXiv:nucl-ex/9908012. 1999.

Wilson, J.W., et al., *Transport Methods and Interactions for Space Radiations*. NASA RP 1257. 1991.

Yao, W.M., et al., (Particle Data Group), *J. Phys. G* 33, 1. 2006.

Zeitlin, C., et al., *Heavy fragment production cross sections from 1.05 GeV/nucleon ^{56}Fe in C, Al, Cu, Pb, and CH₂ targets*. *Physical Review C*, Vol. 56, n 1. 1997.